UiT
THE ARCTIC
UNIVERSITY
OF NORWAY

Faculty of Science and Technology
Department of Physics and Technology

Arctic Cirrus Clouds: A Comparison of Properties Derived from Measurements by Ground-Based and Spaceborne Lidar Systems

—

Ingrid Margrethe Vestnes Hanssen

FYS-3931 Master's thesis in space physics

December 2015

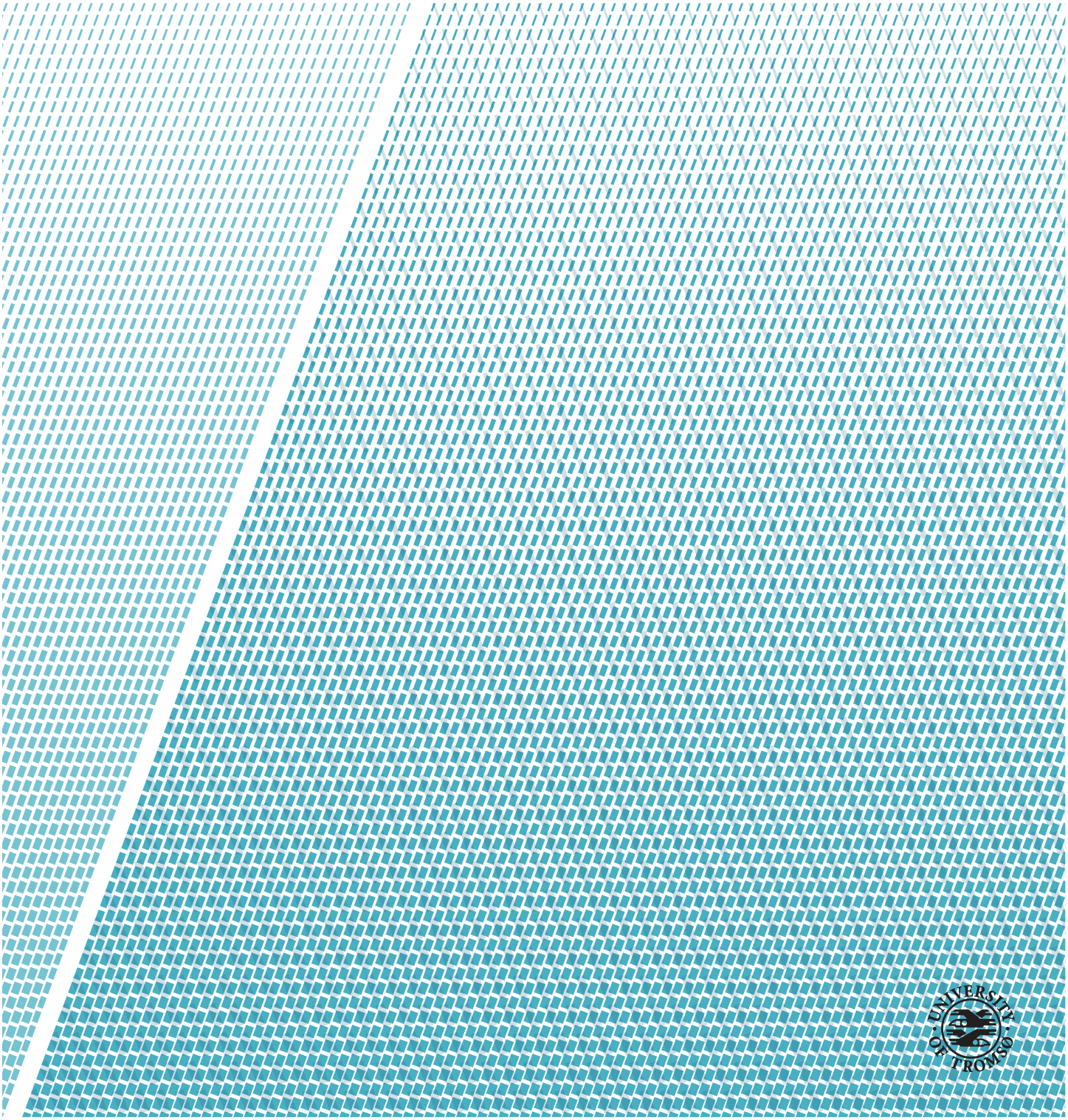

Abstract

The purpose of this thesis is to investigate Arctic cirrus clouds. In this work, data from the ground-based lidar system at ALOMAR, Andøya Space Center. and the spaceborne lidar onboard the CALIPSO satellite is used.

Cirrus clouds are an important factor in modeling climate changes, which is one of the major research fields of this time. Most of the cirrus cloud research concentrates on investigating the phenomenon in the tropical regions as some of the generating mechanisms of cirrus clouds are more common there. The study of cirrus clouds in the Arctic has been sparse due to lack of instrumentation. The ALOMAR facility offers instrumentation and database suitable for such research.

Two lidar systems with similar properties are used in the thesis. The stationary system at Ramnan, Norway (379 meter above sea-level) has been in operation since 2005, and gives access to long-term data. The system measures the troposphere with good quality up to 15-20 km, and can also detect major events in the stratosphere up to 61 km.

The CALIPSO satellite was launched in 2006 and has been operating steadily since 2007. The satellite orbits sun-synchronously, with two daily overpasses near Andøya. The onboard lidar has the same capabilities as the stationary system in Northern Norway, and the two datasets can be compared.

Analysis of the data indicate that there is around 50% cirrus clouds in the Arctic region, with CALIPSO registering 48% and the ALOMAR Troposphere lidar finding 56%. Mean base height is found to be between 6600-7000 meters above sea-level for the two systems and clouds are relatively thin with a mean thickness of 1166 and 1464 meters for ALOMAR and CALIPSO, respectively. In tropical regions, base heights of 8-10 km and thickness of 2-3 km are common.

Several interesting cases of cirrus clouds near the stratosphere are detected over ALOMAR. These cases require special attention, and indicate that cirrus clouds reside at higher altitudes than expected in the Arctic region.

Acknowledgements

While working on this project, I have received guidance and support from several people who deserve thanks.

UiT The Arctic University of Norway have provided me with 5 interesting years as a student, filled with important life experiences. A big thanks to Unni-Pia Løvhaug for supervising me in a wonderful way, it has been a great help!

I wish to thank Andøya Space Center and ALOMAR for the opportunity to work on this exciting project. Thank you for giving me access to both lidar data and the system itself, as well as answering all of my annoying questions along the road and making me feel welcome at any time.

A big thank you to Michael Gausa for being my supervisor and never getting tired of explaining things again and again. I also have to thank you for arranging a study trip to Yale University, allowing me to learn from people with experience in cloud research.

I wish to thank Trude Storelvmo at Yale for introducing me to New Haven and helping me along with fruitful discussions about data processing and results. It is always an inspiration to learn from people with experience and passion.

I also have to thank my fiancé for allowing me to spend so much time away from home without to many complaints and for keeping up with nervous rambling and physics talk. And for babysitting the dog enough for me to finish my work!

Satellite data from the CALIPSO satellite has been used in this thesis. These data were obtained from the NASA Langley Research Center Atmospheric Science Data Center.

Contents

List of Figures

List of Tables

List of Abbreviations

ALOMAR Arctic Lidar Observatory for Middle Atmosphere Research

APD Avalanche Photodiode

ASC Andøya Space Center

CALIOP Cloud-Aerosol Lidar with Orthogonal Polarization

CALIPSO Cloud-Aerosol Lidar and Infrared Pathfinder Satellite Observations

DIAL Differential-Absorption Lidar

ESA European Space Agency

ECMWF European Centre for Medium-Range Weather Forecasts

FARS Facility for Atmospheric Remote Sensing

IGRA Integrated Global Radiosonde Archive

IPCC Intergovernmental Panel on Climate Change

ITCZ Intertropical Convergence Zone

IWC Ice-Water Content

LaRC Langley Research Center

Lidar Light Detection and Ranging

NASA National Aeronautics and Space Administration

NOAA National Oceanic and Atmospheric Administration

Nd:YAG Neodynium-Doped Yttrium Aluminium Garnet

Radar Radio Detection and Ranging

RMR Rayleigh-Mie-Raman

SVC Sub-Visual Cirrus

UiO University of Oslo

UiT University of Tromsø

WMO World Meteorological Organization

Nomenclature

Cirrus Cloud Theory

A is inversely related to thermal conductivity

B is inversely related to vapor pressure and vapor diffusivity in air

C Geometrical factor of the crystal

F Ventilation term

m Crystal mass

P Power

Q Shape Parameter

σ Supersaturation term

τ Optical Depth

Lidar Theory

A effective detection area of the system

α extinction coefficient

$\beta(R)$ range-dependent backscatter coefficient for a lidar system

c speed of light

$G(R)$ range-dependent measurement geometry for a lidar system

K system-dependent factor for a lidar system

λ wavelength of transmitted light

η system efficiency

$O(R)$ overlap function between the laser beam and the telescopes field of view

P_0 averaged transmitted power

$P(R)$ range-dependent received power for a lidar system

R^2 accounts for the scattering geometry of the measurement region, which is formed as part of a sphere.

$T(R)$ range-dependent transmission / absorption term for a lidar system

τ pulse length in time

1 Introduction

1.1 Topic and Motivation

Cirrus clouds are one of the major unsolved components in climate research (Liou, 1986). Clouds are recognized by their phase, which refers to the state of its majority constituents. The cloud phase is either ice, liquid or mixed. Cirrus have been known to mankind as ice-phase clouds for centuries (Lynch, 2002), but research only started after the second world war. Technological advances due to the Cold War and the Space Race lead to the invention of lidars which have been used for cirrus-studies ever since.

Todays scientists are motivated by the well-known, but unsolved climate changes (Liou, 1986). Cirrus clouds are known to admit solar radiation into the Earths atmosphere as well as trapping parts of the infrared radiation from the ground. This will in time lead to a heating of the atmosphere which contributes to the global warming.

1.2 Previous Work

Much research has been conducted on the topic, but most of it is focused on cirrus at mid- and lower latitudes, leaving the Arctic cirrus clouds virtually unexplored.

The first report summarizing current knowledge about cirrus clouds was pub-

lished in 1957 by Robert Stone, after it became apparent during World War 2 that cirrus clouds impaired the pilots view (Stone, 1957). It focused mostly on the prediction of cirrus clouds. Liou (1986) published a report summarizing the current knowledge of cirrus clouds with a climate perspective. This paper is still cited as the major motivation for ongoing research (Sassen *et al.* , 2008; Noel *et al.* , 2002).

In 2006, the National Aeronautics and Space Administration (NASA) launched the Cloud-Aerosol Lidar and Infrared Pathfinder Satellite Observation (CALIPSO) satellite. Its purpose was to obtain improved measurements and increase understanding of, amongst other things, cirrus clouds (Winker *et al.* , 2003). Data from this satellite has resulted in some papers with a global perspective on the macrophysical properties of cirrus (Sassen *et al.* , 2008). When it comes to microphysics, most scientists agree that this must be researched with a more limited spatial coverage, as the properties are likely to vary with geography (Sassen & Benson, 2001).

In the Arctic region, not much work has been done with respect to cirrus clouds. Guasta *et al.* (1994) published a short research letter following a light detection and ranging (lidar) campaign in Finland (at $66^{o}N$). The intent of the campaign was to study the effects of the volcanic eruption of Mt. Pinatubo in 1991, but as a bi-product, cirrus clouds were measured.

Some campaigns over Svalbard combining airborne lidars with other instruments have been conducted to study clouds in general, but little research has focused on cirrus clouds (Lampert, 2010). A master thesis written through the University of Oslo (UiO) focused on case studies of a few cirrus clouds over Andøya Space Center (ASC) in 2007 (Larsgard, 2008).

Leading up to this master's thesis, a preliminary study of the geometrical properties of cirrus clouds over Andøya Space Center was conducted. This was presented in a project paper at UiT, The Arctic University of Norway (Hanssen, 2015). The statistical results from this paper is attached in Appendix C for convenient reference.

1.3 The Aim and Purpose of this Study

This thesis aims to disclose macrophysical properties of cirrus clouds in the Arctic region by use of both a local ground-based lidar system located at the Arctic Lidar Observatory for Middle Atmosphere Research (ALOMAR) and the spaceborne lidar onboard the CALIPSO satellite.

Important macrophysical features such as cloud geometry (cloud altitudes and thickness) and temperature will be explored in datasets from 2007-2013 for both systems.

Both lidar systems used in the thesis has depolarization capabilities. For the ALOMAR troposphere lidar, these measurements have never been calibrated and checked against verified measurements. The CALIPSO satellite can give an overall statistics of depolarization within the clouds. This is an important step toward disclosing microphysical properties of Arctic cirrus clouds. Initial comparison of the data from ALOMAR and CALIPSO will be conducted.

Investigating the cirrus cloud cover at high latitudes is important for modeling climate changes. Even more important is the investigation of microphysical properties of cirrus clouds, which are assumed to vary geographically (Sassen & Benson, 2001). As there have been no extensive studies of such properties in the Arctic region, this is cause for major uncertainties in climate models.

Results in this thesis will also highlight topics that require closer focus in future research.

1.4 Organization of the Thesis

In chapter 2, theory about cirrus clouds is presented.

In chapter 3 the theory about lidars in general and the systems used in this thesis will be presented.

In chapter 4 the statistical analysis of macrophysical properties over ALOMAR and measured by CALIPSO are presented.

In chapter 5, some interesting cases of cirrus clouds near and possibly above the tropopause are presented.

In chapter 6, the uncovered results are further discussed and the initial study of depolarization ratio from ALOMAR is presented. A summary of the work and future challenges is presented in chapter 7.

The appendices contain macrophysical properties with respect to season, results from the preliminary project study and other relevant information for the thesis.

2 Cirrus Clouds

In this chapter, theory about cirrus clouds is presented. This will help emphasize the motivation for researching Arctic cirrus clouds and indicate which areas require more focus.

2.1 Definitions According to the World Meteorological Organization

The World Meteorological Organization (WMO) publishes the International Cloud Atlas as a guide for weather observers to identify the various kinds of clouds and other natural phenomenons (WMO, 1975). The atlas gives morphological descriptions of clouds as a way to distinguish them from each other.

There are three main generas of cirrus clouds, according to the WMO; Cirrus, cirrostratus and cirrocumulus clouds. Each of the three generas are further divided into species and varieties according to individual appearance. The division can be seen in figure 2.1, reproduced from WMO (1975).

Cloud Classification					
Genera	Species	Varieties	Features	Mother-cloud	
				Genitus	Mutatus
Cirrus	Fibratus, Uncinus, Spissatus, Castellanus, Floccus	Intortus, Radiatus, Vertebratus, Diplicatus	Mamma	Cirrocumulus, Altocumulus, Cumulonimbus	Cirrostratus
Cirruocumulus	Stratiformis, Lenticularis, Castellanus, Floccus	Undulatus, Lacunosus	Virga, Mamma	-	Cirrus, Cirrostratus, Altostratus
Cirrostratus	Fibratus, Nebulosus	Duplicatus, Undulatus	-	Cirrocumulus, Cumulonimbus	Cirrus, Cirrocumulus, Altostratus
Altocumulus	Stratiformis, Lenticularis, Castellanus, Floccus	Translucidus, perlucidus, opacus, duplocatus, undulatus, radiatus, Lacunosus	Virga, Mamma	Cumulus, Cumulonimbus	Cirrocumulus, Altostratus, Nimbostratus, Stratocumulus
Altostratus	-	Translucidus, Opacus, Duplicatus, Undulatus, Radiatus	Virga, Praecipitatio, Pannus, Mamma	Altocumulus, Cumulonimbus	Cirrostratus, Nimbostratus
Nimbostratus	-	-	Praecipitatio, virga, mamma	Cumulus, Cumulonimbus	Altocumulus, Altostratus, Stratocumulus
Stratocumulus	Stratiformis, Leticularis, Castellanus	Translucidus, Perlucidus, Opacus, Duplicatus, Undulatus, Radiatus, Lacunosus	Mamma, Virga, Praecipitatio	Altostratus, Nimbostratus, Cumulus, Cumulonimbus	Altocumulus, Nimbostratus, Stratus
Stratus	Nebulosus, Fractus	Opacus, Translucidus, Undulatus	Praecipitatio	Nimbostratus, Cumulus, Cumulonimbus	Stratocumulus
Cumulus	Humilis, Mediocris, Congestus, Fractus	Radiatus	Pileus, Velum, Virga, Praecipitatio, Arcus, Pannus, Tuba	Altocumulus, Stratocumulus	Stratocumulus, Stratus
Cumulonimbus	Calvus, Capillatus	-	Praecipitatio, Virga, Pannus, Incus, Mamma, Pileus, Velum, Arcus, Tuba	Altocumulus, Altostratus, Nimbostratus, Stratocumulus, Cumulus	Cumulus

Figure 2.1: The World Meteorological Organizations division of clouds into generas, species and varieties. The figure is reproduced from the International Cloud Atlas, Volume 1, 1975-edition.

The three generas of cirrus clouds are defined according to WMO by the following morphological descriptions:

***Cirrus**: Detached clouds in the form of white, delicate filaments or white or most white patches or narrow bands. These clouds have fibrous hair-like appearance, or a silky sheen, or both.*

***Cirrostratus:** Transparent, whitish cloud veil or fibrous (hair-like) or smooth appearance, totally or partly covering the sky, and generally producing halo phenomenon.*

***Cirrocumulus:** Thin, white path, sheet or layer of cloud without shading, composed of very small elements in the form of grains, ripples, etc., merged or separate, and more or less regularly arranged; most of the elements have an apparent width of less than one degree.*

As the above definitions show, identifying cirrus clouds by morphology requires a clear view of the clouds, which can be difficult to achieve. This obstacle accompanied with the clouds impact on Earth and its population has lead to increasing scientific interest in the topic.

2.2 History

Luke Howard was the first person to name cirrus clouds, dating back to 1803 (Sassen, 2002). This was the first latin naming of clouds, and it relates to the appearance of the clouds. Well pre-dating the naming of the clouds, they were thought to be ice phase clouds as early as 500 BC.

Cirrus clouds research began after World War 2. Cirrus clouds were recognized as an important factor for pilots during the war, and military organizations in several countries were motivated to investigate the phenomenon (Lynch, 2002).

The first American report on the topic was published in 1957 by Robert Stone. The report was ordered by the American government to disclose the current knowledge of cirrus clouds and forecasting, as the clouds had proven detrimental for pilots view. The report illustrated well the need for further research.

With the Space Age and the Cold War motivating technological developments, new equipment became available for cloud research (Lynch, 2002). However, other cloud and weather phenomenon took precedence over cirrus clouds, as

they appeared harmless compared to for example storms and precipitation (Sassen & Mace, 2002).

In 1986, a new report ordered by the American government was published, this time with a climate perspective on cirrus clouds (Liou, 1986). The report summarized the current knowledge and highlighted the areas to investigate in order to estimate the cirrus effect on the global climate changes. Today, this report is still cited by most authors as the main motivation for researching cirrus clouds, as they remain unsolved with respect to climate changes and the Earths radiation budget.

2.3 Current Research and Motivation

The main motivation for researching cirrus clouds remains the disclosure of their effect on the climate changes occurring today. Since 1986, the topic has been intensively studied, but most of the research focuses on the mid- and lower latitudes, where one has believed the main occurrence of these clouds to be. The satellite cover and population density is also larger here, making research easier.

In 2007, the satellite CALIPSO was launched, allowing for cirrus cloud research with a more global perspective. Several papers have been published using data from this satellite, with both global and local perspectives(Sassen *et al.* , 2008; Huo & Lu, 2014; Adhikari *et al.* , 2012).

Sassen *et al.* (2008) published one of the papers with a global perspective. The authors found a cirrus cover in the tropical region of close to 60%, with a decreasing trend toward the polar regions.

With an Arctic perspective, little research has been reported. In 1994, a research letter was published reporting on cirrus cloud detection in Finland, at $66^{o}N$ (Guasta *et al.* , 1994). The clouds were detected during lidar research on the effect of the Pinatubo volcanic eruption in 1991, and 50% cirrus cover over a two month-period was found.

With the foundation of the Arctic Lidar Observatory at Andøya, Norway in 1994, the motivation was researching the middle section of the atmosphere (Skatteboe, 1996). The observatory was mainly dedicated to lidar research, but with time it has expanded to host passive instruments like radiometers as well as being in charge of all scientific instruments for radio detection and ranging (radar) at Andøya Space Center.

The lidar instrumentation park was expanded in 2005 with the installation of a troposphere lidar, intended to research clouds and aerosols in the lower parts of the atmosphere (Frioud *et al.* , 2006). Cirrus cloud research has been named as one of the main topics to research using this instrument. This has resulted in one previous master thesis looking at cirrus clouds using the first year of data from the ALOMAR troposphere lidar (Larsgard, 2008).

Leading up to this thesis, a preliminary paper was written, containing a brief statistics of cirrus clouds above ALOMAR. This thesis disclosed a large occurrence of cirrus clouds in measurements, which motivates further research on the topic (Hanssen, 2015).

As mentioned, cirrus clouds are currently researched due to their climate effects. Their properties reveal that they will lead to a certain degree of heating in the atmosphere as they admit the incoming solar radiation and trap parts of the outgoing radiation from Earth (Stephens, 2002).

The Arctic region appears to have a net warming effect from clouds throughout the year (Lampert, 2010). There is also an increased snow and ice-cover in this region, causing the effects of heating in the atmosphere to be more notable and devastating.

In 2001, the Intergovernmental Panel on Climate Change (IPCC) presented their fourth report on climate changes. This report contained a figure illustrating the level of understanding for some of the elements causing radiative heating and cooling on the Earths climate. Cirrus clouds were listed as one of the elements with the lowest degree of scientific understanding (IPCC, 2001). This figure is reproduced in figure 2.2.

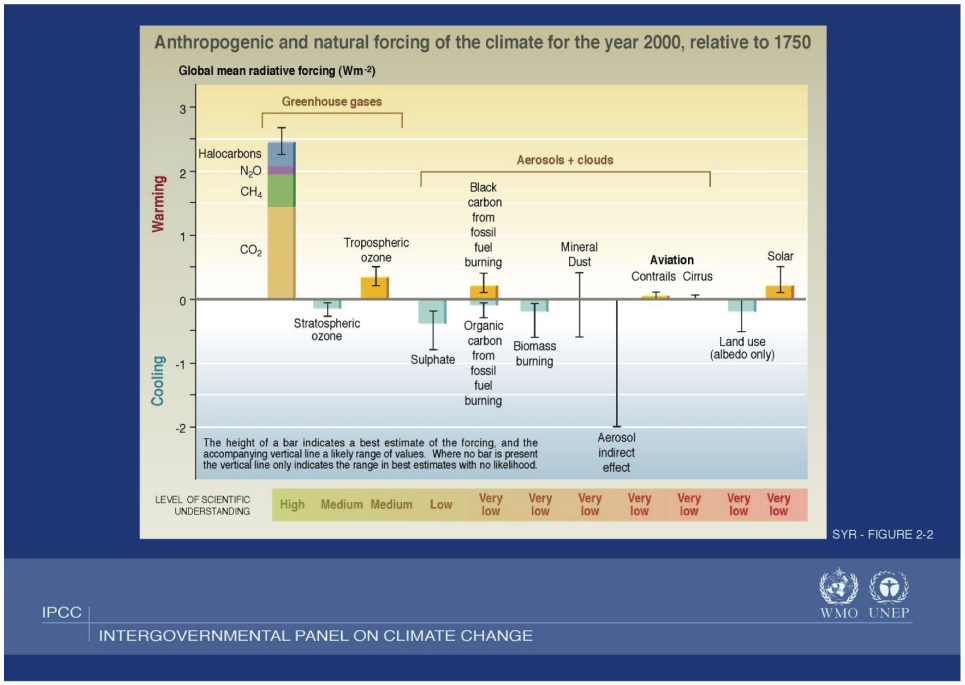

Figure 2.2: IPCC's presentation of the current level of scientific understanding for various sources of radiative heating and cooling from IPCC's report on climate changes from 2001. The figure illustrates the need for further research to increase the level of scientific understanding of several components in climate models, including cirrus clouds and contrails.

To be able to model cirrus cloud effects on the climate, a higher level of understanding is required. As much research has been conduced at lower latitudes, disclosing features of Arctic cirrus clouds is an important step toward a global understanding of them.

2.4 Types of Cirrus Clouds

In section 2.1, the cirrus cloud definitions according to the WMO were presented. There are two types of cirrus clouds not currently included in the International Cloud Atlas, namely Contrail Cirrus Clouds (hereafter: contrails) and Subvisual Cirrus Clouds (SVC) (Lynch, 2002).

They were both discovered during World War 2, but much of the research has been conducted at a later time (Schumann, 2002; Lynch & Sassen, 2002). This may very well be one of the reasons they are not included in the current edition of the International Cloud Atlas, which was published in 1975. An update of the

International Cloud atlas is currently pending, which may lead to the inclusion of these clouds as acknowledged cirrus clouds [1].

2.4.1 Contrail Cirrus Clouds

Contrails is an abbreviation for "condensation trail clouds", and they are related to aircrafts. They were first discovered in connection with propeller aircrafts in the early 20th century and later named by pilots in the British Royal Air Force during World War 2 (Schumann, 2002).

They are one of the most well-studied varieties of cirrus clouds, as they are man-made. With growing in interest climate changes, especially the ones manmade, studies to disclose environmental causes started soon after their discovery (Schumann, 2002). Research is still ongoing, and recent papers have looked at the effect contrails have on the total cirrus cloud cover (Stordal *et al.* , 2005).

Contrails are formed from the exhaust of aircrafts due to rapid cooling in ice-supersaturated air (Schumann, 2002). Due to large particle pollution from the exhaust, they form where no natural clouds would, but they may persist and transform into "normal" cirrus clouds given the right circumstances (Minnis *et al.* , 2004). The transformation of contrails to natural cirrus is not the only way air traffic affects cirrus cloud cover. The pollution of particles from airplane exhaust will leave numerous nuclei for natural cirrus to form at a later time(Schumann, 2002).

Studying contrail cirrus clouds can give better understanding of natural cirrus clouds, as the conditions under which they form is well-known and their location is clearly accessible for in-situ measurements from other aircrafts as well as active remote sensing equipment such as lidars [2].

Previously mentioned studies by Stordal *et al.* (2005) revealed what might be an increasing trend in the total cirrus cover due to contrails. The study estimated a radiative forcing significantly larger than the one estimated for air traffic due to other effects than cirrus clouds. Radiative forcing is defined as the number of watts per square-meter contributed to by various sources of heating or cooling.

1. Published as newsflash on the WMO webpage, found at this URL: `https://www.wmo.int/media/content/international-cloud-atlas`. Last checked: September 22nd 2015 13:14LT
2. See chapter 3 for more information about lidars

Even though there are some challenges in estimating effects of contrails and researching them, they have been shown to affect the climate and the total cirrus cloud cover. The size of their contribution should be considered uncertain, but it cannot be ignored (Stordal *et al.* , 2005).

2.4.2 Subvisual Cirrus Clouds

As previously mentioned, sub-visual cirrus clouds were first discovered during World War 2. Pilots reported seeing clouds at high altitudes that were not observed from the ground (Lynch & Sassen, 2002). Since the 1970's, lidars have been used to measure SVC's. The clouds are characterized by an optical depth [3] of 0,03 or less, which makes them invisible to the naked eye when looking in a vertical direction. Passive instruments also have difficulties observing the clouds, and as they are vertically thin, horizontal detection is expected to be unlikely (Lynch & Sassen, 2002).

SVC's are linked to the tropopause, and they reside at higher altitudes than other cirrus clouds. They are also found at lower temperatures, well below the threshold for homogeneous nucleation at -40^oC (Lynch & Sassen, 2002). Several generating mechanisms have been linked to these clouds. According to Sassen *et al.* (2008), they are caused by cold traps in the tropopause. This is listed as their generating mechanism in table 2.1, even though there is no definitive proof yet.

Other mechanisms such as anvils from thunderstorms which are injected into, and above, the tropopause, as well as orographically caused gravity waves and jet streams are investigated as possible causes for SVC's.

At higher latitudes, subvisual clouds may be remnants of optically thicker clouds rising, but they are assumed to be less common than in the tropical region (Lynch & Sassen, 2002). This was supported in some degree when looking at statistical results from the project paper, revealing that the majority of cirrus clouds over ALOMAR were at great distance from the local tropopause (Hanssen, 2015).

It is evident that their generating mechanism is still under investigation and the present knowledge does not allow for conclusive definitions.

The lack of knowledge and detection possibilities for these clouds may lead to an underestimation of the total cirrus cloud cover. This again will affect estimates of the climate impacts from such clouds (Sassen *et al.* , 2008). The

3. See section 2.6.3 for more information about optical depth

launch of CALIPSO in 2006 was intended to help the situation, and other satellites continuing its work will hopefully contribute to this research.

2.5 Generating Mechanisms

There is a number of known generating mechanisms for cirrus clouds, and in table 2.1, the currently acknowledged ones are listed (Sassen *et al.* , 2008). The various mechanisms have been disclosed at different times throughout cirrus cloud research, and as late as 1986, only synoptic generation of cirrus clouds was known, along with contrails (Liou, 1986).

Table 2.1: The currently acknowledged generating mechanisms of cirrus clouds (Sassen *et al.* , 2008)

Category	Mechanism
Synoptic (Jet stream, frontal etc)	Top-down generation
Injection cirrus	Thunderstorm anvils
Mountain-wave updraft	Orographic, terrain-induced
Cold trap	Tropopause-topped thin layer (SVC's)
Contrail cirrus	Rapid cooling of aircraft exhaust

The mechanisms resulting in cirrus clouds are clearly geographically dependent. The occurrence of cold trap cirrus clouds is believed to be more pronounced in the tropical region than the Arctic due to their possible relations to thunderstorms and gravity waves (Sassen *et al.* , 2008). When looking at results from the preliminary project paper, this seems likely as such clouds are generally located around or near the tropopause [4].

Also other mechanisms will have a clear dependence on geography, such as orographic cirrus clouds, which occur in mountain-rich areas. Contrail cirrus clouds will also be detected more over areas with busy air traffic than calm, undisturbed air in more remote locations (Guasta & Vallar, 2003).

Injection cirrus clouds are related to convective events, which are most pronounced in the Intertropical Convergence Zone (ITCZ). This region is known for strong convective cloud events in the summer season, which have the ability to transport ice and water into the tropopause and beyond. Such clouds have a higher ice water content (IWC) compared to clouds undergoing homogeneous freezing (Sassen *et al.* , 2008).

4. Statistical results from project paper is found in appendix C

Other mechanisms, such as synoptic systems are less geography dependent, as these weather patterns evolve all around the globe.

2.6 Macrophysical and Optical Parameters

The previously stated definitions of cirrus clouds in the International Cloud Atlas is the only official definition of cirrus clouds. However, following technological advances, other parameters than morphology have been made available through remote and in-situ measurements, allowing for more precise detection of cirrus clouds (Sassen, 2002).

There are no commonly accepted parameter definitions to distinguish cirrus clouds from other clouds and aerosol layers. There are some general intervals where height, temperature and optical depth are assumed to lie for all cirrus clouds, but there is also agreement among scientists that there will be local variations in these criterions.

For instance, global studies tend to use more restrictive criterions, such is the case in the global study of CALIPSO-data, conducted by Sassen *et al.* (2008). This minimizes chances of misclassifying mixed-phase clouds as cirrus, while also opening for excluding cirrus clouds from the statistics. The behavior of these parameters should therefore be investigated at different latitudes to adapt criterions to geography.

2.6.1 Height

One of the important parameters for cirrus cloud research, is cloud height. Cirrus clouds are closely related to the upper region of the troposphere and the tropopause (Sassen & Mace, 2002). The local tropopause altitude varies with latitude, and the Arctic tropopause is continuously monitored by radar systems located at Svalbard (Hall *et al.* , 2011).

The radar tropopause for the period 2007-2010 never exceeded 13 km with the corresponding radiosonde tropopause located at approximately 11 km. The radiosonde tropopause height is used as a basis for this study, and the height region investigated above Andøya Space Center is therefore chosen to be between 4 and 12 km.

Although height can be used for a rough screening for cirrus clouds, they are not exclusively present in this region. Mixed-phase clouds rising from lower altitudes and polar stratospheric clouds can both be present in the same height

region during winter. Therefore, other parameters such as temperature or visual optical depth should be applied as well (Sassen *et al.* , 2008).

2.6.2 Temperature

Cirrus clouds consist almost exclusively of ice crystals, and temperature can therefore be chosen as a parameter to eliminate clouds of mixed phase. The theoretical limit for homogeneous freezing of water is set to -40^oC, which could be used as a criterion for cirrus classification. This has been applied in global studies, like in Sassen *et al.* (2008).

However, cirrus clouds can also form at higher temperatures through heterogeneous freezing in the presence of a condensation nuclei. Eliminating all clouds warmer than -40^oC therefore excludes some cirrus clouds. Combining the temperature criterion with for example optical thickness will allow for a better screening without eliminating actual cirrus clouds. Other studies have used higher temperature thresholds, such as Huo & Lu (2014) which used -20^oC as the limit for cirrus clouds.

It is also important to consider the generating mechanism of such clouds when investigating temperature. Clouds generated "top-down", may have warmer temperatures at the cloud base, while the cloud top, where the actual freezing of the water droplets occur may be well below the threshold for homogeneous freezing. With time cirrus clouds descend to lower altitudes, and the surroundings will cause melting of the ice and a transition into a mixed- or water-phase cloud.

2.6.3 Optical Depth

Classification based on optical depth is useful when separating cirrus clouds from other high-altitude ice clouds as well as mixed-phase altostratus clouds (Sassen *et al.* , 2008). The parameter describes the optical transparency of the cloud ranging from invisible (like SVC's) to opaque where cirrus clouds transform into altostratus.

According to Sassen *et al.* (2008), cirrus clouds have optical depths ranging from $\tau \in \langle 0.03, 3.0]$, whereas altostratus clouds have optical depths greater than 3.0 (Sassen, 2002). However, cirrus clouds undergoing altostratus transition can have greater optical depths.

2.7 Cirrus Clouds and the Tropopause

Cirrus clouds reside in the upper part of the troposphere, and the tropopause altitude at the location of measurements is therefore interesting to study (Noel *et al.* , 2006). There are different algorithms for calculating the location of the tropopause, and non are applicable independent of geography and time of year (Zängl & Hoinka, 2001).

According to the World Meteorological Organization, the thermal tropopause, which can be derived from radiosonde measurements, is defined as

The lowest level at which the lapse rate decreases to 2 K/km or less, provided also the average lapse rate between this level and all higher levels within 2 km does not exceed 2 K/km (Zängl & Hoinka, 2001)

Experience shows that this definition is ill-suited for locating the tropopause in polar regions during the winter season (Zängl & Hoinka, 2001; Hoinka, 1999). There are other methods for locating the tropopause, for example by use of radar measurements (Hall *et al.* , 2011).

The tropopause region has other characteristics, such as sharply decreasing relative humidity and absence of gases present in the stratosphere such as ozone (Zängl & Hoinka, 2001). Neither property leads to a clear line separating the troposphere and stratosphere.

Radiosonde data is used for temperature data in the thesis, and is also used to find the tropopause location for cases of special interest. Even though the thermal definition of the tropopause is considered unreliable in the polar regions, an attempt is made to calculate the local tropopause for the ALOMAR location.

The satellite data contains information about the tropopause altitude at the point of measurement, obtained from weather models. These numbers are compared to the radiosonde data in chapter 5.

2.8 Microphysical Properties

2.8.1 Cloud Nucleation

As cirrus clouds are ice-phase clouds, they are clearly temperature dependent. The clouds are formed on ice nuclei, which either freeze homogeneously or heterogeneously (Cotton, 2011).

Homogeneous freezing is so-called spontaneous freezing where no particles are required (Wallace, 2006). This process is limited by an upward temperature of approximately -40^oC, above which only heterogeneous freezing is assumed possible. It has been shown that the chance of supercooled liquid occurring at this temperature is very low. Should this be the case, it would be short-lived and unstable (Cotton, 2011).

The temperature threshold of homogeneous freezing has been used as a criterion to distinguish cirrus clouds from mixed-phase clouds (Sassen *et al.* , 2008). However, this would exclude cirrus where the ice nuclei is heterogeneously nucleated.

Cirrus cloud droplets have been found at temperatures upto -13^oC, which is a great deal warmer than homogeneous nucleation (Wallace, 2006). There are several mechanisms which can cause heterogeneous freezing: Vapor-deposition, condensation freezing, immersion freezing and contact freezing (Cotton, 2011).

Vapor deposition involves a transfer of vapor to a nucleus which results in freezing (Cotton, 2011). It requires supersaturated air with respect to ice and a low temperature. Condensation freezing is the result of vapor condensation, forming an ice nuclei which then freezes.

Immersion freezing is when a liquid droplet freezes on an ice nuclei, while contact freezing occurs when ice nuclei come in contact with supercooled droplets and freeze (Cotton, 2011). This is the most efficient heterogeneous freezing mechanism.

2.8.2 Ice Crystals

Once there are frozen cloud droplets present, crystal growth is initiated (Wallace, 2006). This is achieved by ice multiplication, which can be caused by a variety of reasons. Examples of multiplication reasons are fractioning, either due to fragile crystals or the freezing process itself, and riming on secondary freezing (Cotton, 2011).

The growth equation describes the rate of growth in crystals (Hallett *et al.* , 2002):

$$\frac{dm}{dt} = \frac{CF\sigma}{A+B} \tag{2.1}$$

where

A is inversely related to thermal conductivity

B is inversely related to vapor pressure and vapor diffusivity in air

C is the geometrical factor of the crystal

F is the ventilation term

m is the crystal mass

σ is the supersaturation term

No precise definition of the terms A and B is found, but they represent the relation between growth and thermal conductivity, vapor pressure and vapor diffusivity.

Important features of cirrus clouds are particle size, shape and orientation. These features are in general not well understood as they are hard to measure, but the topic has received much attention. Aircrafts have conducted in-situ probing of cirrus clouds to collect crystals for laboratory analysis (Hallett *et al.* , 2002). These measurements are geographically limited and there is a near infinite range of crystal shapes and sizes. As it is expensive to perform and with limited results, it is less common today (Sassen *et al.* , 2008).

Another method to get information about crystals is to use polarization-sensitive lidars (Sassen, 1991). This method is cheaper than conducting in-situ measurements with an acceptable accuracy. However, it is not possible to get the exact shape and size for all individual particles in the clouds, as they are far to numerous (Noel *et al.* , 2006). The polarization lidar technique will be able to classify regions of clouds with families of shapes and sizes, which is adequate for radiation modeling. The method is described more thoroughly in section 2.8.3.

2.8.3 Depolarization Ratio as a Guide to Crystal Properties

When transmitting light into the atmosphere from a lidar system, the properties of the laser is known to the observer. This includes the polarization of the light. A lidar system with depolarization capabilities measures the polarization of the returned signal. By dividing it into perpendicular and parallel polarization with respect to the transmitted light, the depolarization ratio can be calculated (Sassen, 1991).

The depolarization ratio, in its simplest form is written in equation 2.2 (Chen

et al. , 2002).

$$\delta = \frac{\sum P_{\perp}}{\sum P_{\parallel}} \tag{2.2}$$

The linear depolarization ratio is extremely sensitive to the microphysical properties of cirrus clouds (Noel *et al.* , 2006). It has therefore been used by multiple authors to obtain information about the microphysics of cirrus clouds.

One of the methods was presented by Noel *et al.* (2002). It involves ray-tracing simulations looking at three parameters: Index of refraction, aspect ratio Q and crystal orientation. According to Noel *et al.* (2006), the index of refraction shows little variation. The aspect ratio or shape parameter Q can therefore be determined within limits of a range by assuming random orientation.

When using depolarization ratio, one must take care not to misidentify horizontally aligned plate-like crystals as spherical, liquid droplets (Sassen & Benson, 2001). When measuring cirrus clouds from the Facility for Atmospheric Remote Sensing (FARS) in the U.S., the lidar was tilted a few degrees off-zenith for some shots during measurements. The same is done at ALOMAR. However, there measurements are always conducted with a 3 degree tilt with respect to zenith.

Ones the ALOMAR measurements are verified, the depolarization information from them will give an indication of the shape class for the crystals. The shape class refers to the crystals manor of scattering, not the actual shape one would find by imaging the crystals (Noel *et al.* , 2006).

The relation between depolarization ratio and the shape parameter Q is shown in table 2.2:

Table 2.2: Relations between depolarization ratio and shape parameter Q according to Noel *et al.* (2006)

Depolarization Ratio	Shape Parameter Q
$\delta < 0.25$	$Q < 0.1$
$0.25 < \delta < 0.5$	$0.1 < Q < 1.5$
$\delta > 0.5$	$Q > 1.5$

2.9 Radiative Properties and Climate Effects

Radiative properties of clouds determine their effect on the atmosphere (Liou *et al.* , 2002). For so-called warm clouds (clouds in water-phase), the radiation is modeled as blackbody-radiation (Liou, 1986). Ice phase clouds however, have a lower number density and can therefore not be simplified to blackbodies.

In order to estimate the radiation effect from ice clouds, the optical properties of ice are important. The shape, size and orientation of the crystals affect how they scatter incoming radiation from the sun, as well as the trapping of outgoing radiation from Earth.

Attempts have been made to numerically model the index of refraction, which is vital in determining the scattering properties of ice crystals (Liou, 1986). The result is a real part that changes little with conditions, and an imaginary part altering the absorption coefficient depending on wavelength.

Estimating the radiation effect from clouds is important in modeling how they affect the climate. Cirrus clouds will affect the radiation properties in the atmosphere, but radiation also affects cirrus properties (Stephens, 2002). The same two-way link applies to the connection between cirrus clouds and water vapor in the atmosphere. With cirrus affecting the climate and the climate affecting cirrus clouds, determining which came first and to what extent is difficult.

3

Light Detection and Ranging

Throughout the course of this thesis, data obtained from the troposphere lidar system at ALOMAR and the Cloud-Aerosol Lidar with Orthogonal Polarization (CALIOP) lidar onboard the NASA-satellite CALIPSO will be used. This chapter contains theory about lidar instruments in general as well as the specific instruments used in the thesis.

There is a general consensus that lidar is the best suited instrumentation for remote sensing of cirrus clouds (Sassen *et al.* , 2008; Sassen & Mace, 2002). ALOMAR is located within the Arctic region and has a well-developed infrastructure. This makes it ideally suited for long-term research on clouds in the Arctic region.

The CALIPSO-satellite is equipped with, among other instruments, a polarization-sensitive lidar, CALIOP (Winker *et al.* , 2003). The satellite is intended for cloud and aerosol research, and the data products delivered contain all parameters necessary for comparing local data from ALOMAR with data from a larger geographical region in the Arctic area.

3.1 Lidar Theory

For measuring cirrus cloud altitudes, lidar is considered the best instrumentation available for remote sensing (Sassen & Mace, 2002). Lidars can be utilized both as ground-based instruments, and also onboard airplanes (Lampert, 2010) or satellites (Winker *et al.* , 2003).

In addition, both lidar systems used for this thesis are so-called polarization-sensitive lidars. This allows for extractions of more parameters and eventually microphysical properties of cirrus clouds (Sassen & Benson, 2001).

3.1.1 The Lidar Principle

In remote sensing there are two main families of instruments; passive and active remote sensing instruments. Lidars are among the active remote sensing instruments, which means that they both transmit and receive signals to and from the measuring volume. The same principle is applied in for instance radar theory.

Lidar stands for Light Detection and Ranging, which describes the process in an accurate manor. Light pulses are transmitted into the measuring volume and the returned backscatter is detected by the detection system (Wandinger, 2005a). In todays lidar systems, lasers are used as transmitters, but in theory any light source can be utilized.

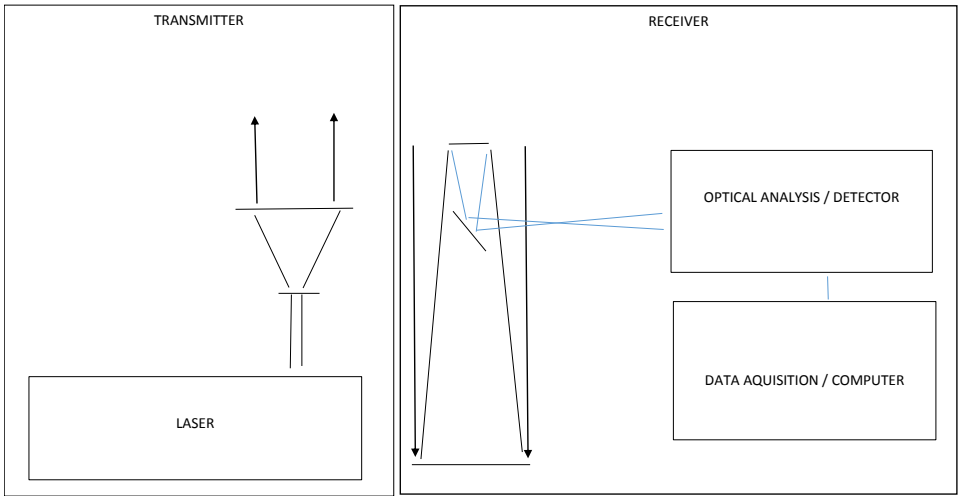

Figure 3.1: Basic lidar setup showing the components featured in most lidar systems today. In most cases each system is adapted to the desired science and specific location of the system.

The basic setup of a lidar-system is illustrated in figure 3.1 (Wandinger, 2005a). The system contains a transmitter and a receiver part, as previously described. All systems currently in operation use one or more lasers for transmitters. The laser properties are adapted depending on the scientific requirements. The systems also require some transmitter optics, such as beam expanders and guiding mirrors to direct the beam into the measurement volume.

Lasers used in lidar systems are often pointed horizontally, and the beam is guided into the atmosphere by use of mirrors. This will ensure a more precise alignment of the beam, as the laser itself can be altered due to for example temperature changes. By using steerable mirrors, the beam can always be found within the telescopes field of view.

The receiver system consists of a telescope with the desired size. Depending on the altitude one wishes to investigate, the telescope size is determined. From the telescope, the returned photons are focused into fiber optical cables and transported to the detection-part of the system. The design of such detectors is individual for each system depending on requirements. From the detectors, the resulting signal is recorded using the data acquisition part of the system, usually consisting of one or more computers and hard drives.

3.1.2 The Lidar Equation

The lidar equation describes the detected signal as a function of atmospheric and system-dependent parameters. The basic form of the equation is given in equation 3.1 (Wandinger, 2005a).

$$P(R) = KG(R)\beta(R)T(R) \tag{3.1}$$

where

$P(R)$ is the received power

K is the system factor

$G(R)$ is the range-dependent measurement geometry

$\beta(R)$ is the backscatter coefficient

$T(R)$ is the transmission term / absorption term

The system factor and the geometry of the measurement field is determined by the lidar-system itself and all the information about the atmosphere is contained in the last two terms.

The system factor K depends on system design, and is therefore known and controllable (Wandinger, 2005a). A general description for such a factor is given in equation 3.2

$$K = P_0 \frac{c\tau}{2} A\eta \tag{3.2}$$

where

P_0 is the averaged transmitted power

c is the speed of light

τ is the pulse length in time

A is the effective detection area of the system

η is the system efficiency

The efficiency-parameter in this term will account for the properties of all the optical components within the system.

The geometrical factor is written as

$$G(R) = \frac{O(R)}{R^2} \tag{3.3}$$

where

$O(R)$ is the overlap function between the laser beam and the telescopes field of view

R^2 accounts for the scattering geometry of the measurement region, which is formed as part of a sphere.

The third term in the equation, called the backscatter term contains information about the atmospheres capability to scatter the signal back in a 180^o direction (Wandinger, 2005a). It depends on both range and wavelength of the transmitted light and for atmospheric measurements it can be divided into the contribution from molecular and aerosol scattering.

The transmission term accounts for the part of the signal that is lost in the scattering process (Wandinger, 2005a). Also this parameter can be divided into contributions from various particle types, and it is also divided into absorbed and scattered light. Signal lost through scattering accounts for photons scattered in any other direction than backward. The transmission term is expressed as equation 3.4:

$$T(R,\lambda) = \exp\left[-2\int_0^R \alpha(r,\lambda)dr\right] \tag{3.4}$$

where

α is the extinction coefficient

λ is the transmitted wavelength

and the factor 2 accounts for two-way ray path. This gives the following form to the lidar equation (Wandinger, 2005a):

$$P(R,\lambda) = P_0\frac{c\tau}{2}A\eta\frac{O(R)}{R^2}\beta(R,\lambda)\exp\left[-2\int_0^R \alpha(r,\lambda)dr\right] \tag{3.5}$$

3.1.3 Scattering Mechanisms

There are different scattering mechanisms for light and some of these have given rise to various lidar techniques (Wandinger, 2005a). The most common ones will be presented here.

The scattering mechanisms are

- Elastic-backscatter
- Inelastic (Raman) scattering
- Differential-absorption
- Resonance fluorescence

The elastic backscatter lidar is based in Rayleigh- and Aerosol or Mie scattering (Wandinger, 2005a). This technique is the most basic lidar technique, and such systems emit and detect the same wavelength, thus looking at backscatter with unaltered frequency.

Rayleigh scattering is scattering from particles with small size compared to the emitted wavelength (Young, 1982). This is the scattering mechanism which accounts for the blue sky due to scattering of sunlight and has been known since lord Rayleigh named it in the 19th century. A clean atmosphere with no aerosols or clouds can be modeled by Rayleigh scattering.

Aerosol scattering accounts for scattering of any particle size and shape, but is most commonly used to describe large particles of the same or larger size than the emitted wavelength (Wandinger, 2005a). The Mie-approximation of aerosol scattering is adapted for spherical particles such as rain droplets, of a large size compared to the wavelength. For small particles, the shape is irrelevant.

Raman scattering is inelastic scattering based on energy change in molecules (Wandinger, 2005a,b). Applying this to lidar measurements allow for example for temperature measurements and monitoring water vapor. By detecting backscattered photons with up- or downshifted frequencies, the Raman signal can be calculated. In both the troposphere lidar and the larger Rayleigh-Mie-Raman (RMR)-system at ALOMAR, all three scattering mechanisms listed above are used (Frioud *et al.* , 2006; von Zahn *et al.* , 2000)

Differential absorption is based on absorption properties for the studied constituents in the atmosphere (Wandinger, 2005a). The Differential Absorption Lidar (DIAL) technique is used at ALOMAR for the ozone-lidar (Skatteboe, 1996). The lidar emits two wavelengths, one which is absorbed by the gas and one which remains unaltered. By comparing the backscattering of both wavelengths, the amount of the gas studied can be calculated (Gimmestad, 2005)

Resonance fluorescence lidars rely on the matching of the emitted wavelength and the transition energy in the atoms of the element one wishes to study (Wandinger, 2005a). The lasers must be tuned to the exact wavelength of the constituent investigated (Abo, 2005). However, these lidars make due with a lot less emitted power than for example Rayleigh and Mie lidars, as they receive photons emitted by the gas in the atmosphere, and not the same ones they transmitted. Such lidar systems are present at ALOMAR, one being the Weber-Sodium lidar (Skatteboe, 1996).

3.1.4 Polarization Lidar

For researching microphysical properties of cirrus clouds, using a polarization-sensitive lidar is one of the best methods (Sassen *et al.* , 2008). The properties of the transmitted laser pulses are known, among them the polarization of the light. In pulsed lasers, which are used in many lidar systems, the light has a

natural linear polarization (Sassen, 2005).

When looking at depolarization in the backscattered signal, two detection channels are required for the same wavelength. One channel looking at polarizations parallel to the transmitted light and one looking at orthogonal polarization (Sassen, 2005). By comparing the two channels, and calculating the ratio of them, the amount of depolarization caused by the atmosphere is found. This can give important information about the particle size, shape and orientation (Sassen & Benson, 2001).

For both systems used in this thesis, the lidars have depolarization channels for the 532 nm wavelength channels (Frioud *et al.* , 2006; Winker *et al.* , 2003). As previously stated, the Troposphere lidar at ALOMAR is not yet verified with respect to this parameter. For future research, this system can be used to disclose microphysical properties of cirrus clouds at Arctic latitudes.

3.2 ALOMAR

The ALOMAR observatory is located on top of the mountain Ramnan, 379 meters above sea level. It was founded in 1994 as a result of international cooperation within the scientific community (Skatteboe, 1996). Originally, the observatory was equipped to investigate the atmosphere between 10 and 100 km. In 2005, the troposphere lidar system was set in operation (Frioud *et al.* , 2006). This expanded the observatories lidar range of operation to cover the entire atmosphere, from the mountain top to above100 km altitude (Skatteboe, 1996; Frioud *et al.* , 2006).

The main purposes of the observatory when founded were exploration of the Arctic atmosphere, the middle atmosphere and conducting trend measurements of atmospheric parameters (Skatteboe, 1996). The Arctic atmosphere is unique with respect to existing state of the climate and its sensitivity to changes. The Arctic region is less investigated, and the location of ALOMAR within this region with an already established infrastructure gives unique possibilities for studies here.

The middle atmosphere was originally the goal of the investigation, as is indicated in the observatory's acronym. This region of the atmosphere is less understood and harder to access than the lower atmosphere (von Zahn *et al.* , 2000). Rockets are expensive and only offer short-term in-situ measurements, and satellites are impaired by the higher layers in the atmosphere. The often-used radar instrumentation is unable to measure in the stratosphere.

3.2.1 The Troposphere Lidar at ALOMAR

The troposphere lidar at ALOMAR was initially a cooperation between Andøya Space Center and the University of Oslo. Currently, the instrument is fully owned by ASC. The scientific goals of the system include the exploration of Arctic cirrus clouds, along with tropospheric aerosols and air-trajectories (Frioud *et al.* , 2006).

The lidar system has close resemblance to the larger Rayleigh-Mie-Raman (RMR) lidar system at ALOMAR (von Zahn *et al.* , 2000). The transmitter is a Neodymium-Doped Yttrium Aluminium Garnet (Nd:YAG) laser emitting infrared light at 1064 nm along with the lasers second and third harmonics, 532 and 355 nm (Frioud *et al.* , 2006). The emitted second harmonic is linearly polarized, thus the system is a depolarization-lidar system. Specifications of the transmitter is found in table 3.1:

Table 3.1: Transmission system of the tropospheric lidar system at ALOMAR.

	Transmitter
Laser	Seeded Nd:Yag Quanta Ray
Wavelengths	1064, 532 and 355 nm
Polarization	Linear polarization
Laser Energy	1020 mJ
Repetition rate	30 Hz
Pulse energies	610, 290 and 120 mJ, respectively
Beam divergence	400 μrad

The receiver system is a Newtonian telescope with a parabolic primary mirror (Frioud *et al.* , 2006). The focal box and detection units are divided into several wavelength channels, allowing for maximum information. Signals are detected both analogue and digitally. Analog channels have 12 bit digital resolution and 7.5 meters height resolution. The photomultipliers and Avalanche Photodiodes (APDs) has a 250 MHz count rate.

Table 3.2: Detection system of the tropospheric lidar system at ALOMAR.

	Detectors
1064 o nm	Non-polarized, detected by APD
532 p nm	Parallel polarization, deteceted by photomultiplier
532 s nm	Cross-parallel polarization, deteceted by photomultiplier
387 o nm	Non-polarized, detected by photomulitplier. Raman-channel
355 o nm	Non-polarized, detected by photomultiplier

The system previously had detection channels for 607 nm backscattered light,

used for Raman scattering. This channel has been removed during the last maintenance period and will not be used for future measurements due to low signal quality (Michael Gausa, private communication, 2015).

As the system is meant to investigate depolarization properties, the system is tilted 3^o off-zenith for routine measurements (Michael Gausa, private communication, 2015). This is in accordance with procedures at other facilities researching cirrus clouds (Sassen & Benson, 2001).

3.3 The Cloud-Aerosol Lidar and Infrared Pathfinder Satellite Observation Mission

In 2006, NASA launched the CALIPSO satellite. The satellite carries along a lidar and two passive instruments for infrared and visible imaging (Winker *et al.* , 2003). The satellite was launched to aid in measuring and modeling climate changes due to aerosol and cloud effects. Compared to greenhouse gases, these effects are harder to quantify and therefore requires more attention.

Aerosols are known to have both direct and indirect effects on temperature in the atmosphere (Winker *et al.* , 2003). They will directly influence the earths radiation budget through scattering and trapping of radiation from the Sun and the Earth. In addition, they provide condensation nuclei for clouds and affect cloud properties, which in turn affects the climate.

Clouds are one of the dominant feedback processes in temperature alterations in the atmosphere (Winker *et al.* , 2003). Estimating the amount of heating or cooling produced by clouds is therefore crucial to improve models. In addition, different microphysical properties of clouds will alter their effect on the climate.

The satellite delivers global datasets of aerosol and cloud profiles derived from lidar data. Combining this with data from passive instruments onboard gives a more extensive dataset with several additional parameters. In addition the satellite flies in the "A-train" constellation, which allows for several other instruments to be applied to the science. Orbiting sun-synchronously, the satellite covers the entire globe between 82^oS and 82^oN (Winker *et al.* , 2003).

3.3.1 The CALIOP Lidar

The lidar onboard CALIPSO is a polarization sensitive lidar emitting two wavelengths (Winker *et al.* , 2003). It is the first polarization-sensitive lidar in orbit to provide long-term measurements. The specifications of the CALIOP lidar are found in table 3.3. For laser safety in the atmosphere, the laser footprint size is chosen to be rather small.

Table 3.3: Specifications of the CALIOP lidar

CALIOP	
Wavelength	532, 1064 nm
Polarization	532 nm linearly polarized
Laser energy	110 mJ
Repetition rate	20,16 Hz
Pulse length	20 ns
Footprint diameter	70 m
Receiver Field of View	90 m
Footprint spacing	335 m

4

Macrophysical Properties of Arctic Cirrus Clouds

This chapter contains the macrophysical properties of cirrus clouds in the Arctic derived from measurements by the lidar system at ALOMAR and the satellite CALIPSO. Section 4.1 contains information about the dataset and method of analysis used for the ALOMAR data. Section 4.2 contains results from ALOMAR. In section 4.3, the properties of the CALIPSO dataset is presented along with the obtained results in section 4.4.

All the results are presented in monthly means and standard deviations. The data is illustrated with tables and plots.

4.1 ALOMAR data

In this section, the data from the ALOMAR troposphere lidar is presented, along with a description of the dataset and methods applied in analysis.

Figure 4.1: The ALOMAR Observatory Location in Northern Norway. The observatory is located on $69,3^oN, 16.0^oE$.

4.1.1 Dataset

The troposphere lidar at ALOMAR has been in operation since 2005. The first 18 months were used for testing and adapting the system, and therefore only data from 2007-2013 is used for this thesis. The instrument has later been undergoing major maintenance since April 2013 and is expected to be back in operation from 2016.

In total, the dataset contains 313 measurements of satisfying quality and duration for cirrus cloud research. Cases where cirrus clouds have been visually identified, but MATLAB has been unable to detect cloud base are excluded from the investigation. This only occurred in measurements of poor quality.

4.1.2 Method of Analysis

For the years 2007-2009, height and temperature are used as criterions to determine the presence of cirrus clouds. The height interval where cirrus

clouds are expected to occur in the Arctic region is said to lie within 4-12 km.

The temperature data is obtained from radiosonde measurements released from Bodø, approximately 240 km away [1]. Temperature can be assumed to be relatively stable over long distances (Noel *et al.* , 2006), and the radiosonde measurements are therefore used. For future research using data from ALOMAR, there is a new radiosonde station at Andenes about 5 km away from the observatory.

For every measurement, intensity-profiles of backscattering are plotted and compared to the cirrus cloud heights retrieved by the analysis software. Cases where the temperature at cloud-top is above -20^oC are classified as non-cirrus clouds. This temperature limit allows for both heterogeneous and homogeneous freezing of cirrus ice crystals.

For the years 2010-2013, the depolarization ratio is also applied as a criterion for cirrus clouds. As the ALOMAR troposphere lidar is permanently tilted 3 degrees off-zenith during measurements, only spherical particles like water droplets can be assumed to give low depolarization values (Sassen & Benson, 2001).

Manual screening of time-height plots containing color-coded depolarization ratios is used to find valid cirrus cloud regions for this period. This eliminates possible water-phase clouds to be misclassified as cirrus. The same procedure has been used by for example Sassen & Benson (2001).

The geometrical properties of cirrus clouds from 2010-2013 at ALOMAR was briefly investigated during the preliminary project study conducted in the spring of 2015. The results from this study are attached in Appendix C. All results presented in this chapter contain data from the entire dataset from June 2007-April 2013.

4.1.3 Data Corrections

Data analysis of lidar data requires certain corrections before-hand. These are applied to all lidar-datasets, but some of the steps vary depending on the system design.

1. The distance is measured using Google Maps. Print screen of the map with distance measurement is found in Appendix D.

Deadtime correction

The lidar-system at ALOMAR has dual reception for all wavelengths, as the backscatter is recorded by an analog and a photon count channel to cover both near and far-range. The analog channel has no deadtime-correction, but for the photon count channels, the sensors require some corrections.

The devices used for photon count channels are either photomultipliers or APDs. They have a counting frequency limit such that photons entering with too short temporal spacing will be counted as a single photon. This is corrected using the following formula (Mielke, 2005):

$$\text{Signal}_{\text{deadtime-corrected}} = \frac{\text{Signal}_{\text{original}}}{1 - \text{Signal}_{\text{original}} \times \text{deadtime}} \tag{4.1}$$

For the ALOMAR-system, the deadtime-factor is set to 0.004 ns, as provided by the manufacturer (Mielke, 2005).

Background subtraction

Despite narrow filters in the detection system, background light will be present in the data recordings. There are different methods for eliminating the background from a lidar signal. In this case, it is estimated from the highest part of the signal, from where no "true" backscatter is received. The background is estimated for each datafile from each channel, to give the best possible estimate of background at any given time.

Separate measurements of background noise with no laser-light transmitted can also be used. However, the background signal changes with time, and for long-duration measurements, estimating background from each datafile gives a more accurate background.

Different channels will have a varying amount of noise, and time time of day will also affect the background. As ALOMAR is located in the Arctic region, there is daylight around the clock for at least two months every year. During the winter season, one would think that there is less noise. However, moonlight, northern lights and lights from other lidars will disturb the measurements despite the lack of daylight.

Plotting the estimated background as is done in figure 4.2, illustrates how it varies both seasonally and diurnally. Measurements during summer shows a more stable background, as the light conditions don’t change much. During

winter, the background changes with time of day, but is not necessarily less than the summer season.

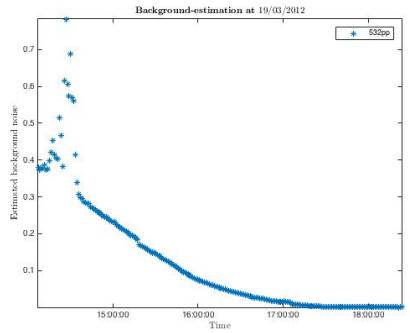

(a) Background estimate from March 19th 2012

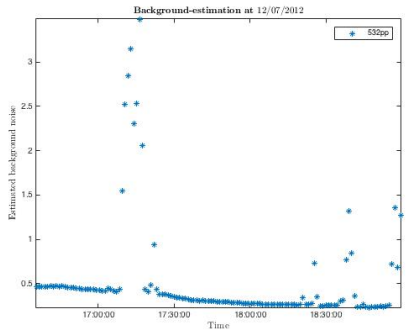

(b) Background estimate from July 12th 2012

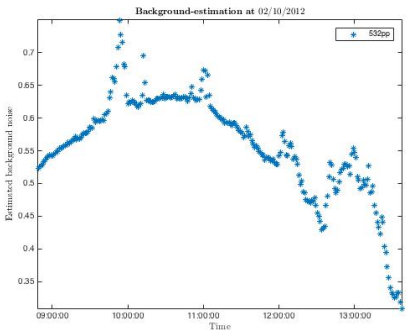

(c) Background estimate from October 2nd 2012

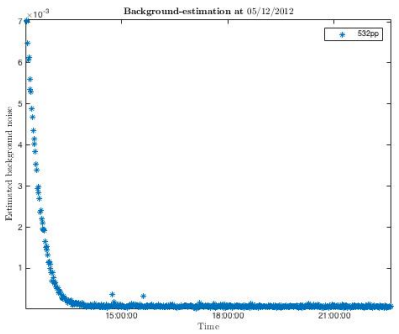

(d) Background estimate from December 6th 2012

Figure 4.2: The figure shows background estimates from all four seasons. The background shows a clear variation with time of day as well as season. In March, the background decreases as late evening approaches. In July, the background is more stable. In October, the background grows from the morning, before decreasing as afternoon approaches. In December, the background has a sharp peak around mid-day before it decreases rapidly (The figure is reproduced from Hanssen (2015))

Range correction

A monostatic lidar system has a telescope with a limited field of view and the laser beam is emitted within that field. When the beam hits particles in the atmosphere, it undergoes volume scattering. Only parts of that scattering is directed back to the telescope and detected. To correct for the scattering geometry limitations, the following formula is applied to the signal

$$\text{Signal}_{\text{corrected}} = \text{Signal} \times \text{range}^2 \tag{4.2}$$

The range is found by multiplying the bin number with its height resolution, which for the ALOMAR system is 7,5 meters / bin.

Figure 4.3 is reproduced from Wandinger (2005a) and shows the scattering geometry for a monostatic lidar system. Both systems used in this thesis are approximately monostatic.

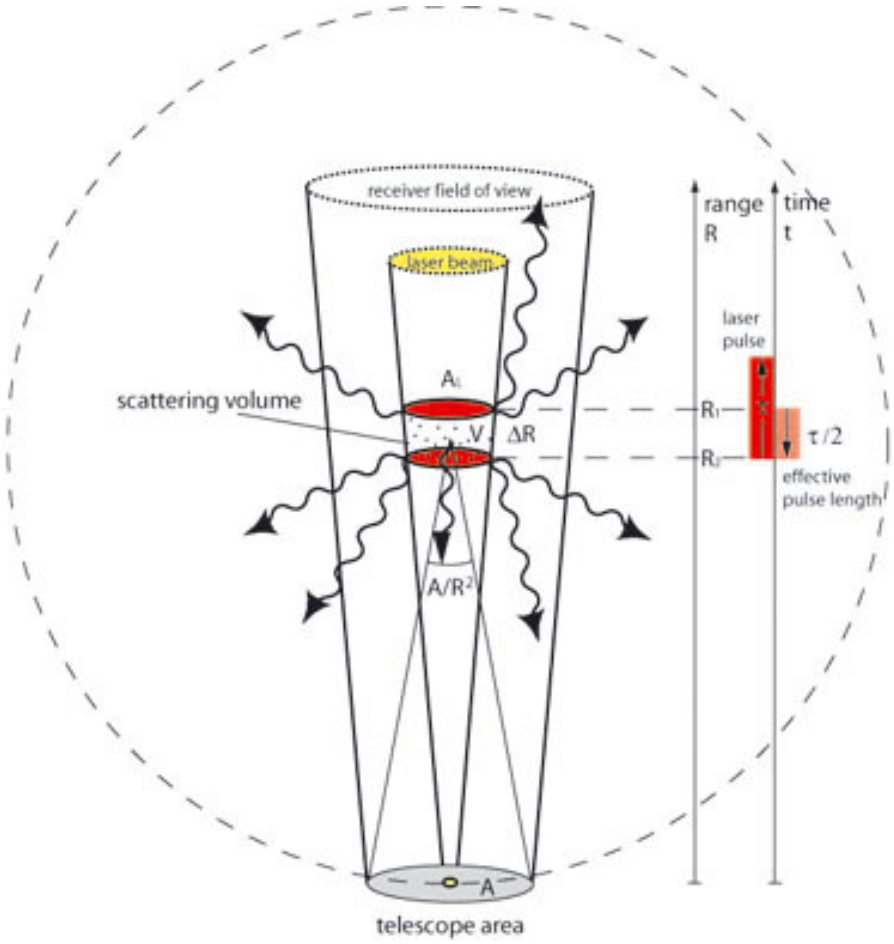

Figure 4.3: Scattering geometry for a lidar system. The figure is reproduced from Wandinger (2005a)

Time averaging

The final step before analysis is conducted, is averaging over time. Each datafile from ALOMAR consists of 2000 laser shots, and have a duration of 66 seconds. To obtain smoother profiles for easing the cloud detection, the files are averaged over a given time period.

The software used for analysis in this thesis is designed so that the averaging period can easily be adapted from day to day. Most of the cases from 2010-2013 are averaged over 11 minutes / 10 datafiles. For 2007-2009, most cases are averaged over 5.5 minutes / 6 files. Some measurements are averaged over shorter periods due to short measurement durations.

4.1.4 Software

The software used for analysis of the data is a combination of ALOMAR-supplied and self-written MATLAB-code. The file structure in datafiles from the troposphere lidar is complex, and software exists to load data from measurement files into MATLAB. Software for data corrections and analysis is written by the author.

Plots used for manual screening of depolarization ratios are delivered by the ALOMAR lidar staff. The plots are also available online for public inspection [2].

Figure 4.3 shows an example of an intensity plot for the 532 nm parallel channel after all data corrections have been applied, as well as the corresponding quickplot.

2. So-called Quickplots from the ALOMAR troposphere lidar are found at the following URL: `http://alomar.andoyaspace.no/tropolidar/Data-Overview.html` (Last checked: October 12th, 2015)

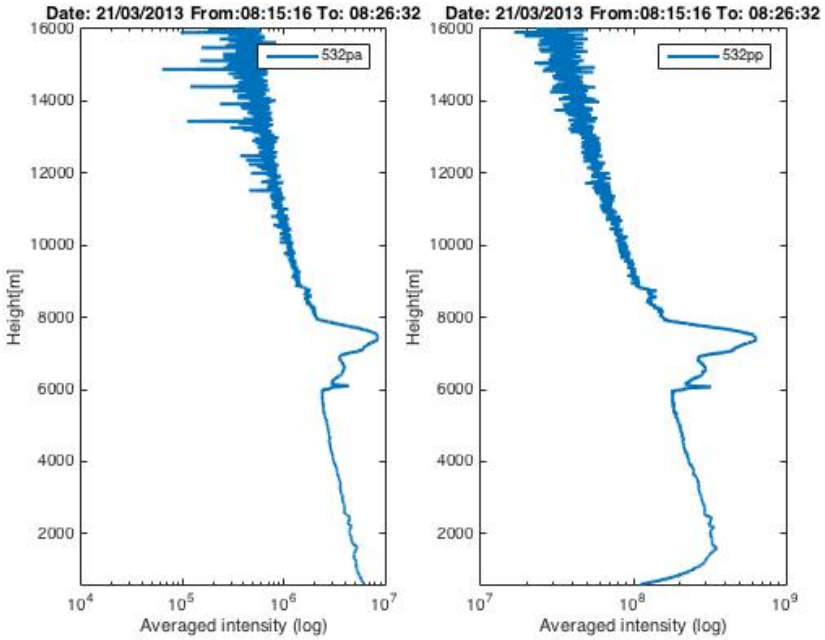

(a) Backscattering intensity profile for the analog (left) and photon count (right) channels of visible light with polarization parallel to the transmitted light (532nm)

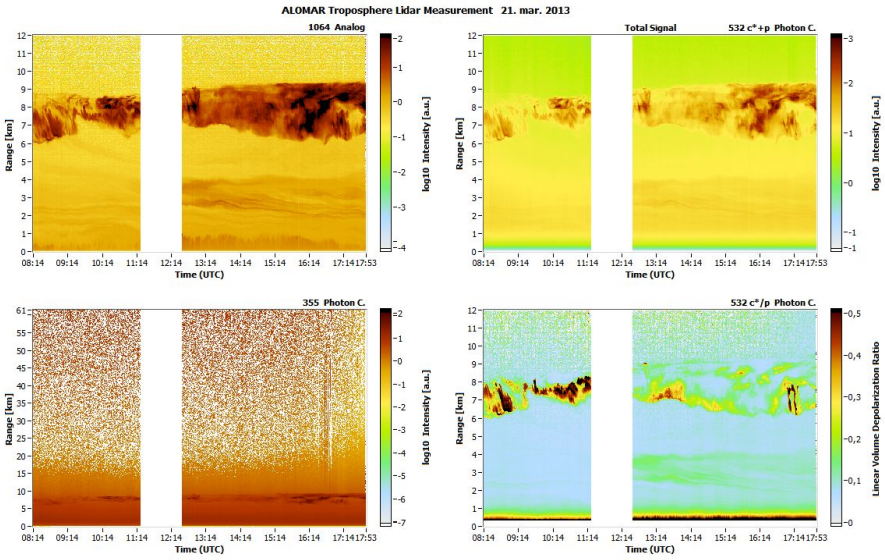

(b) Quickplot corresponding to the above intensity profile

Figure 4.4: Backscattering intensity profile and Quickplot from March 21st 2013. The upper panel shows clear Mie-scattering from approximately 6000-8000 meters, where the cloud is present. The time-height plot in the lower panel shows how the same cloud developed through the measurement.

4.2 Results from ALOMAR

This section presents statistical results obtained from the lidar located at ALOMAR. All statistics from both ALOMAR and CALIPSO are, as previously stated, presented with monthly means. The seasonal statistics for ALOMAR data is available in Appendix A. This is done to ease comparison with results obtained in the project paper (Hanssen, 2015). These results were presented in terms of season, and are available in Appendix C for convenient reference.

Before the macrophysical properties of the clouds are presented, the measurement distribution is shown in figure 4.5a. The figure shows that there is a minimum of measurements in September, and in general the coverage of the fall season is low compared to the rest of the year.

The reason for the low measurement number appears to be caused by weather conditions limiting measurements. Inspection of the maintenance schedule for the system reveals for the most cases even distribution of these periods with respect to time of year. It is not uncommon to have unstable weather in Northern Norway during the fall months accompanied by precipitation, preventing measurements.

In figure 4.5b, the cirrus cloud occurrence in ALOMAR data is illustrated. The overall mean is represented by the red line, indicating an overall cirrus occurrence in measurements of 56 %. There is a clear minimum in occurrence in January, with a more even distribution throughout the rest of the year. April, June and September have high numbers of cirrus cases. For September, this could be partly due to the low number of measurements. April and June however, has an average number of measurements and high number of cirrus cases.

Table 4.1 shows the cirrus occurrence in measurements from ALOMAR for the entire period from 2007-2013.

Table 4.1: Monthly occurrence of cirrus clouds in measurements over ALOMAR

Month	Occurence [%]
January	35 %
February	52 %
March	52 %
April	69 %
May	49 %
June	69 %
July	58 %
August	50 %
September	58 %
October	71 %
November	54 %
December	65 %
Overall Mean	56 %

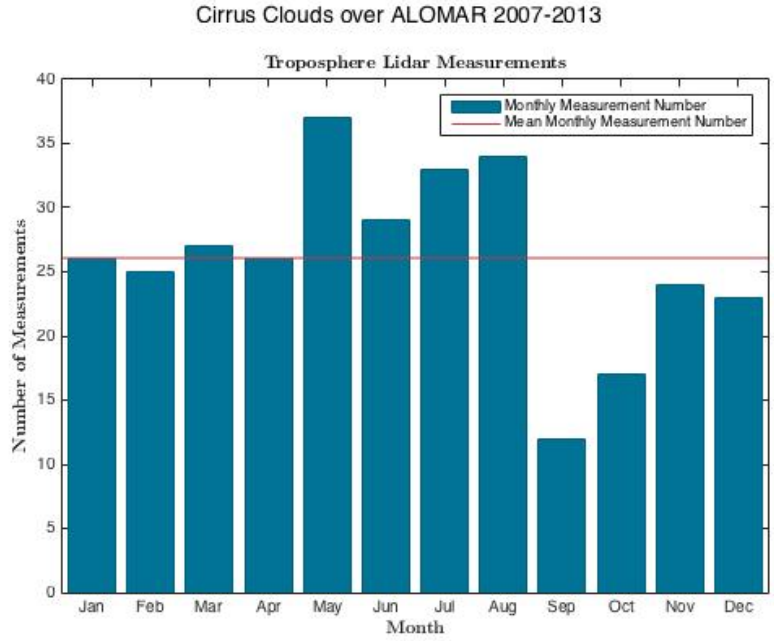

(a) Measurement distribution with respect to month

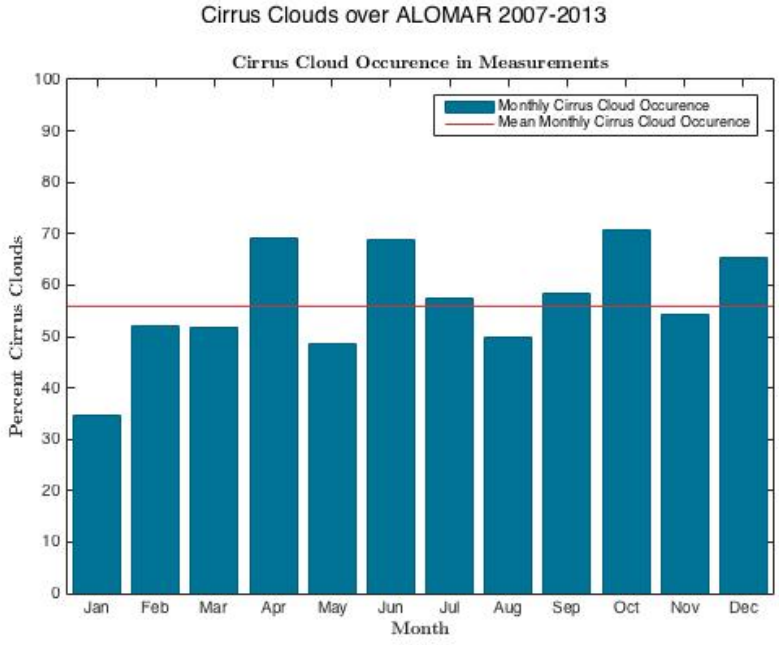

(b) Cirrus cloud occurrence with respect to month

Figure 4.5: Measurement distribution and cirrus clouds occurrence with respect to month. The upper panel shows the distribution of measurements, where the spring and summer months have a clear maximum. The lower panel shows the cirrus occurrence, with maximum in April, June and October and a minimum in January.

4.2.1 Macrophysical Properties

In this section, the macrophysical properties height and thickness of cirrus clouds over ALOMAR is presented. Temperature data for the cloud cases is also presented. This data is obtained from radiosonde measurements released with balloons from Bodø.

Height

Table 4.2 shows the mean base height and standard deviation with respect to month. The overall mean base height is 6647 meters over ALOMAR[3].

The upper panel of figure 4.6 shows the mean base height with respect to month. There is a peak in September, and a minimum in the spring months March and May.

The lower panel of the figure shows the standard deviation of the base height. For most of the months with mean base height above the overall mean, the standard deviation is also increased.

Table 4.2: Monthly mean base height and standard deviation for cirrus clouds over ALOMAR

Month	Base Height [m]	Standard Deviation [m]
January	7076	± 1778
February	6476	±1035
March	5657	±1456
April	6263	±1416
May	5695	±1209
June	6981	±1892
July	6786	±1932
August	7454	±1289
September	9434	±1903
October	6799	±1282
November	6889	±1725
December	5988	±1365
Overall	6647	±1695

3. Note that ALOMAR is located approximately 379 meters above sea-level (Skatteboe, 1996)

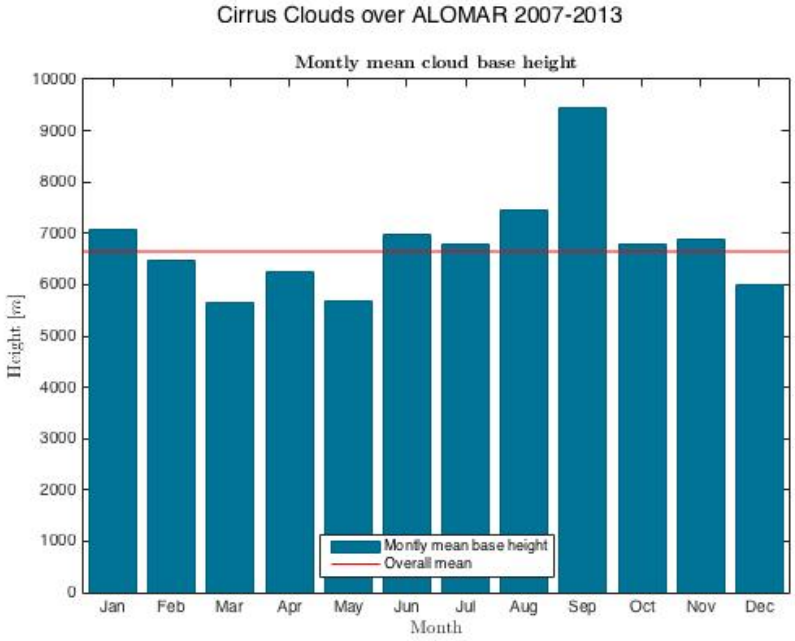

(a) Cirrus cloud base height

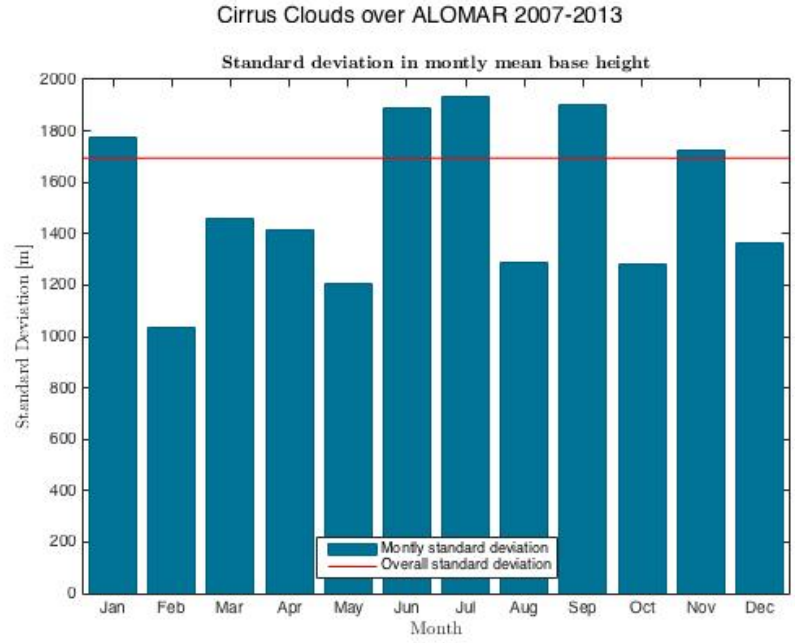

(b) Base height standard deviation

Figure 4.6: The figure shows base height and standard deviation over ALOMAR. The upper panel shows increased base height during summer and fall, and a minimum in the late winter. The standard deviation reaches maximum in the months with highest base height.

Thickness

In table 4.3, the thickness and its standard deviation for cirrus cases over ALOMAR is presented. The overall thickness of these clouds is 1166 ± 726 meters, which is fairly thin.

The same parameter is illustrated in figure 4.7. The upper panel shows that January, July and August have the thinnest clouds. The spring months show increasing thickness, and in the lower panel, it is evident that also the standard deviation increases during these months. The fall season seems to have thicker clouds with a relatively low standard deviation, thus a more stable thickness throughout the season.

Table 4.3: Monthly mean thickness and standard deviation of cirrus clouds above ALOMAR

Month	Thickness [m]	Standard Deviation [m]
January	916	±406
February	1250	±930
March	1146	±723
April	1298	±916
May	1383	±1026
June	1287	±530
July	1067	±560
August	884	±509
September	1358	±624
October	1409	±568
November	1186	±752
December	1389	±778
Overall	1166	±726

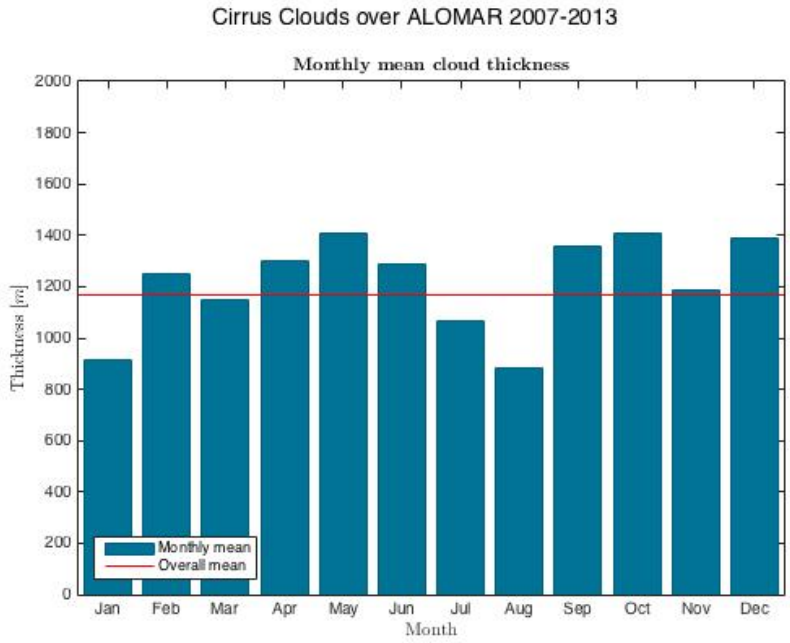

(a) Cirrus cloud thickness

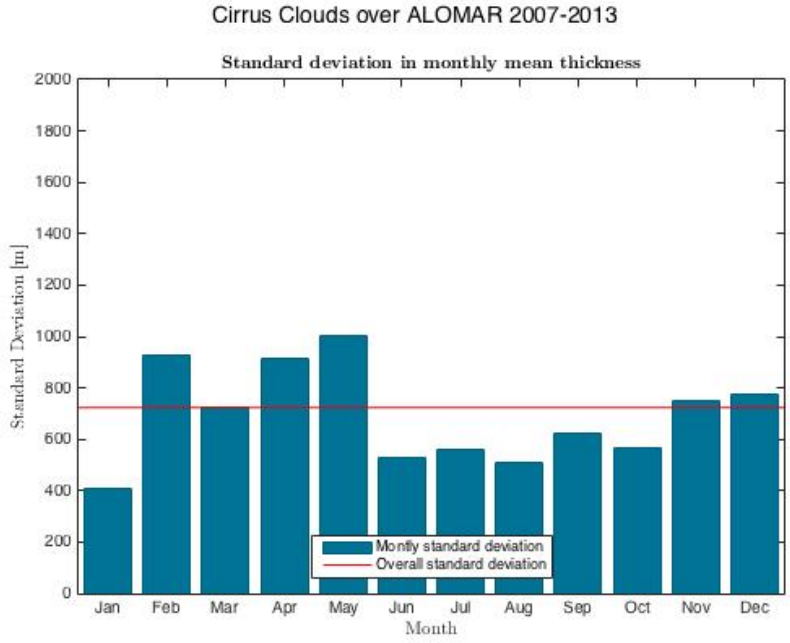

(b) Thickness standard deviation

Figure 4.7: The figure shows cirrus thickness and standard deviation over ALOMAR. The upper panel shows how the thickness is fairly stable throughout the year, with a maximum in spring and fall, and minimum during summer and winter months. The standard deviation shows more variation during spring and more stable clouds during summer and fall.

Temperature

Being ice phase clouds, cirrus are temperature dependent. The entire dataset is screened based on height and temperature, and no clouds with top temperature above -20^oC are classified as cirrus.

Table 4.4 shows the mean top and base height temperatures along with standard deviations. The same parameters are illustrated in figure 4.8. The standard deviation reveals fairly stable temperatures in the region.

Overall, the top cloud temperature is -43 ± 11^oC, which is well below the homogeneous freezing point for water. As expected, the base temperature is slightly higher, with a mean temperature of $-34^oC \pm 11^oC$.

From the figure, it is evident that the temperature rises throughout the summer season, while September has a clear minimum. This is correspondent with the increased mean base height during this month, leading to cirrus clouds in colder regions of the atmosphere. It must therefore not be taken as a measure of troposphere temperature in September as a general, only related to cirrus measurements.

Table 4.4: Monthly cloud temperatures and standard deviation for cirrus clouds above ALOMAR

Month	Top Temperature [^oC]	Standard deviation [^oC]	Base Temperature [^oC]	Standard deviation [^oC]
January	-50	±10	-42	±11
February	-50	±9	-41	±8
March	-47	±8	-37	±10
April	-43	±7	-33	±9
May	-35	±12	-25	±10
June	-38	±10	-29	±12
July	-38	±10	-29	±8
August	-37	±12	-28	±10
September	-52	±12	-47	±11
October	-46	±8	-34	±10
November	-46	±10	-37	±13
December	-48	±11	-36	±9
Overall	-43	±11	-34	±11

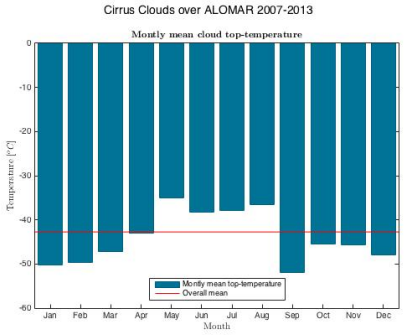

(a) Top cloud temperature has an overall mean of less than -42.75^oC.

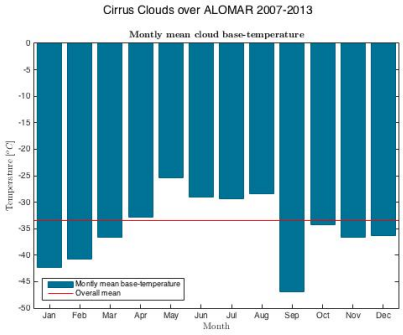

(b) Base cloud temperature has an overall mean of -33.5^oC.

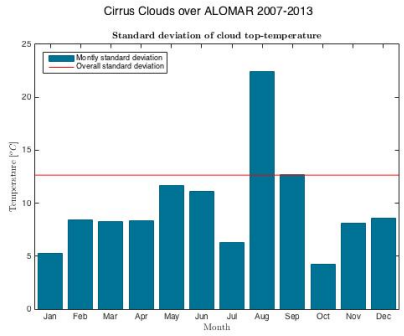

(c) Standard deviation of top-cloud temperature

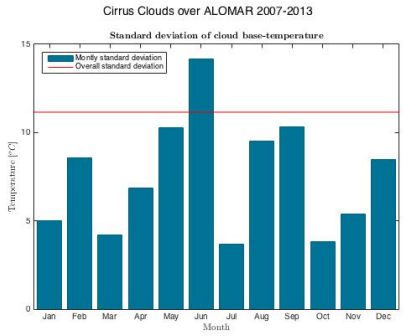

(d) Standard deviation of base-cloud temperature

Figure 4.8: The figure shows temperature at cloud altitudes, measured by radiosondes released over Northern Norway. The upper panels shows the top and base-altitude temperatures for cirrus clouds cases, and the lower panels show the corresponding standard deviation.

4.2.2 The Tropopause over Northern Norway

The tropopause altitude over Northern Norway is calculated from radiosondes released from Bodø on days corresponding to cirrus observations over ALOMAR. The thermal definition of the tropopause is used for calculations. Results are found in table 4.5 and illustrated in figure 4.9.

Table 4.5: Tropopause altitude over Northern Norway estimated from the definition of thermal tropopause altitude

Month	Altitude [m]	Standard Deviation [m]
January	8769	±1267
February	9047	±758
March	8385	±483
April	9095	±1077
May	9276	±1039
June	9849	±660
July	9626	±626
August	10271	±668
September	8851	±939
October	9562	±1517
November	9883	±1637
December	8754	±768
Overall	9578	±1052

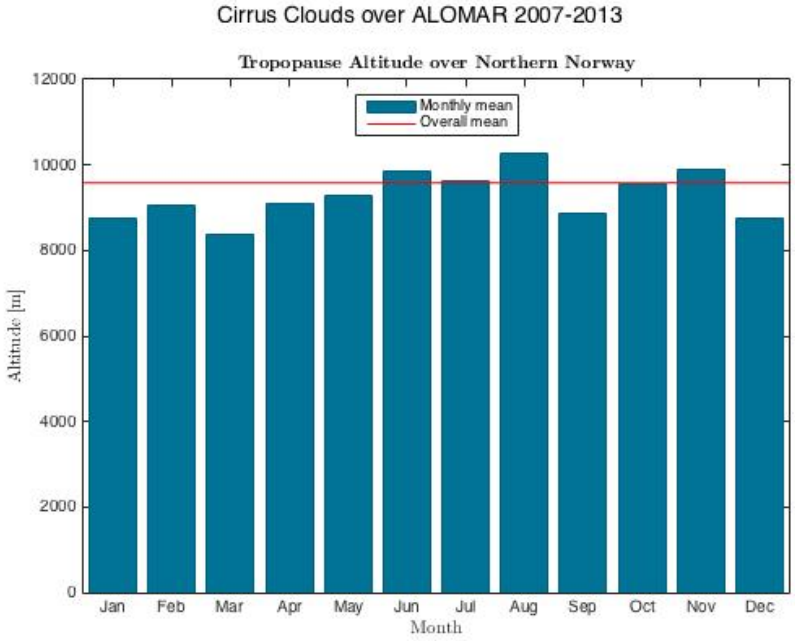

(a) Mean tropopause altitude

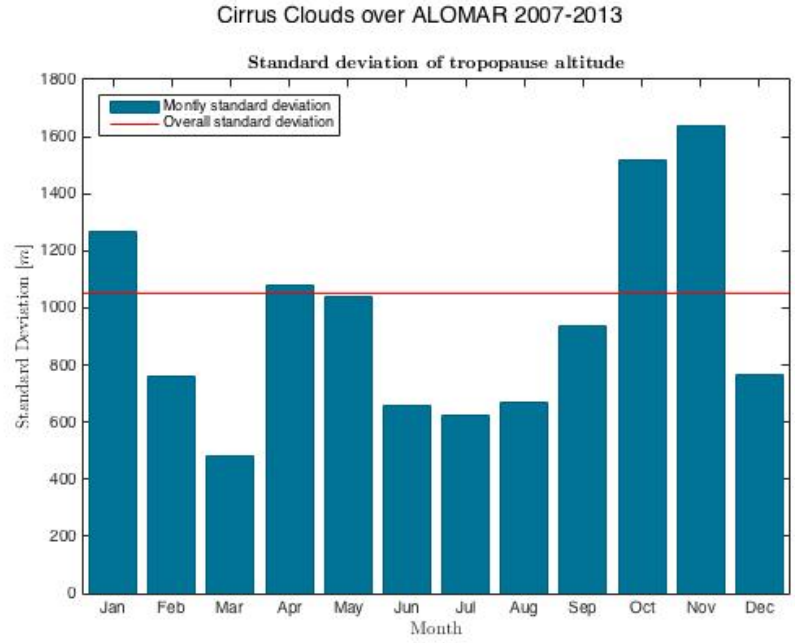

(b) Standard deviation of tropopause altitude

Figure 4.9: Tropopause altitude over Northern Norway. The upper panel shows the monthly mean tropopause altitude, while the lower panel shows the standard deviation. It is evident that the thermal troposphere lies within 8-10 km throughout the year.

4.3 CALIPSO data

Data from the CALIPSO satellite is available for the public through the Langley Research Center (LaRC) (Winker *et al.* , 2003). The global, long-term dataset has already been used in several studies of clouds and aerosols and is considered to be one of a kind with regard to cloud research. There are other satellites planned to carry on the work of CALIPSO, but non have been launched so far.

A typical orbiting pattern for a 24 hour period is plotted in figure 4.10, along with the location of ALOMAR. Over time, the satellite will cover the entire region.

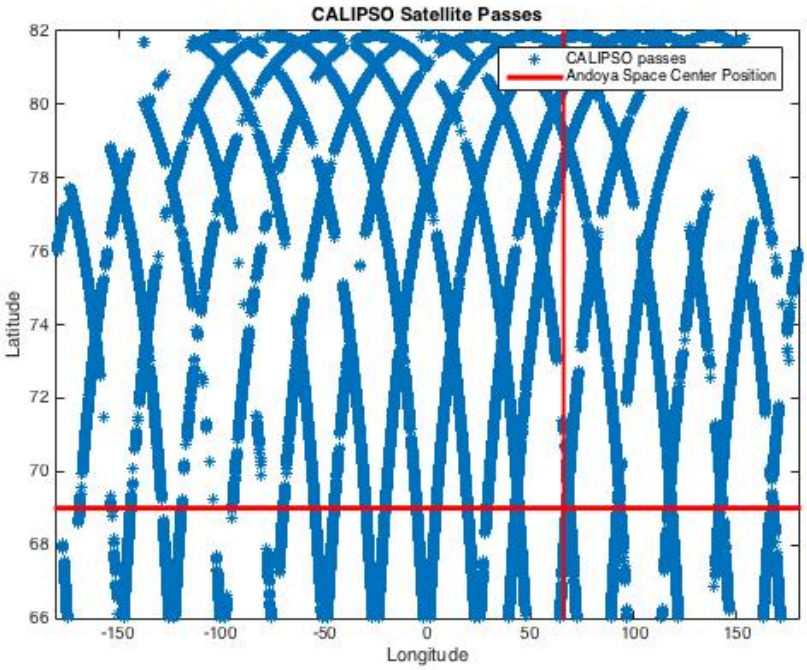

Figure 4.10: CALIPSO passes in the Arctic region during a 24 hour period on July 2nd, 2009. ALOMAR is located where the red lines intersect.

Dataset

Several data products are available from CALIPSO with different degrees of processing performed by LaRC (Winker *et al.* , 2003). For this thesis, the level 2 cloud layer dataset with a 5 km horizontal resolution is used. This dataset includes macrophysical properties such as height and thickness, as well

as optical depth, backscatter profiles, depolarization and ice water content (Powell *et al.* , 2013). Data from 2007-2013 is used to correspond with the time period covered at ALOMAR.

The dataset is screened for Arctic data by use of latitude. In addition, cirrus clouds are determined using the same criterions as the ALOMAR dataset; height is limited between 4 and 12 km, and the top-cloud temperature is not allowed above -20^oC.

The overall occurrence of cirrus clouds in the Arctic region is found to be 48%, as shown in table 4.6. This is slightly less than the ALOMAR dataset, but still more than previous global studies has indicated. The occurrence with respect to month is shown in figure 4.11.

Table 4.6: Monthly cirrus cloud occurrence in the Arctic region as measured by the CALIPSO satellite.

Month	Occurrence
January	49 %
February	44%
March	55%
April	53%
May	45%
June	44%
July	49%
August	50%
September	47%
October	45%
November	47%
December	48%
Overall	48%

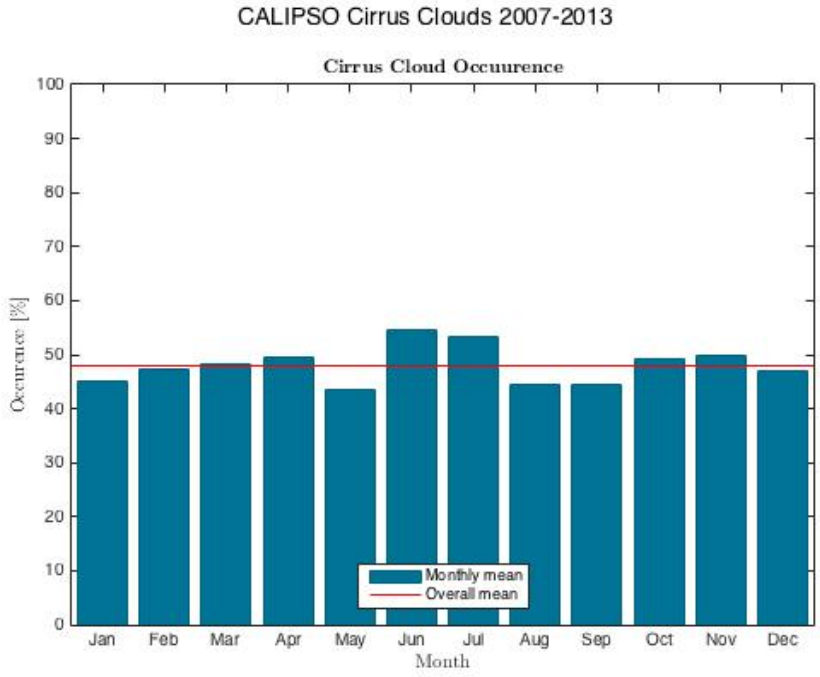

Figure 4.11: Cirrus cloud occurrence measured by CALIPSO. The figure shows a maximum occurrence in January and a minimum in March and April. The occurrence is quite even with small variations.

4.4 Macrophysical Properties

In this section, the macrophysical properties height and thickness of cirrus clouds detected by the CALIPSO satellite is presented, as well as the temperature and tropopause data.

Height

Table 4.7 and figure 4.12 shows the base height and its standard deviation with respect to month. The base height is fairly stable with time, and so is the standard deviation. The maximum base height corresponds to the maximum standard deviation, indicating a larger variation in base height for periods with increased cloud altitude. The overall mean base height is 6665 ± 1525 meters above sea-level.

Table 4.7: Monthly mean base height and standard deviation for cirrus clouds in the Arctic region as measured by the CALIPSO satellite

Month	Base Height [m]	Standard Deviation [m]
January	6572	± 1544
February	6240	± 1400
March	6392	± 1460
April	6394	± 1410
May	6552	± 1445
June	6947	± 1563
July	7210	± 1609
August	7012	± 1671
September	6863	± 1632
October	6600	± 1506
November	6498	± 1481
December	6527	± 1530
Overall	6665	± 1525

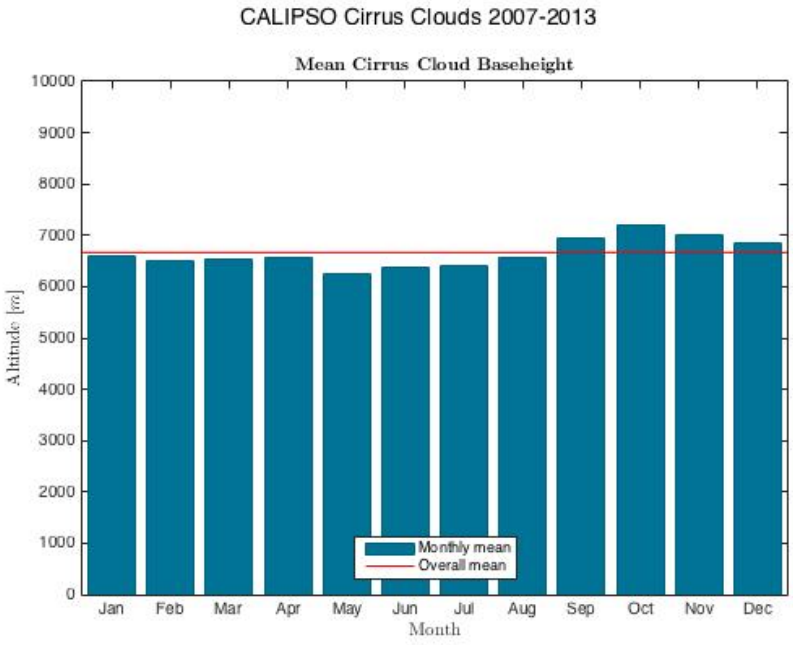

(a) Cirrus cloud base height with respect to month

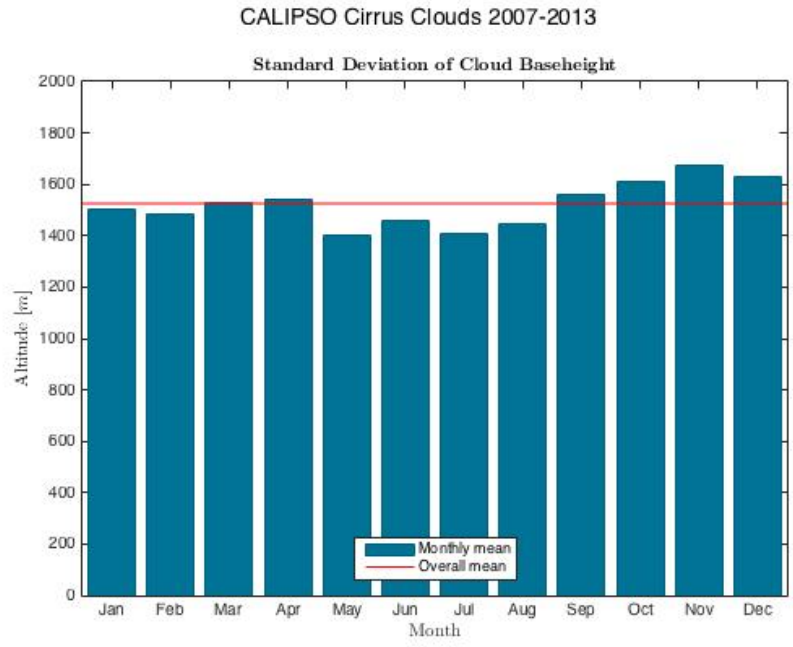

(b) Standard deviation of cirrus cloud base height

Figure 4.12: Cirrus cloud base height measured by CALIPSO. The upper panel shows the mean base height with respect to month. There is a maximum during the spring season, but overall the height is stable. The lower panel shows the standard deviation of the base height, which also has a maximum during spring.

Thickness

The cloud thickness is illustrated in table 4.8 and figure 4.13. The clouds are thickest during the spring season where thickness increases dramatically. The standard deviation follows the same trend as the thickness itself, indicating that thin cirrus during the spring season are less stable than the thicker clouds in the fall. Mean cloud thickness is found to be1464 ± 1122 meters.

Table 4.8: Monthly mean thickness and standard deviation for cirrus clouds in the Arctic region as measured by the CALIPSO satellite

Month	Thickness	Standard Deviation [m]
January	1812	± 1366
February	1490	± 1141
March	1426	± 1104
April	1311	± 1031
May	1189	± 935
June	1204	± 931
July	1257	± 955
August	1314	± 1017
September	1465	± 1119
October	1613	± 1229
November	1689	± 1278
December	1787	± 1355
Overall	1464	± 1122

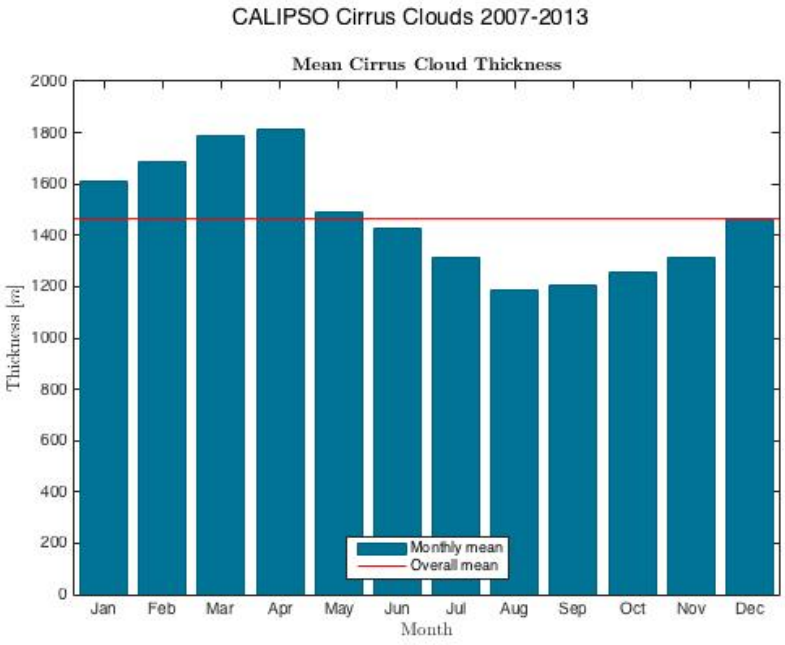

(a) Cirrus cloud thickness with respect to month

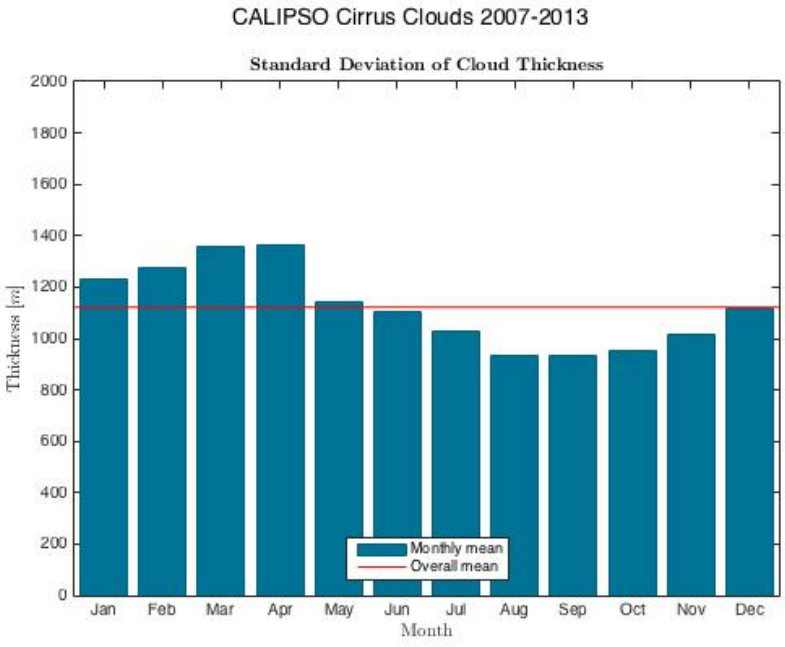

(b) Standard deviation of cirrus cloud thickness

Figure 4.13: Cirrus cloud thickness measured by CALIPSO. The upper panel shows how thickness increases throughout the year toward the fall season. The lower panel shows a similar behavior of the standard deviation.

Temperature

Figure 4.14 shows the temperature of the clouds, both at cloud top and base heights. Their behavior is almost equal, with the top temperature being lower than the base temperature as expected. The standard deviations are also similar, with little variation. The overall mean top-cloud temperature is -49^oC and base-cloud temperature is -38^oC, as can also be seen in table 4.9.

Table 4.9: Monthly cloud temperatures and standard deviation for cirrus clouds in the Arctic region measured by the CALIPSO satellite

Month	Top Temperature [^oC]	Standard deviation [^oC]	Base Temperature [^oC]	Standard deviation [^oC]
January	-58	±9	-47	±10
February	-54	±8	-45	±9
March	-45	±8	-38	±9
April	-50	±8	-42	±9
May	-45	±8	-37	±9
June	-42	±9	-34	±10
July	-41	±10	-23	±10
August	-42	±10	-33	±10
September	-46	±10	-37	±11
October	-51	±8	-29	±10
November	-54	±8	-44	±10
December	-57	±9	-46	±11
Overall	-49	±9	-38	±10

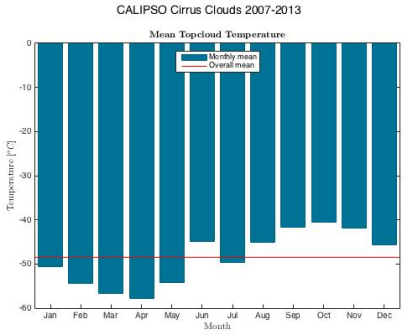

(a) Cirrus cloud top temperature with respect to month

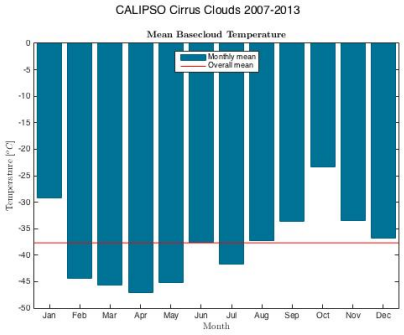

(b) Cirrus cloud base temperature with respect to month

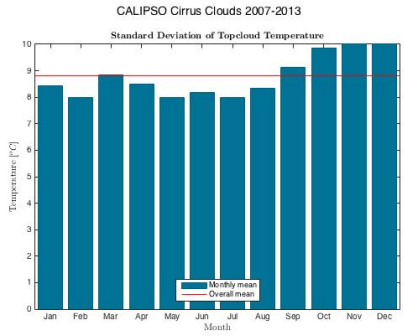

(c) Standard deviation of top-cloud temperature

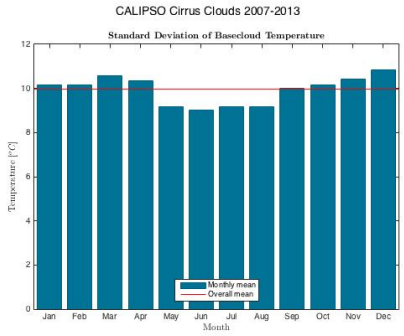

(d) Standard deviation of base-cloud temperature

Figure 4.14: Cirrus cloud temperatures measured by CALIPSO. The upper panels show the temperature at top and base height of the clouds. The lower panel shows the standard deviation of the temperatures.

The Tropopause

The CALIPSO dataset contains information about the tropopause altitude at the location of measurement. This information is extracted for all measurements in the Arctic region containing cirrus clouds.

The local tropopause measured by CALIPSO in terms of monthly mean altitude is presented in table 4.10. It shows that the overall mean tropopause altitude in the Arctic region is found to be approximately 9 km.

In figure 4.15 the monthly heights are presented along with the standard deviation. The measurements show a lower altitude during the summer months, while spring and autumn appears to have a generally higher tropopause.

Table 4.10: Monthly mean tropopause altitude and standard deviation for cirrus clouds in the Arctic region as measured by the CALIPSO satellite

Month	Tropopause Altitude [m]	Standard Deviation [m]
January	9171	± 1086
February	8693	± 1099
March	8760	± 1102
April	8698	± 1034
May	8973	± 950
June	9492	± 987
July	9862	± 963
August	9804	±923
September	9546	± 903
October	9178	± 956
November	9028	± 980
December	9204	± 1100
Overall	9222	± 1004

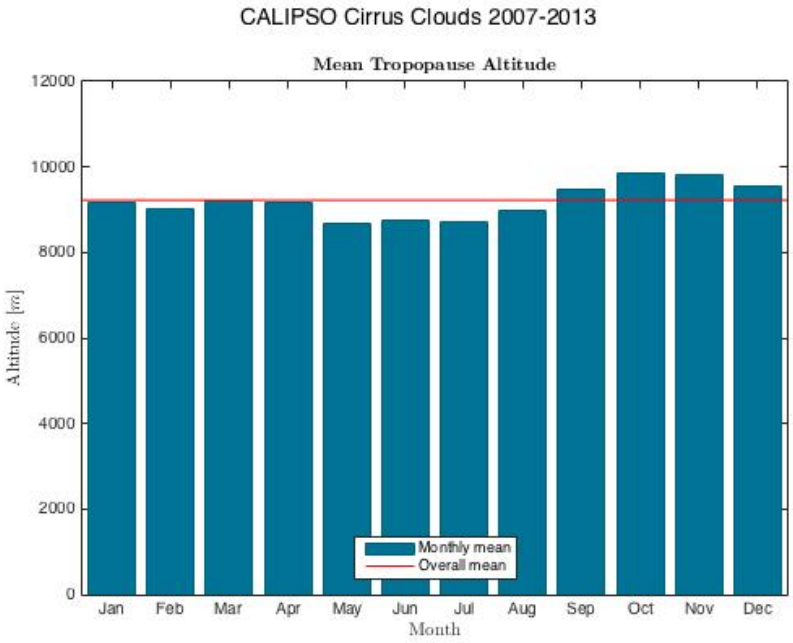

(a) Tropopause altitude with respect to month

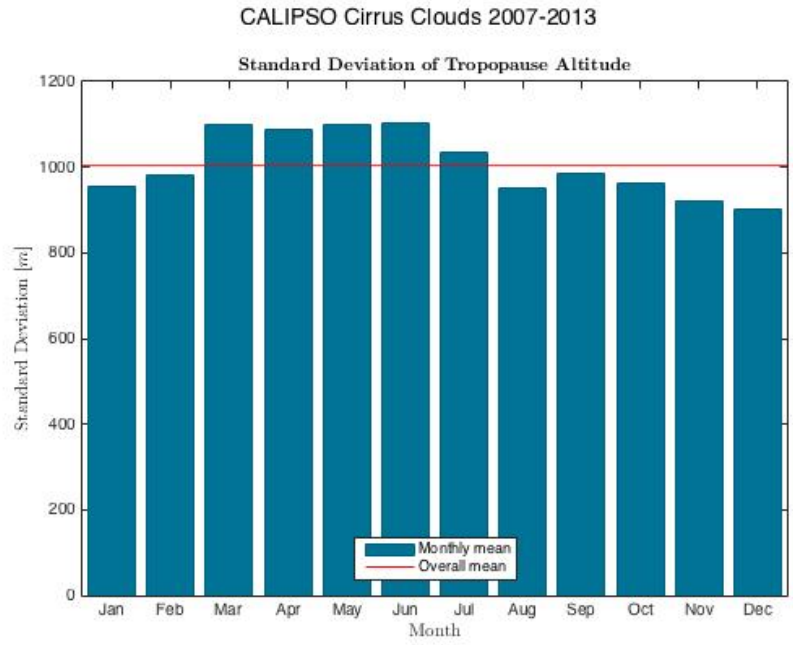

(b) Standard deviation of tropopause altitude

Figure 4.15: Tropopause altitude corresponding to cirrus cloud measurements by CALIPSO. The upper panel shows the tropopause altitude and the lower panel its standard deviation. The maximum tropopause corresponds to the lowest standard deviation, indicating a more stable tropopause height.

/5

Cirrus Clouds in the Arctic Tropopause Region

Several cases of thin cirrus clouds residing in the upper part of the troposphere for long periods of time have been identified by looking at quickplots from ALOMAR. As the mean tropopause altitude in Arctic region is 9 km (Zängl & Hoinka, 2001) which is also supported by the findings in chapter 4, further investigations of cirrus cases at 10-12 km is an interesting study.

One of these cases is shown in figure 5.1. This figure clearly shows a stable cirrus clouds at around 11 km altitude. There are in total 9 cases like this investigated closer throughout this thesis.

Cirrus clouds in the upper troposphere and lower stratosphere are not uncommon, especially when looking at tropical cases during convective events (Sassen, 2002). However, the tropopause cases from ALOMAR are stable and thin clouds, indicating that they are not caused by convective events. One possible answer could be that these are in fact SVC's.

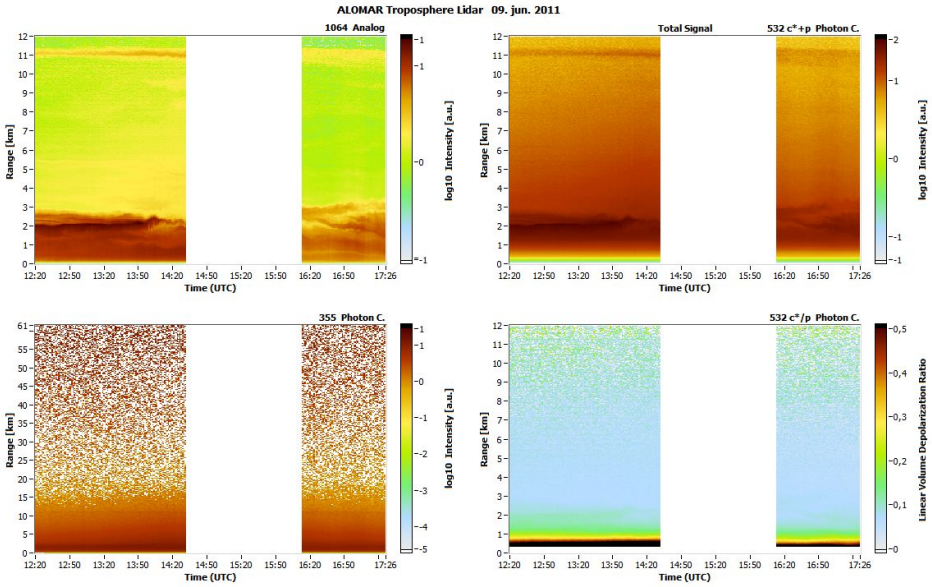

Figure 5.1: Quickplot from ALOMAR June 9th 2011. The figure shows a stable cloud layer at high altitudes in the troposphere, lasting for the entire measurement

5.1 Cases of Near-Tropopause Cirrus Clouds

As previously stated, there is no proven definition of the tropopause altitude which can be used globally and throughout the year. However, 7 of 9 cases investigated here occurs during spring and summer, when the thermal tropopause is assumed more accurate (Zängl & Hoinka, 2001). This definition is therefore applied for these cases.

Plots for all the cases of cloud altitude with temperature and humidity from radiosonde measurements from Bodø are found in Appendix B. The plots have been investigated to identify cases where clouds are located above the thermal tropopause.

- The first case from August 2010 in figure B.1 shows that the cloud altitude is around the thermal tropopause for the entire measurement. As the tropopause definition carries some uncertainty when only using radiosonde measurements, the cloud can be said to be within the tropopause region.

- The second case is from April 2011, shown in figure B.2. In this case, the cloud top never exceeds above the thermal tropopause altitude, and the cloud most likely resides in the troposphere and not the lower strato-

sphere.

- In May 2011, the third case was found. As is seen in figure B.3, the cloud altitude is below the thermal tropopause for this day, but still in the very upper part of the troposphere.

- In June 2011, several cases of high cirrus clouds around the tropopause were identified. The first case from June 9th (Shown in figure 5.2), has cloud altitudes above the thermal tropopause for the entire sounding. The other cases shown in figure B.4 and B.5 are located just below the tropopause.

  As the definitions for where the troposphere ends and the stratosphere begins are unclear, it is too early to conclude whether the case of June 9th 2011 is actually located in the stratosphere or in the tropopause region. This case will be further debated in section 5.2.

- Two cases in October and November 2011 shown in figures B.6 and B.7 were also identified as possible tropopause cirrus clouds. The thermal tropopause is said to be less reliable in polar regions, particularly during the winter season.

  Both these cases show cloud altitudes below the thermal tropopause. When comparing the tropopause altitude calculated here with the relative humidity in the same altitude, the result may seem plausible.

  Relative humidity is an uncertain parameter from radiosondes due to sonde properties, but it also gives an indication of the location of the tropopause (Hoinka, 1999). The relative humidity clearly falls above the thermal tropopause is both cases, which supports the theory that these clouds reside in the upper tropopause.

- The last case investigated was found on April 21st 2012. This case also has cloud altitude just below the thermal tropopause for the entire measurement period.

This leads to the conclusion that only one case requires further attention. Note that these cases are from a subset of the ALOMAR data where quickplots are available. Future research looking at the entire dataset could reveal more cases like the following.

5.2 June 9th 2011

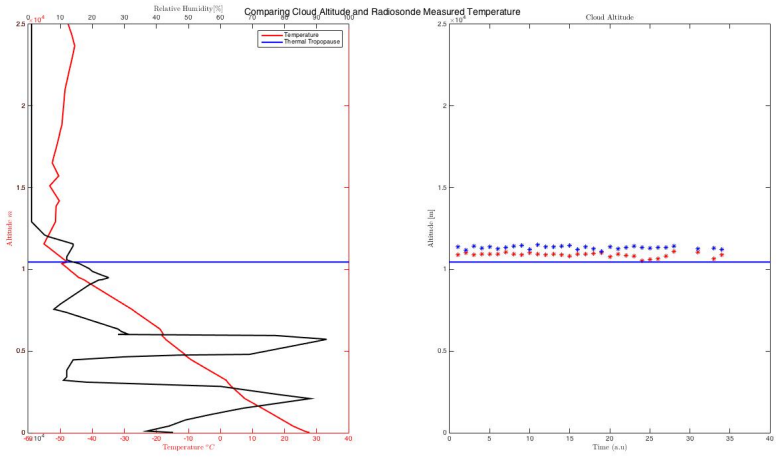

Figure 5.2: Atmospheric variables and cloud altitude from June 9th 2011. The figure shows that the cloud altitude above the thermal tropopause for the entire sounding. Note that the temporal axis is unscaled. Time stamps in UTC is found in figure 5.1

Table 5.1: Cloud properties for June 9th 2011

Property	Value
Mean Base Height	10715 ± 346 meters
Mean Cloud Thickness	603 ± 397 meters
Top cloud temperature	$-48.75^{O}C$
Base cloud temperature	$-52.25^{O}C$
Local Tropopause Altitude	10217 meters

The case of June 9th 2011 shows cloud base above the thermal tropopause for the entire measurement. The measurement lasted for 3,3 hours in total, with a break of about 2 hours in the middle. The radiosonde was released at 12:00 UTC, which in local time is at 13:00, thus during the first part of the measurement.

Looking at the atmospheric variables for this day in figure 5.3, the minimum temperature and minimum relative humidity are also plotted. The cloud height was found close to the thermal tropopause, and lies in the region between thermal tropopause and minimum relative humidity.

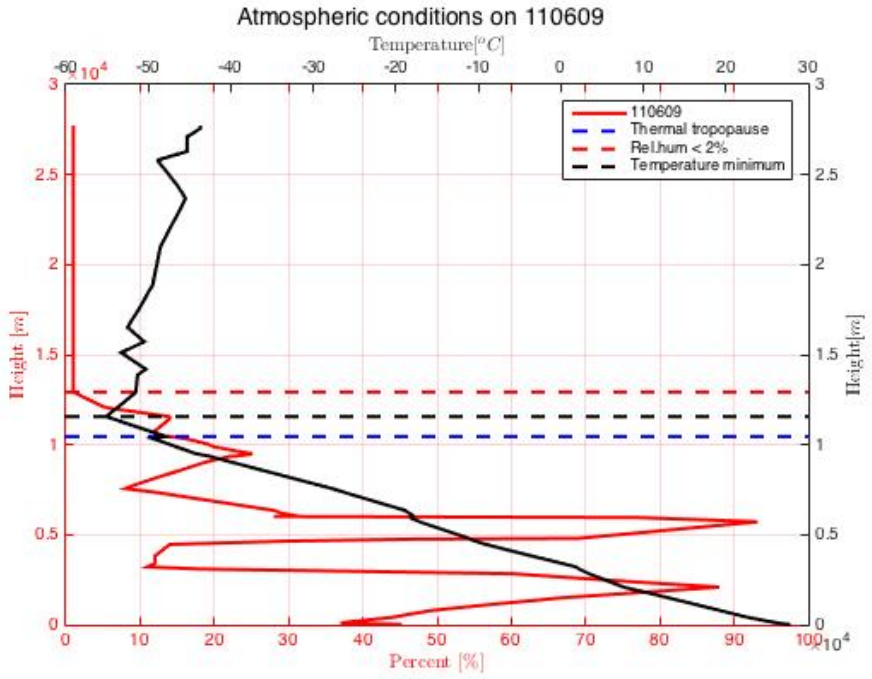

Figure 5.3: Atmospheric variables and cloud altitude from June 9th 2011. The figure shows that the cloud altitude above the thermal tropopause for the entire sounding.

Based on the atmospheric conditions of this day, it is plausible that the cloud is within the tropopause region. It is however not possible to conclude that the cloud is in the stratosphere and not the troposphere.

The case raises interesting questions, and forms the basis of further research. As measurements are about to continue at ALOMAR, it is possible to determine whether this occurs on a regular basis or if the cases found in the sub-dataset from 2010-2013 are unique.

6 Discussion

Comparing results from the geographically limited system at ALOMAR and the widespread measurements from CALIPSO will give an important indication whether the results from Andøya are representative for the entire region. This is important for future research, as campaigns with various instrumentations can be launched from the already established research infrastructure at Andøya Space Center.

Table 6.1 gives a summary of all the properties mapped in chapter 4 for both measurement systems. In the following sections, these properties will be discussed further and compared to previous studies.

Table 6.1: Properties of cirrus clouds in the Arctic Region

Property	ALOMAR	CALIPSO
Occurence	56 %	48 %
Base Height	6647 ± 1695 m	6665 ± 1525 m
Cloud Thickness	1166 ± 726 m	1464 ± 1122 m
Top-cloud Temperature	-43 ± 11^oC	-49 ± 9^oC
Base-cloud Temperature	-34 ± 11^oC	-38 ± 10^oC
Tropopause altitude	9578 ± 1052 m	9222 ± 1004m

6.1 Occurence

The presence of cirrus clouds in polar regions has long been assumed low compared to lower altitudes and especially the tropical regions (Sassen *et al.* , 2008). However, results from both ALOMAR and the polar-orbiting satellite CALIPSO (Winker *et al.* , 2003), indicate a large presence.

In the dataset from ALOMAR, which is located on the Norwegian coast dominated by synoptic systems throughout the year, 56 % occurrence of cirrus clouds in measurements is found. The dataset contains 313 measurements over 6 years, which is somewhat limited for a complete climatology.

The results from analyzing lidar data from CALIPSO supports the large presence of cirrus clouds in the Arctic, as 48% of the CALIPSO measurements in the Arctic region contain cirrus clouds. The temporal distribution of occurrence is shown in figure 6.1.

Even though the two systems have some difference in the occurrence, the variations with time are similar. January and May have low occurrence in both datasets, as well as August. The satellite data shows a more stable behavior than the fixed system, but also this can be explained by the amount of data available.

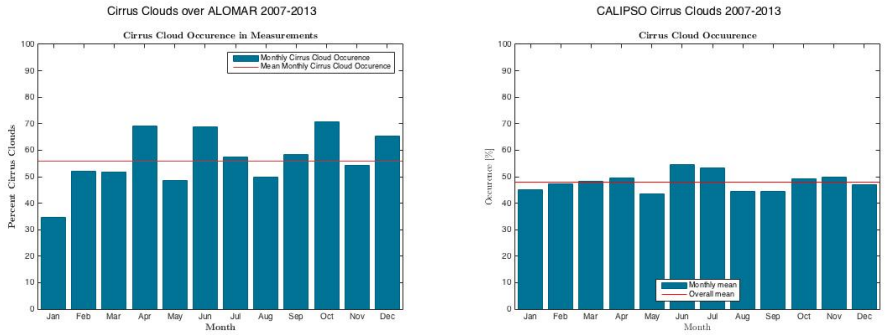

(a) Cirrus cloud occurrence measured at ALOMAR

(b) Cirrus cloud occurrence measured by CALIPSO

Figure 6.1: Cirrus cloud occurrence in the Arctic region measured by two different lidar systems. The upper panel shows the occurrence from ALOMAR while the lower panel show the occurrence measured by CALIPSO

6.2 Geometrical Cloud Properties

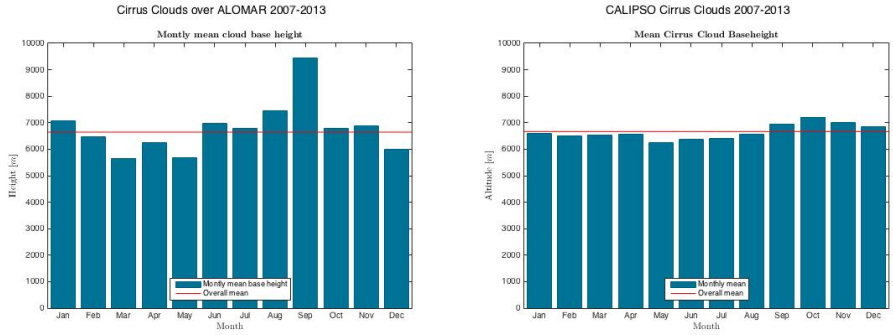

(a) Base height of cirrus clouds over ALOMAR

(b) Base height of cirrus clouds measured by CALIPSO

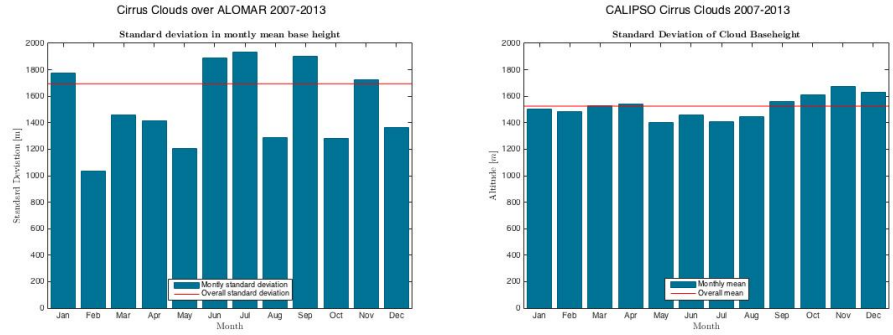

(c) Base height standard deviation of cirrus clouds over ALOMAR

(d) Base height standard deviation of cirrus clouds measured by CALIPSO

Figure 6.2: Comparing base height of cirrus clouds measured from ALOMAR and CALIPSO. The ALOMAR data shows a larger variation than the CALIPSO measurements.

Cloud altitude is presented in figure 6.2, illustrating once again how the ALOMAR dataset has larger variations than the satellite. Variations in base height and its standard deviation follows the same trend. For months with high mean base height, this is an indication of both very high cirrus clouds and more normal clouds being present in the same period.

The overall mean of the two datasets are less than 10 meters apart, as can be seen in table 6.1. This indicates that cloud base height is similar for the entire Arctic region. Note, however that the altitude above ALOMAR is measured at 379 meters above sea-level, causing the difference in overall mean height to be just less than 400 meters.

When comparing to studies conducted at other latitudes, cirrus clouds are found at higher altitudes further south. Sassen & Campbell (2001) found a base height of cirrus clouds at 8,79 km, which is about 2 km above the Arctic result. Rolf (2012) also found a higher base height in a similar study of cirrus over Germany.

When taking into account the relationship with the tropopause, the lower cloud altitude in the Arctic region is plausible. The troposphere is generally thinner at higher latitudes, and studies have shown that the mean tropopause altitude over this region is only around 9 km compared to about 16 km close to the Equator (Hoinka, 1999).

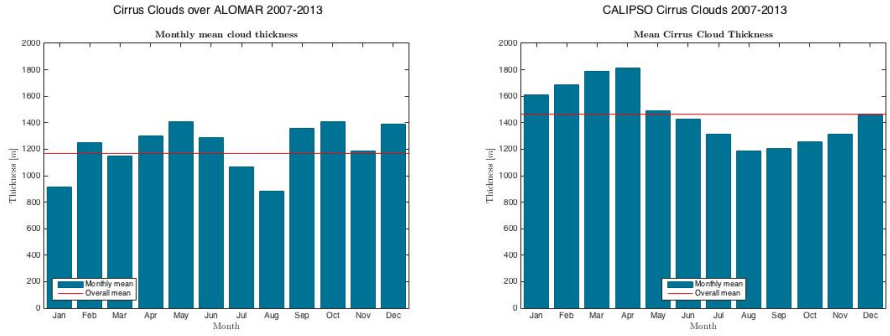

(a) Thickness of cirrus clouds over ALOMAR

(b) Thickness of cirrus clouds measured by CALIPSO

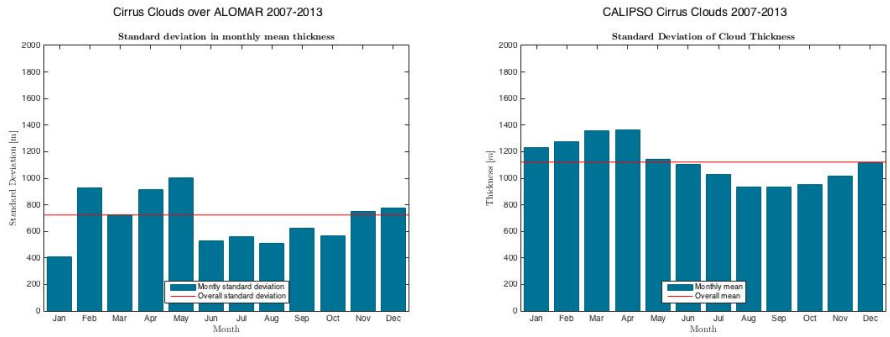

(c) Thickness standard deviation of cirrus clouds over ALOMAR

(d) Thickness standard deviation of cirrus clouds measured by CALIPSO

Figure 6.3: The thickness of cirrus clouds in the Arctic Region. The CALIPSO data shows a more seasonal distribution of thickness, while the ALOMAR dataset varies with month.

Figure 6.3 compares the cloud thickness measured by the two systems. The fixed system at the coast of Norway shows thinner and more stable clouds than the satellite. This could be explained by local differences in for instance

generating mechanism of the clouds. The satellite covers the entire Arctic region, and variations in generating mechanisms can occur.

Compared to lower latitudes, Arctic cirrus clouds appear thinner and more stable. Rolf (2012) found an average thickness of cirrus over Germany to be 2.8 km. This result was also compared to midlatitude cirrus clouds over USA and found to correspond well. Also for tropical regions, thickness is expected to be higher.

The thickness of Arctic cirrus clouds indicates that synoptic generation of cirrus clouds due to weather systems is the more likely generating mechanism here. Thunderstorms and large convective events dominate in the tropical region, and will yield thicker cirrus clouds (Rolf, 2012).

6.3 Temperatures

Both the systems display stable temperatures when looking at the standard deviation. Figure 6.4 shows that both systems behave similarly. For the satellite measurements, maximum temperature is found during the fall months, while at ALOMAR this occurs during summer.

With regard to mean temperatures, the overall mean is slightly colder for the satellite data. This could be caused by several things. The satellite covers larger areas of the Arctic region, also parts that are less affected by the Golf Stream, which heats the ocean around Andøya. In addition, temperature measurements for the ALOMAR data are less geographically accurate, as they are obtained by radiosondes. The balloons drifts with winds, and the temperatures can be assumed to be measured within a large area in Northern Norway and Sweden.

The mean temperature at top-cloud height is below the limit for homogeneous nucleation of ice (Hallett *et al.* , 2002). Synoptic generation of cirrus clouds occur from the top, and this temperature is therefore more relevant for the initial freezing of cloud nuclei (Sassen, 2002). Base temperatures are generally higher as ice nuclei melt when falling.

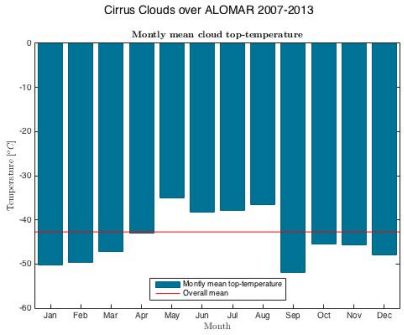

(a) Topheight temperature over ALOMAR

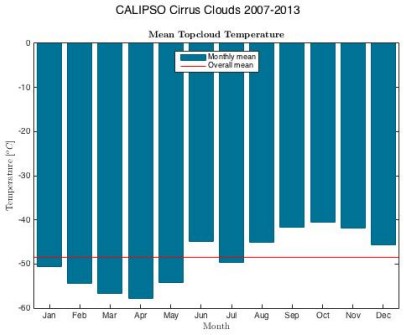

(b) Topheight temperature measured by CALIPSO

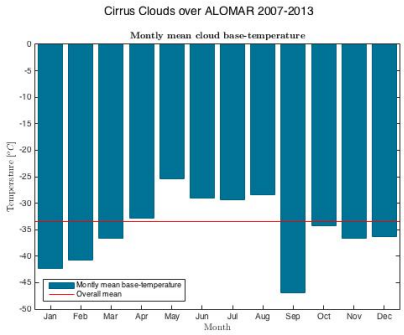

(c) Baseheight temperature over ALOMAR

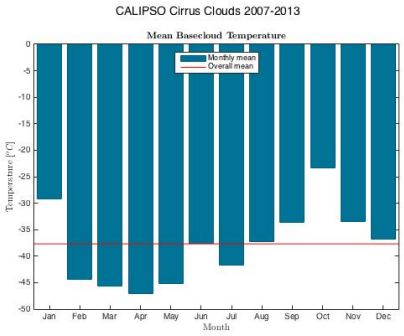

(d) Baseheight temperature measured by CALIPSO

Figure 6.4: Cirrus cloud temperatures measured at ALOMAR and by CALIPSO. The upper panel shows temperatures at the cloud-top altitude, while the bottom panels show the base-height temperature.

6.4 The Arctic Tropopause

The CALIPSO data reveals a mean tropopause altitude in the Arctic region of 9222 ± 1004 meters. Previous tropopause climatologies found a mean polar altitude of 9 km (Hoinka, 1999).

Even though the thermal definition of tropopause altitude is uncertain, it is used in this thesis for the ALOMAR dataset. Radiosondes released from Bodø provide temperature data for almost the entire period. The mean tropopause altitude from this data is found to be 9839 ± 1122 meters.

The same definition has been used in several papers regarding cirrus clouds from various locations on the globe (Rolf, 2012). It is therefore interesting to

compare them to the results found here, even though future studies with other methods of deriving tropopause altitude could give other results.

Compared to the satellite data covering the entire Arctic region, the result from Northern Norway seems plausible. The tropopause altitude for CALIPSO is derived from a global model (Powell *et al.* , 2013). The similarities with radiosonde data is therefore not surprising. The results can be seen in figure 6.5.

Hall *et al.* (2011) found the radar tropopause over Svalbard to be between 10 and 12 km throughout the year, while the corresponding radiosonde measurements were between 8 and 10 km. Thus, using different instrumentation to measure tropopause altitude will give varying results.

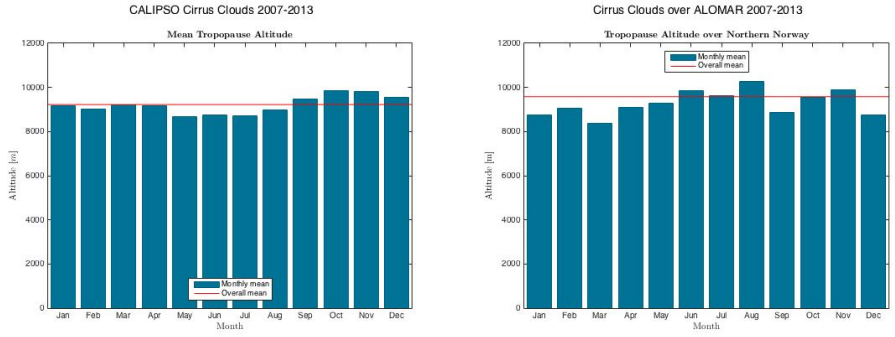

(a) Satellite-measured tropopause altitude

(b) Radiosonde measured tropopause altitude

Figure 6.5: Troposphere altitude derived from model and radiosonde measurements. The left panel shows CALIPSO data, derived from model data. The right panel shows tropopause altitude calculated from radiosonde measurements over Northern Norway. Both plots are based on data corresponding to cirrus observations.

When looking at temperature soundings from summer and winter season in the Arctic region, it becomes apparent why care must be taken when using this parameter for determining tropopause altitude. Figure 6.6 illustrate how the temperature behaves differently during winter, and finding the region where temperature gradients switch from positive to negative can be difficult.

Comparing the ALOMAR results with already published studies in the polar regions, indicate plausible data. However, further studies in the future comparing the radiosonde data with closely located radar measurements from Andenes can confirm or disprove these results.

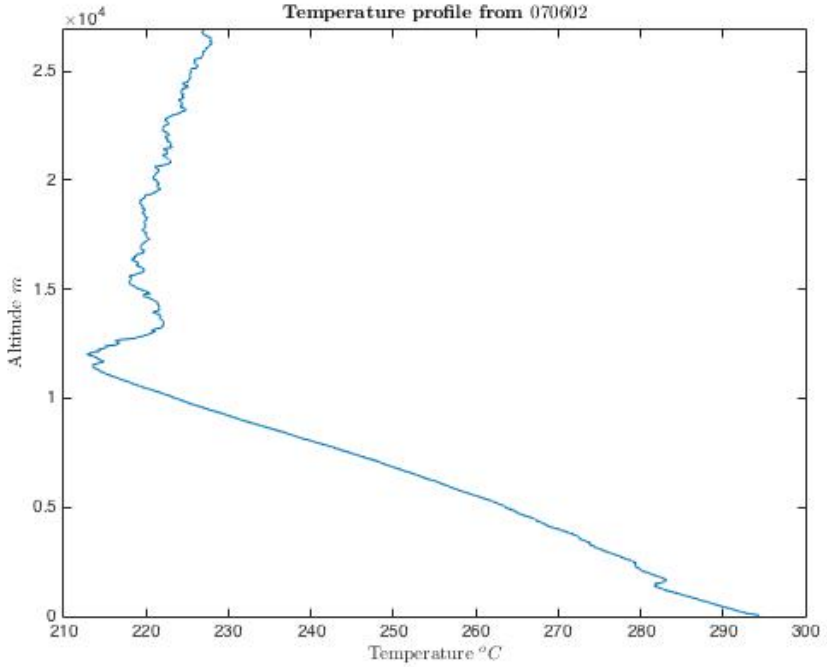

(a) Temperature sounding from Northern Norway measured on June 2nd 2007

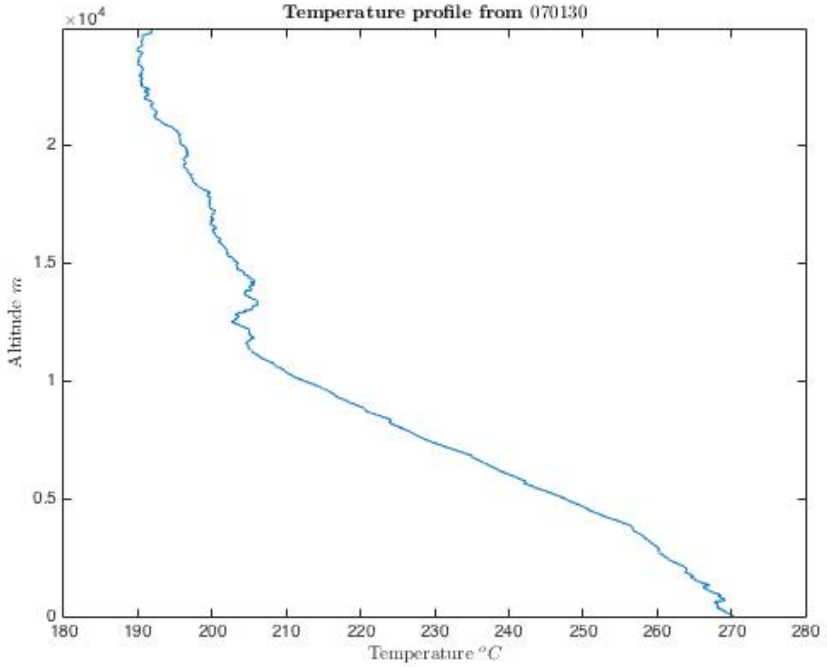

(b) Temperature sounding from Northern Norway measured on January 30th 2007

Figure 6.6: Temperature soundings from both winter and summer season compared. The figure clearly shows a different temperature behavior during winter season, which may cause difficulties when estimating the thermal tropopause.

6.5 Depolarization in Arctic Cirrus Clouds

Even though volume depolarization measured from ALOMAR has never been verified, the mean depolarization ratio is calculated for the available dataset from mid-2010 till 2013. This result is only a preliminary study, but comparing it to measurements from CALIPSO indicate promising measurements.

The overall volume depolarization from ALOMAR is found to be

$$0,1987 \pm 0,0307$$

The CALIPSO dataset has volume depolarization measurements from the entire active period of the satellite. Using data from 2007-2013 as was used when investigating macrophysical properties, the mean volume depolarization ratio is found to be

$$0,2058 \pm 0,1192$$

For the ALOMAR dataset, manual screening of color-coded plots have revealed some cases from early 2010 with poor data quality. The system was upgraded in May 2010 to give reliable depolarization measurements (Gausa, Michael, private communication, 2015), but system logbooks reveal several test measurements until the middle of August. The first day where depolarization ratio is calculated from ALOMAR is therefore August 20th 2010.

Further verification of the ALOMAR dataset is necessary to rely on the dataset completely. This can be done by comparing cirrus measurements from ALOMAR and CALIPSO with close geographical proximity and good data quality. Signal from the ground-based system must reach above the cloud top altitude for the cases to be comparable. In addition, the satellite has a limited number of close passes over ALOMAR.

For the existing data from ALOMAR, there appears to be very few cases where signal is good enough for comparison with spaceborne lidar. The verification is therefore dependent on new measurements.

Following system verification, more thorough studies of individual cases can give indications of crystal shapes in Arctic cirrus clouds. Visual inspection of quickplots already reveal how depolarization ratio changes with falling cloud altitudes and how different atmospheric conditions can affect this parameter.

6.6 Source of Error

For measuring cirrus clouds with lidars, there is always some bias. Measurements from ALOMAR are restricted by local weather conditions, and the limitations for measurements are set in cooperation with owners of other systems at the location. These systems have more restrictive criterions as they are more sensitive to humidity and winds.

The CALIPSO dataset extends over roughly the same time period as the ALOMAR system. It is a much larger dataset, as measurements are unaffected by weather conditions on ground. This is evident in the results in terms of smoother statistics. Some time periods are less covered due to instrument malfunction or maintenance.

For evaluating the upper limit of the troposphere, several definitions exist. For this thesis, the thermal definition according to WMO is used. This definition is less suited in the Arctic winter when comparing to the dynamical tropopause altitude (Zängl & Hoinka, 2001). It is still applied here, as most of the literature used in comparison also uses the thermal tropopause definition. The good correlation with other tropopause measurements can partly be because this definition is widely used despite its limitations.

7

Conclusions

This thesis has focused on revealing the macrophyiscal properties of cirrus clouds in the Arctic region by comparing measurements from both ground-based and spaceborne lidar systems.

The results reveal an occurrence of 56% cirrus clouds over Andøya and 48% in the entire Arctic region measured by CALIPSO. The large presence of cirrus clouds at high latitudes emphasize the need for further research on the topic in this region to complete climate models.

Macrophysical and synoptic properties have also been investigated. Cirrus clouds are found to have a base height of 6647 meters above ALOMAR and 6665 meters above sea-level according to CALIPSO. The results correspond to a low tropopause altitude compared to lower latitudes.

Cloud thickness is found to be 1166 meters and 1464 meters for ALOMAR and CALIPSO data, respectively. Compared to lower latitudes, this shows that the cirrus clouds are thinner and that the variation in thickness is small. The reason for this may be related to the differences in generating mechanisms for cirrus clouds at low and high latitudes.

As cirrus clouds in Northern Norway appear to be mostly synoptic, the top-cloud temperature is of most interest. This temperature is well below the limit of homogeneous nucleation. For the entire Arctic, the temperatures are slightly lower. ALOMAR is located just 2,5 degrees north of the Arctic circle, while the

CALIPSO dataset includes measurements up to 82^o N. This can account for the lower temperature at cirrus altitudes found by CALIPSO.

For all cirrus parameters, the temporal behavior of the two datasets are similar. The ALOMAR dataset shows larger variations, but the available amount of data is much smaller than for the satellite dataset. ALOMAR data is limited by both local weather conditions as well as limited presence of personnel.

7.1 Outlook: Tropopause Definitions in the Arctic

Even though the thermal tropopause is calculated in this thesis, other definitions and instrumentations can be beneficial for future research. The temperature behavior in the stratosphere during winter is likely to cause difficulties in detecting the tropopause altitude, and combining definitions such as the dynamical tropopause (Zängl & Hoinka, 2001) and radar measurements (Hall *et al.* , 2011) can give more exact measurements of the tropopause.

7.2 Outlook: Depolarizing Effects of ice in Cirrus Clouds

One of the initial goals of this thesis, was to disclose some of the microphysical properties of cirrus clouds in the Arctic. However, system limitations prevented a complete examination of the depolarization ratio which is one of the key parameters for such properties. For that reason, no complete results are presented here.

The volume depolarization has been calculated for the ALOMAR dataset from 2010-2013 and the CALIPSO dataset from 2007-2013. The overall mean values are close together, and both display a low depolarization ratio.

The two systems show slightly varying depolarization ratio's, and these differences can most likely be explained by geographical differences in microphysical properties. The most pronounced difference lies in the stability of the depolarization ratio. The ALOMAR data shows a very low standard deviation, which could indicate that cirrus at the coast of Norway have a stable, low depolarization ratio. If this is the case, further research is required to disclose more details about the clouds microphysics.

7.3 Concluding Remarks

This thesis has shown the large potential for long-term cirrus cloud research from the Arctic Lidar Observatory in Northern Norway. The results show similar behavior as the measurements conducted by CALIPSO. For the parameters showing differences, these are explained by varying cloud properties with geography.

The large occurrence disclosed here, shows the importance of more extensive research of cirrus clouds in the Arctic region to complete and improve modeling of climate changes. The former belief that cirrus clouds are less common in the Arctic region is, according to findings in this thesis, proven wrong.

Future satellite missions to continue the work of the CALIPSO satellite are already planned for launch (Wehr, 2006). An important next step is therefore to investigate microphysical properties of cirrus clouds over ALOMAR using the long-term dataset available.

Bibliography

Abo, Makoto. 2005. *Resonance Scattering Lidar*. Springer Series in Optical Sciences. Springer. Chap. 11: Resonance Scattering Lidar, pages 307–323.

Adhikari, Loknath, Wang, Zhien, & Deng, Min. 2012. Seasonal variations of Antarctic clouds observed by CloudSat and CALIPSO satellites. *Journal of geophysical research*, **117**, 1–17.

Chen, Wei-Nai, Chiang, Chih-Wei, & Nee, Jan-Bai. 2002. Lidar Ratio and Depolarization Ratio for Cirrus Clouds. *Applied Optics*, **41**(30), 6470–6476.

Cotton, William. 2011. *Storm and cloud dynamics: the dynamics of clouds and precipitating mesoscale systems*. 2 edn. Vol. 99. Academic Press.

Frioud, Max, Gausa, Michael, Baumgarten, Gerd, Kristijansson, Jon Egill, & Føre, Ivan. 2006. New Tropospheric Lidar System in Operation at ALOMAR (60 degrees N, 16 degrees E). *Pages 179–182 of:* Nagasawa, Chikao, & Sugimoto, Nobuo (eds), *Reviewed and revised papers presented at the 23rd International Laser Radar Conference, 24.-28. July 2006, Nara, Japan*. Nara, Japan: The Conference Steering Committee of the 23rd ILRC, 2006.

Gimmestad, Gary G. 2005. *Differential-Absorption Lidar for Ozone and Industrial Emission*. Springer Series in Optical Sciences. Springer. Chap. 7: Differential-Absorption Lidar for Ozone and Industrial Emission, pages 187–212.

Guasta, Massimo Del, & Vallar, Edgar. 2003. In-cloud variability of LIDAR depolarization of polar and midlatitude cirrus. *Geophysical research letters*, **30**(11).

Guasta, Massimo Del, Morandi, Marco, Stefanutti, Leopoldo, Stein, Bernhard, Kolenda, Jurgen, Rairoux, Patrick, Wolf, J. P., Matthey, Ranaud, & Kyro, Esko. 1994. Multiwavelength LIDAR observation of thin cirrus at the base of the Pinatubo stratospheric layer during the EASOE campaign. *Geophysical research letters*, **21**(13), 1339–1342.

Hall, C. M., Hanssen, G., Sigernes, F., & Ruiz, K.M. Kuyeng. 2011. Tropopause height at 78N 16E: Average seasonal variation 2007-2010. *Atmospheric Chemistry and Physics*, **11**(11), 5485–5490.

Hallett, John, Arnott, William P., Bailey, Matthew P., & Hallet, Joan T. 2002. *Cirrus*. Vol. 2. Oxford University Press. Chap. 3: Ice Crystals in Cirrus, pages 41–77.

Hanssen, Ingrid Margrethe Vestnes. 2015 (June 2015). *Arctic Cirrus Clouds over Andøya Space Center: A Statistical Analysis of LIDAR-data*. Project paper, Department of Physics and Technology, UiT, The Arctic University of Norway.

Hoinka, Klaus P. 1999. Temperature, Humidity, and Wind at the Global Tropopause. *Monthly Weather Review*, **127**(10), 2248–2265.

Huo, Juan, & Lu, Daren. 2014. Physical Properties of High-Level Cloud over Land and Ocean from Cloudsat and Calipso Data. *Journal of Climate*, **27**(December), 8966–8978.

IPCC. 2001. Climate Change 2001: Synthesis Report. A Contribution of Working Groups I, I, III to the Third Assessment Report of the Intergovernmental Panel on Climate Change. *Cambridge University Press*.

Lampert, Astrid. 2010. *Airborne LIDAR observations of tropospheric Arctic clouds*. PhD-thesis, Institute of Aerospace Systems, Technische Universität Carolo-Wilhelmina zu Braunschweig, Hermann-Blenk-Str. 23, D-38108 Braunschweig, Germany.

Larsgard, Nina. 2008 (April). *Characteristics of cirrus clouds over ALOMAR and their dependence on atmospheric conditions*. Masterthesis, University of Oslo, Institutt for geofag, avdeling MetOs.

Liou, K.N., Takano, Y., Yang, P., & Gu, Y. 2002. *Cirrus*. Vol. 2. Oxford University Press. Chap. 13: Radiative Transfer in Cirrus Clouds, pages 265–296.

Liou, Kuo-Nan. 1986. Influence of Cirrus Clouds on Weather and Climate Processes: A global Perspective. *American Meteorological Society: Monthly Weather Review*, **114**(6), 1167–1199.

Lynch, David K. 2002. *Cirrus*. Vol. 2. Oxford University Press. Chap. 1: Cirrus: History and Definition, pages 1–11.

Lynch, David K., & Sassen, Kenneth. 2002. *Cirrus*. Vol. 2. Oxford University Press. Chap. 12: Subvisual Cirrus, pages 256–264.

Mielke, Bernd. 2005. *Analog + Photon Counting*. Tech. rept. LICEL Tech, Licel GmbH, CHausseestr 34/35, 10115 Berlin, Germany.

Minnis, Patrick, Ayers, J. Kirk, Palikonda, Rabindra, & Phan, Dung. 2004. Contrails, Cirrus Trends, and Climate. *Journal of Climate*, **17**(April), 1671–1685.

Noel, Vincent, Chepfer, Helene, Ledanois, Guy, Delaval, Arnaud, & Flamant, Pierre H. 2002. Classification of Particle Effective Shape Ratios in Cirrus Clouds Based on the Lidar Depolarization Ratio. *Applied Optics*, **41**(21), 4245–4257.

Noel, Vincent, Chepfer, Helene, Haeffelin, Martial, & Morille, Yohann. 2006. Classification of Ice rystal Shapes in Midlatitude Ice Clouds from Three Years of Lidar Observations over the SIRTA Observatory. *Journal of the Atmospheric Sciences*, **63**, 2978–2991.

Powell, Kathleen, Vaughnan, Mark, Winker, David, Lee, Kam-Pui, Pitts, Michael, & Trepte, Charles. 2013 (September). *Data Management System: Data Products Catalog for CALIPSO*. Tech. rept. 3.6. National Aeronautics and Space Administration (NASA), Langley Research Center, Hampton, Virginia.

Rolf, Christian. 2012 (December). *Lidar observations of natural and volcanis-ash-induced cirrus clouds*. Ph.D. thesis, Bergische Universität.

Sassen, Kenneth. 1991. The Polarization Lidar Technique for Cloud Research: A Review and Current Assessment. *Bulletin of the American Meteorological Society*, **72**(12), 1848–1866.

Sassen, Kenneth. 2002. *Cirrus*. Vol. 2. Oxford University Press. Chap. 2: Cirrus: A Modern Perspective, pages 11–40.

Sassen, Kenneth. 2005. *Polarization in Lidar*. Springer Series in Optical Sciences. Springer. Chap. 2: Polarization in Lidar, pages 19–42.

Sassen, Kenneth, & Benson, Sally. 2001. A Midlatitude Cirrus Cloud Climatology from the Facility for Atmospheric Remote Sensing. Part 2: Microphysical Properties Derived from Lidar Depolarization. *Journal of the Atmospheric Sciences*, **58**(15), 20103–2112.

Sassen, Kenneth, & Campbell, James. 2001. A Midlatitude Cirrus Cloud Climatology from the Facility for Atmospheric Remote Sensing. Part 1: Macrophysical and Synoptic Properties. *Journal of the Atmospheric Sciences*, **58**(5), 481–496.

Sassen, Kenneth, & Mace, Gerald. 2002. *Cirrus*. Vol. 2. Oxford University Press.

Chap. 8: Ground-based Remote Sensing of Cirrus Clouds, pages 168–196.

Sassen, Kenneth, Wang, Shien, & Liu, Dong. 2008. Global distribution of cirrus clouds form CloudSat /Cloud-Aerosol Lidar and Infrared Pathfinder Satellite Observations measurements. *Journal of geophysical research*, **113**(October).

Schumann, Ulrich. 2002. *Cirrus*. Vol. 2. Oxford University Press. Chap. 11: Contrail Cirrus, pages 231–255.

Skatteboe, Rolf. 1996. ALOMAR: Atmospheric Science using Lidars, Radars and Ground Based Instruments. *Journal of Atmospheric and Terrestrial Physics*, **58**(16), 1823–1826.

Stephens, Graeme. 2002. *Cirrus*. Vol. 2. Oxford University Press. Chap. 20: Cirrus, Climate and Global Change, pages 433–448.

Stone, Robert. 1957 (March). *A Compendium on Cirrus and Cirrus Forecasting*. Air Weather Service Technical Reprot AWS TR 105-130. United States Air Force.

Stordal, F., Myhre, G., Stordal, E. J. G., Rossow, W. B., Lee, D. S., Arlander, D. W., & Svendby, T. 2005. Is there a trend in cirrus cloud cover due to aircraft traffic? *Atmospheric Chemistry and Physics*, **5**(8), 2155–2162.

von Zahn, U., von Cossart, G., Fiedler, J., Fricke, K. H., Nelke, G., Baumgarten, G., Rees, D., Hauchecorne, A., & Adolfsen, K. 2000. The ALOMAR Rayleigh/Mie/Raman lidar: Objectives, Configuration and Performance. *Annales Geophysicae*, **18**, 815–833.

Wallace, John M. 2006. *Atmospheric Science: An introductory survey*. Elsevier Inc.

Wandinger, Ulla. 2005a. *Introduction to Lidar*. Springer Series in Optical Sciences. Springer. Chap. 1: Introduction to Lidar, pages 1–18.

Wandinger, Ulla. 2005b. *Raman Lidar*. Springer Series in Optical Sciences. Springer. Chap. 9: Raman Lidar, pages 242–271.

Wehr, Tobias (Editior). 2006 (November). *EarthCARE: Mission Requirement Document*. Mission Requirement Document 5. ESA and JAXA, EarthCARE Mission Advisory Group.

Winker, David M., Pelon, Jacques R., & McCormick, Patrick. 2003. CALIPSO mission: Spaceborne LIDAR for observation of aerosols and clouds. *SPIE*

Proceedings, **4893**(March), 11.

WMO. 1975. *International Cloud Atlas - Manual on the Observation of Clouds and Other Meteors*. Vol. 1. World Meteorological Organization.

Young, Andrew T. 1982. Rayleigh Scattering. *Physics Today*, **35**(1), 42–48.

Zängl, Günther, & Hoinka, Klaus P. 2001. The Tropopause in Polar Regions. *Journal of Climate*, **14**(14), 3117–3139.

A

Seasonal Statistics

In chapter 4, the statistical results were presented with respect to month. For most of the parameters, variations are better illustrated with monthly statistics. However, in the previously written project paper (Hanssen, 2015), results were presented in terms of season. These results are reproduced in Appendix C.

The seasons are divided as follows:

Winter December, January and February

Spring March, April and May

Summer June, July and August

Fall September, October and November

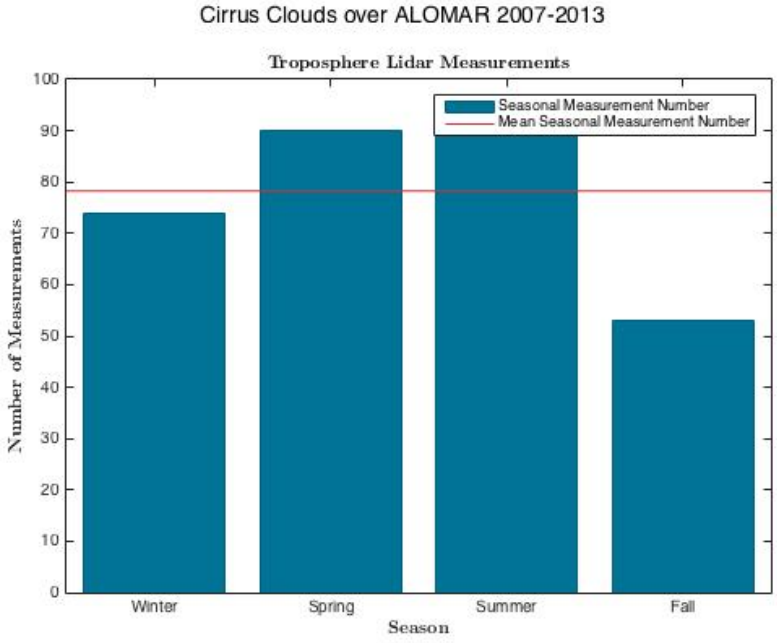

(a) Measurement distribution with respect to season

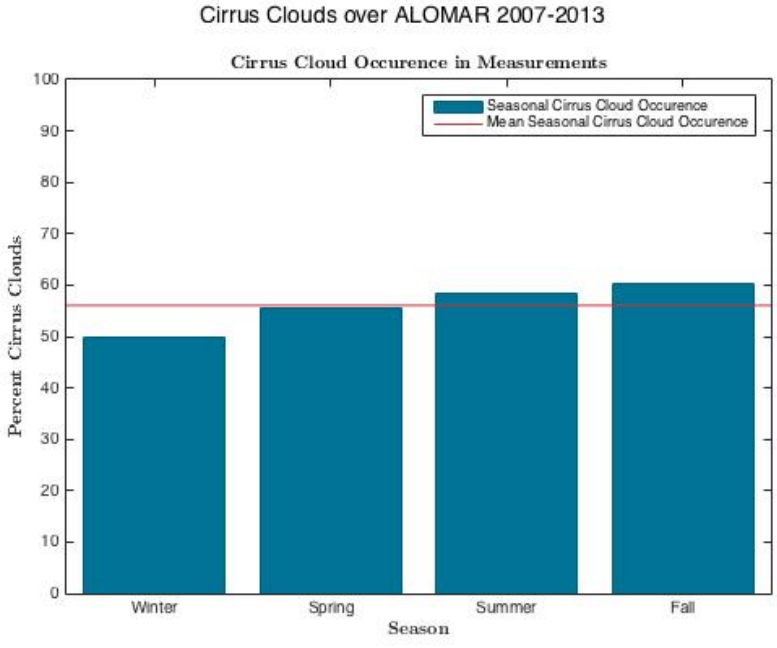

(b) Seasonal cirrus cloud cover with respect to season

Figure A.1: Measurement and cirrus cloud distribution with respect to season. There is no clear seasonal variation, and the monthly statistics presented in chapter 4 illustrates better the change in cover with time.

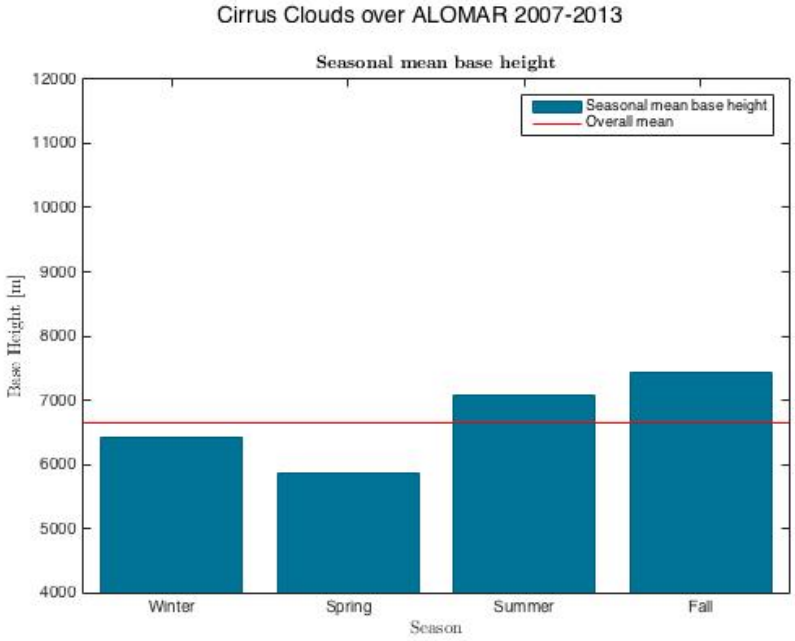

(a) Cirrus cloud base height with respect to season

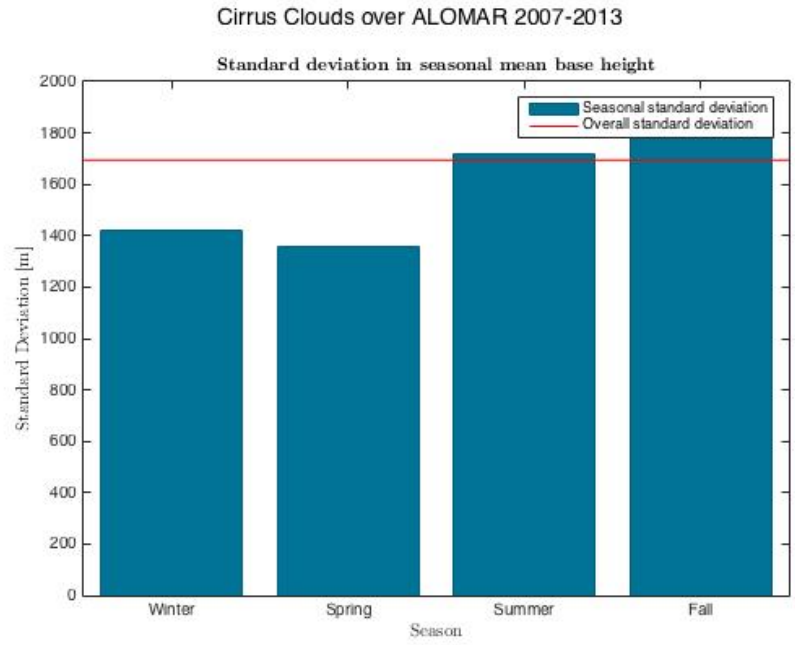

(b) Base height standard deviation with respect to season

Figure A.2: Base height statistics of cirrus clouds over ALOMAR with respect to season. The figure shows low base height during spring, and increased base height during summer and fall. The standard deviation shows the same temporal behavior.

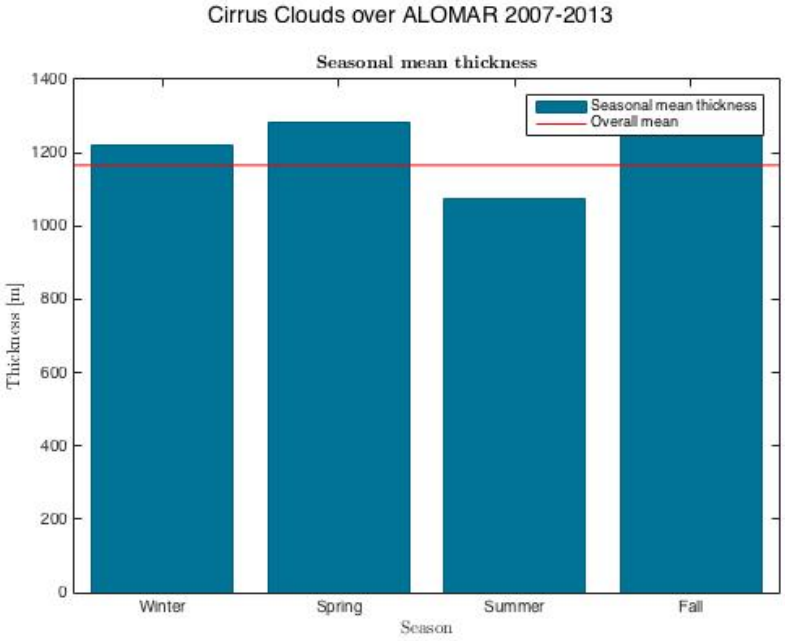

(a) Cirrus cloud thickness with respect to season

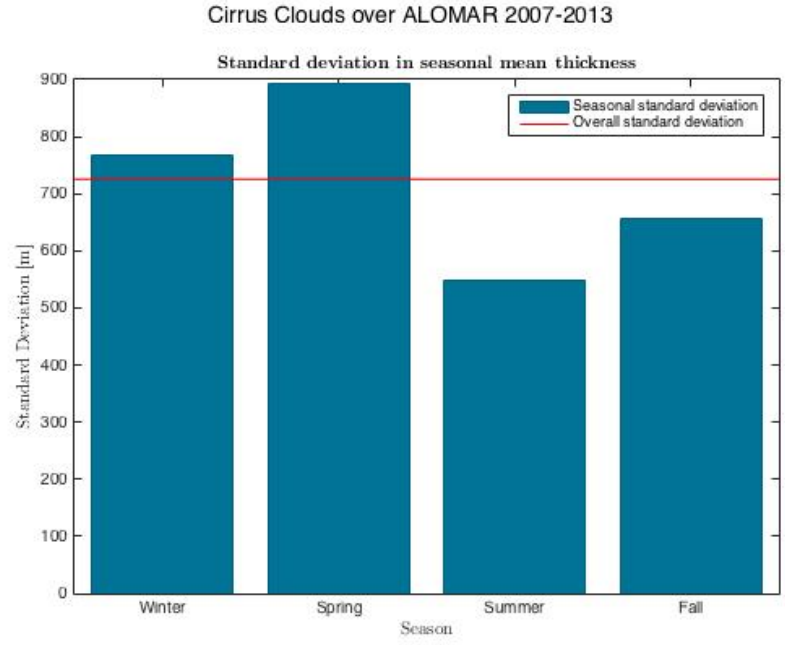

(b) Thickness standard deviation with respect to season

Figure A.3: Cirrus cloud thickness over ALOMAR. The figure shows thicker clouds during spring and fall. Also here, standard deviation follows the same trend.

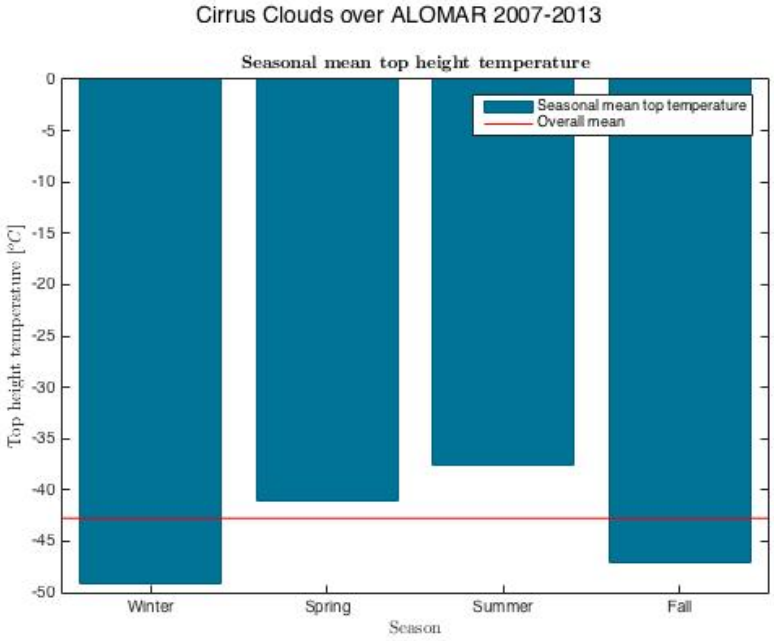

(a) Temperature at cloud top-height as a function of season. The overall mean is found to be -42.75^oC.

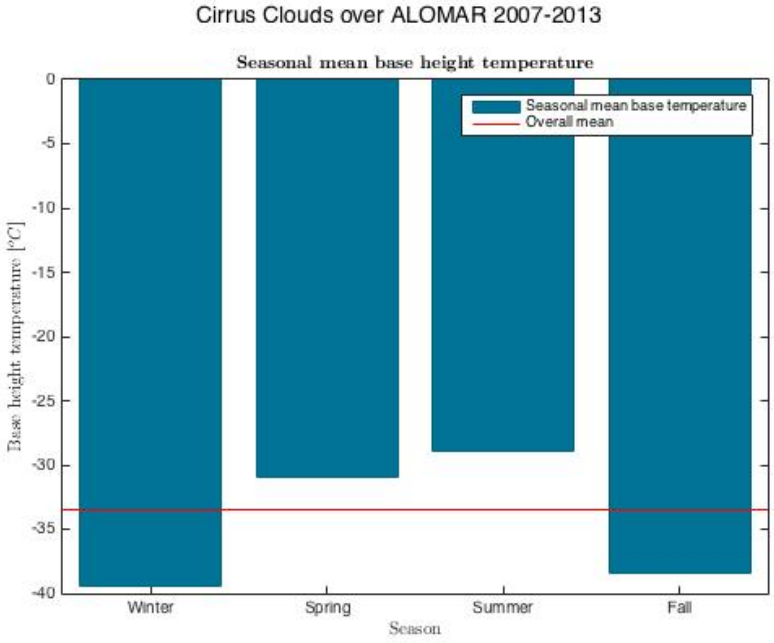

(b) Temperature at cloud base height as a function of season. The overall mean is found to be -33.5^oC.

Figure A.4: Cirrus cloud temperature over ALOMAR show that the temperature rises with warmer seasons, and both top and base temperature behaves similar.

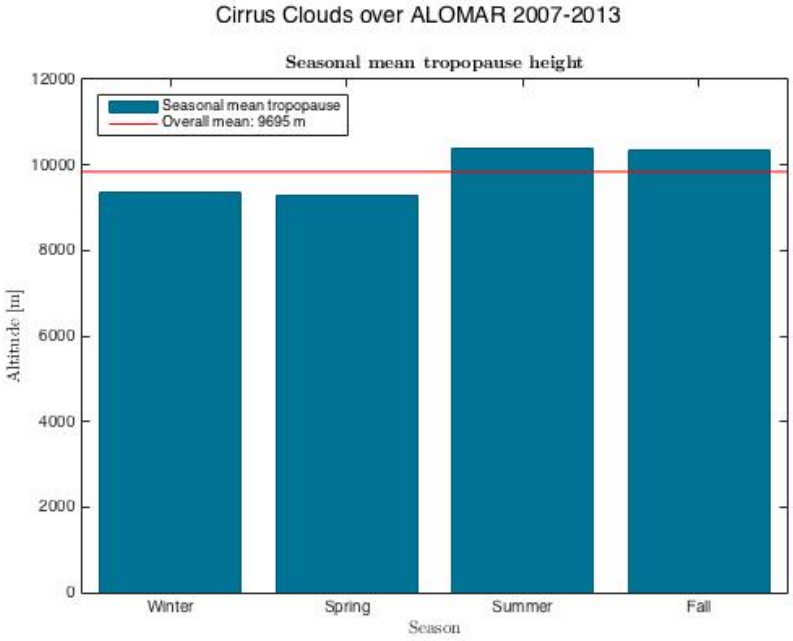

(a) Seasonal mean local tropopause of Northern Norway

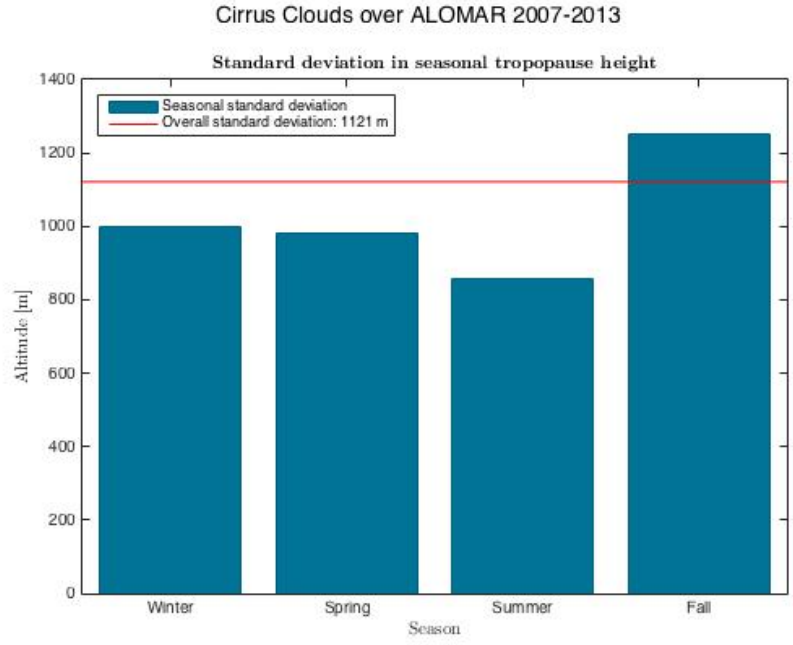

(b) Standard deviation of monthly tropopause

Figure A.5: Local Tropopause of Northern Norway. The upper panel shows how the altitude is highest during summer and fall. The standard deviation is however, smallest during summer, and highest during fall. The altitude is only calculated for days with cirrus present, and is not a complete climatology of the tropopause altitude.

B

Tropopause Cirrus Clouds

The investigation of cirrus clouds near the tropopause was conducted using radiosonde measurements along with lidar data about the clouds. 9 cases in total were investigated, but only one found to clearly reside above the thermal tropopause.

Plots of the cloud altitudes and atmospheric variables for the other cases are found here.

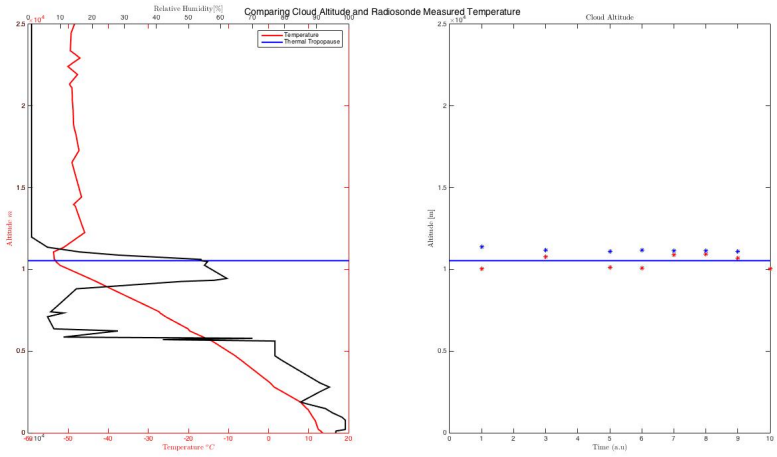

Figure B.1: Atmospheric variables and cloud altitude from August 14th 2010. The figure shows that the cloud altitude is around the thermal tropopause altitude for the entire time period.

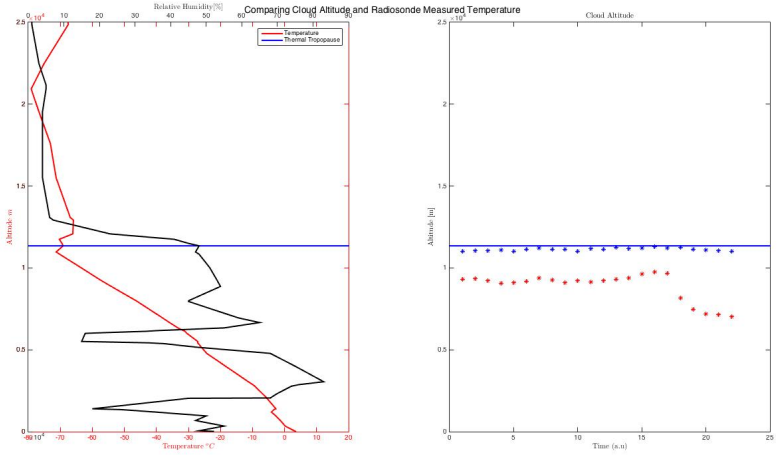

Figure B.2: Atmospheric variables and cloud altitude from April 1st 2011. The figure shows that the cloud altitude is below the thermal tropopause for the entire measurement

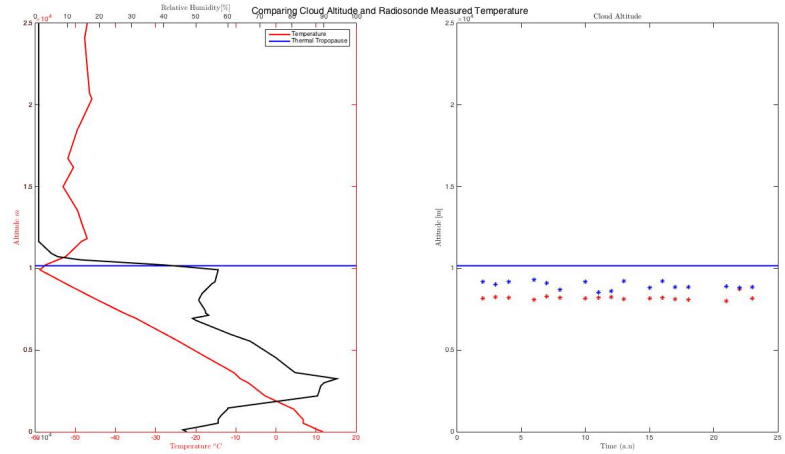

Figure B.3: Atmospheric variables and cloud altitude from May 13th 2011. The figure shows that the cloud altitude below the thermal tropopause for the entire sounding.

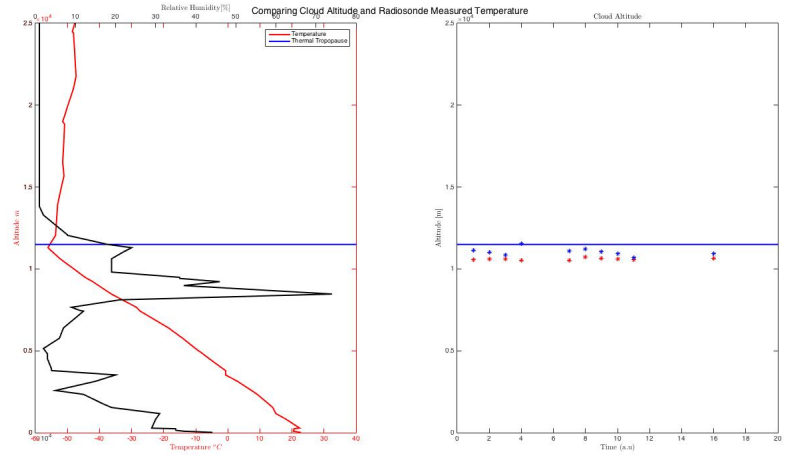

Figure B.4: Atmospheric variables and cloud altitude from June 10th 2011. The figure shows that the cloud altitude is just below the thermal tropopause

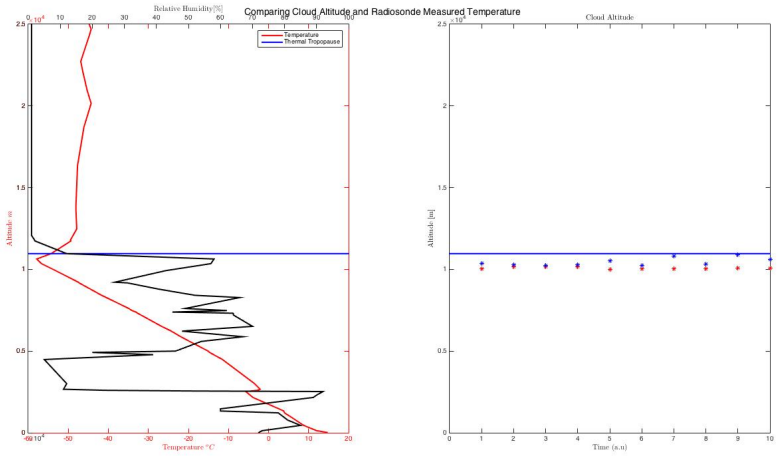

Figure B.5: Atmospheric variables and cloud altitude from June 16th 2011. The figure shows that the cloud altitude is just below the thermal tropopause

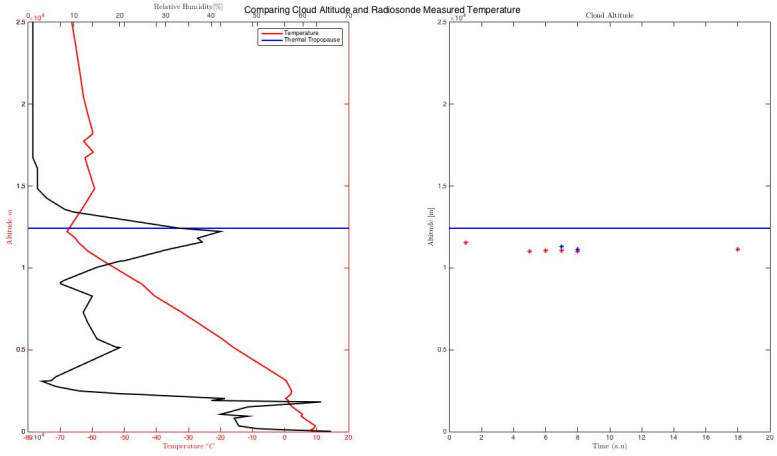

Figure B.6: Atmospheric variables and cloud altitude from October 25th 2011. The figure shows that the cloud altitude is just below the thermal tropopause

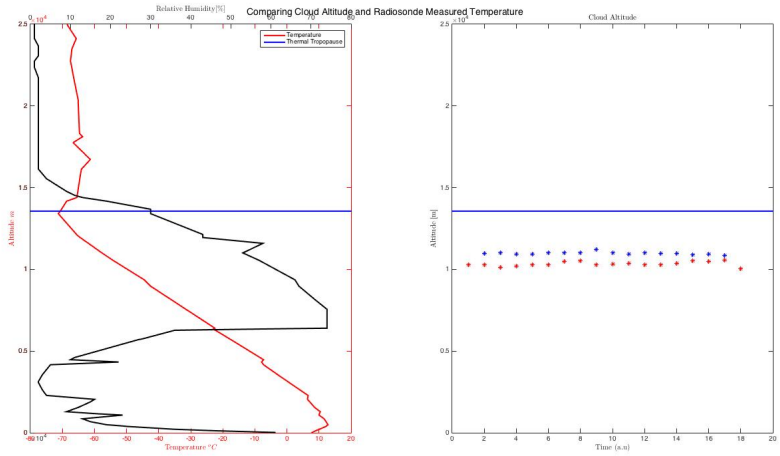

Figure B.7: Atmospheric variables and cloud altitude from November 11th 2011. The figure shows that the cloud altitude is well below the thermal tropopause

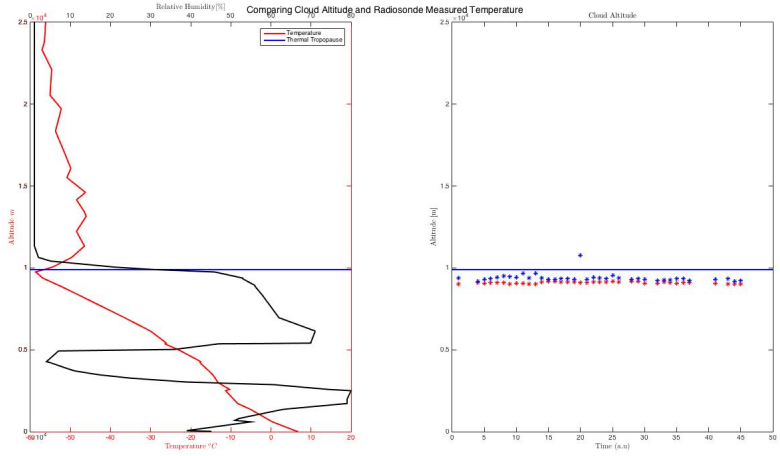

Figure B.8: Atmospheric variables and cloud altitude from April 21st 2012. The figure shows that the cloud altitude is just below the thermal tropopause

C

Macrophysical Results from Project Paper

During the preliminary study for this thesis, macrophysical properties of cirrus clouds over ALOMAR was studied for a subset of the ALOMAR Troposphere lidar dataset. Properties like cloud base height, thickness and temperature was studied for 2010-2013. These results are reproduced in this appendix with respect to season. For further details, see Hanssen (2015).

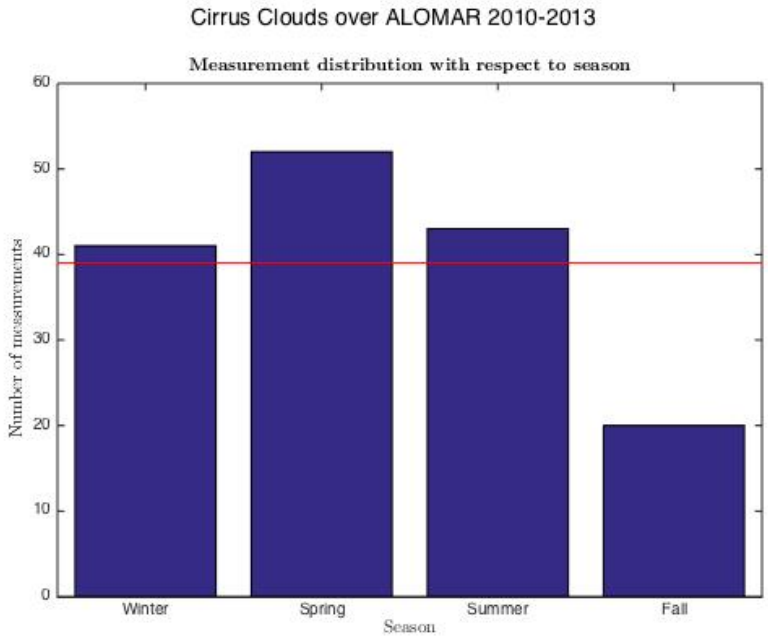

(a) The seasonal distribution of measurements with the tropospheric LIDAR at ALOMAR. Note the low number of measurements during the fall season.

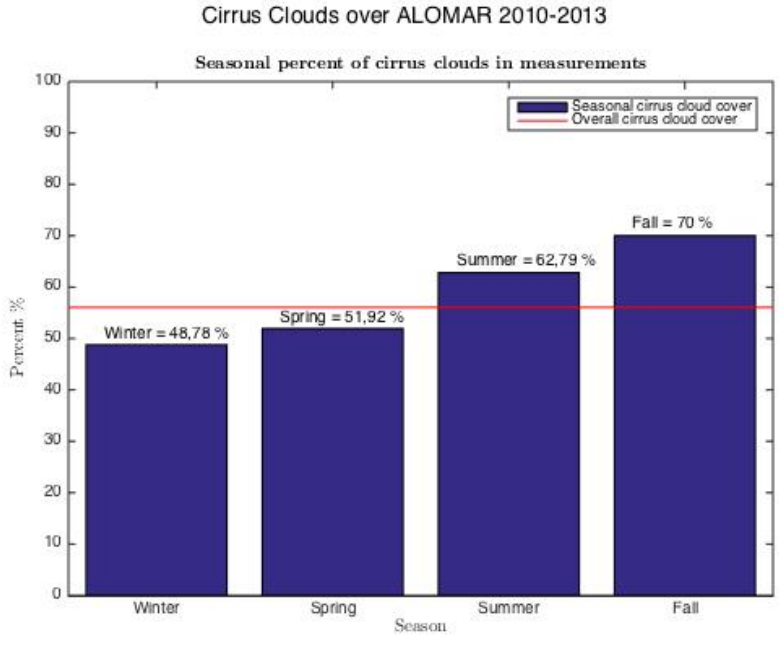

(b) Seasonal cirrus cloud cover in percent. The mean cover is 56.10%.

Figure C.1: The upper panel shows the measurement distribution with respect to season. The lower panel shows the occurrence frequency of cirrus clouds in the data set, also with respect to season. There is a notably lower number of measurements during the fall season, accompanied by a large percentage of cirrus clouds detected.

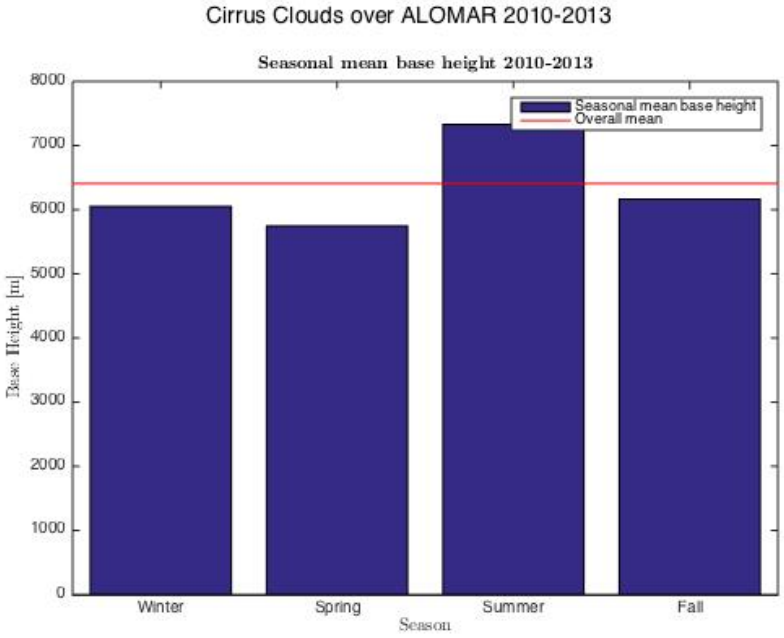

(a) Mean base height

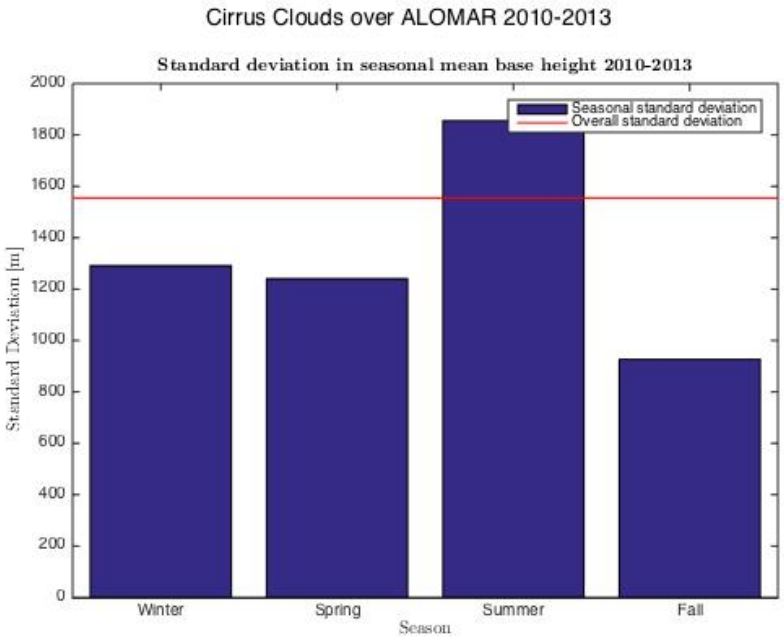

(b) Base height standard deviation

Figure C.2: Upper panel: The seasonal distribution of mean cloud base height. The base height peaks in the summer season. Lower panel: Standard deviation for the base height. The standard deviation also peaks in the summer season.

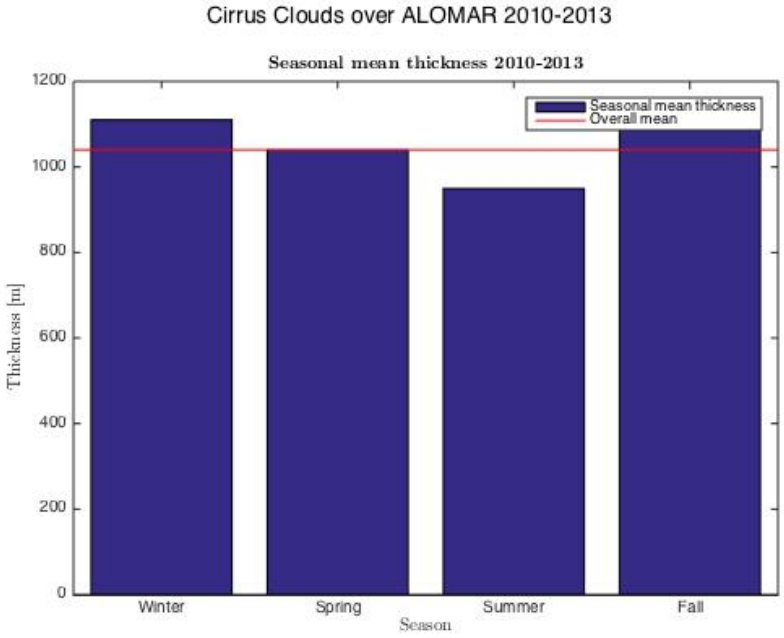

(a) Mean cloud thickness

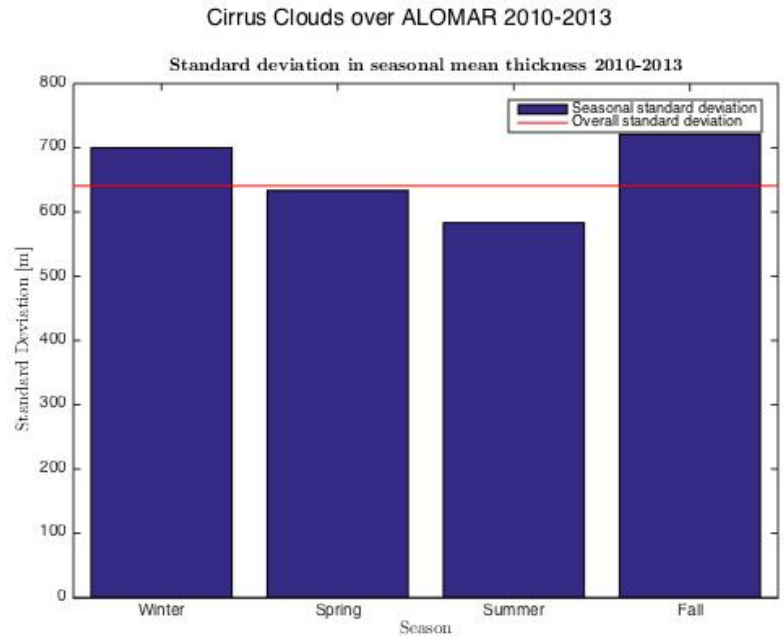

(b) Cloud thickness standard deviation

Figure C.3: Upper panel: The seasonal thickness distribution shows only small seasonal variations. The clouds seem to be thinner during the summer season but the variations are less than 200 meters over the year. Lower panel: The standard deviation of thinkness also shows little variation.

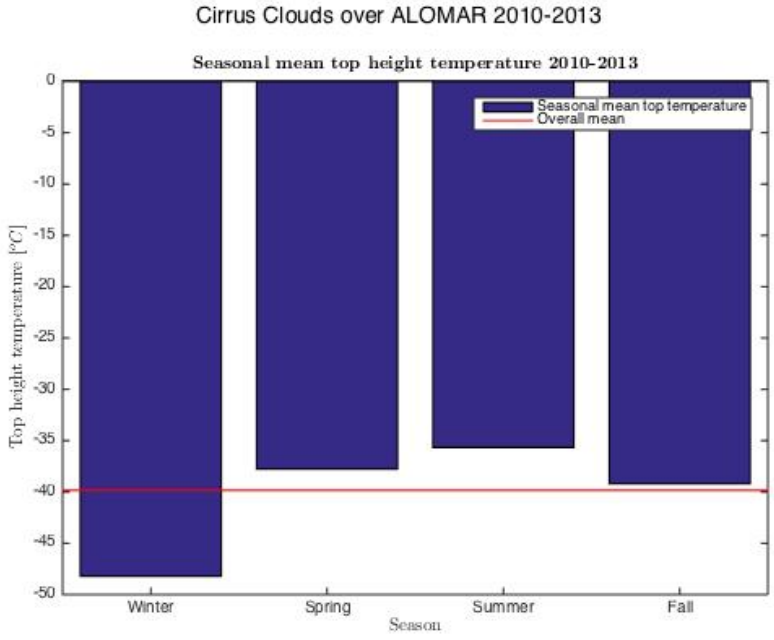

(a) Seasonal top cloud temperature with overall mean

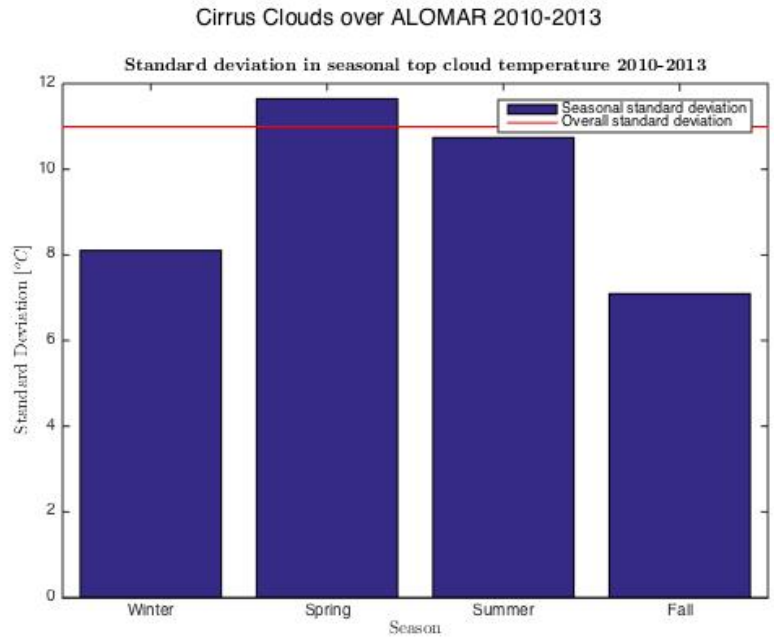

(b) Standard deviation of seasonal top cloud temperature with overall standard deviation

Figure C.4: Upper panel: The seasonal mean top cloud temperature with the overall mean. There is a clear minimum in the winter season. The overall mean is $-39,85^oC$, which is close to the temperature limit for homogeneous freezing. Lower panel: The standard deviation of seasonal temperature. The maximum variations occur in the spring and summer season while the fall season has the smallest standard deviation. The overall standard deviation is 11^oC.

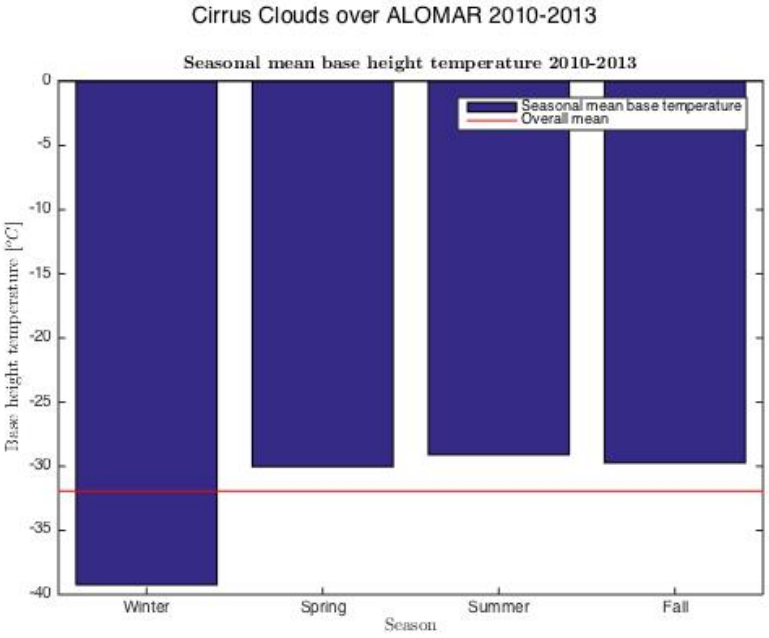

(a) Seasonal base cloud temperature with overall mean

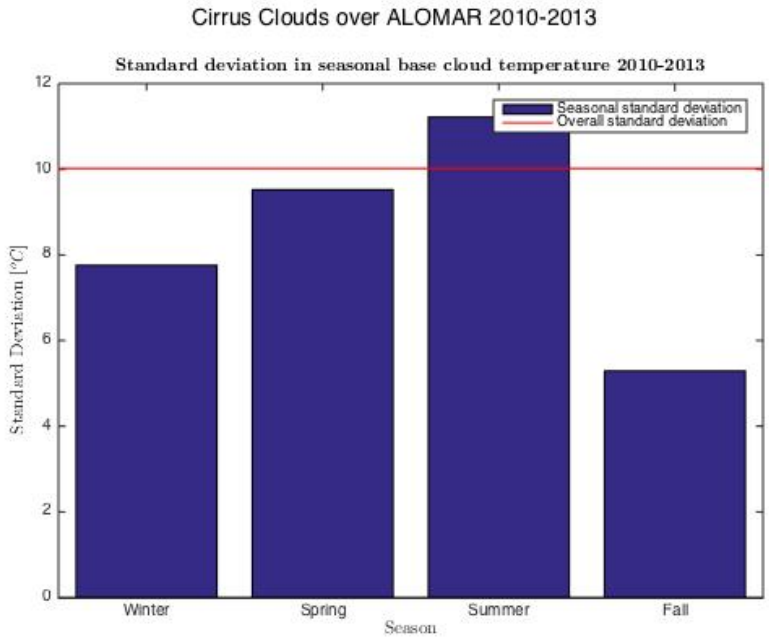

(b) Standard deviation of seasonal base cloud temperature with overall standard deviation

Figure C.5: Upper panel: The seasonal mean base cloud temperature with the overall mean. There is a clear minimum in the winter season. The overall mean is $-31,93^oC$. Lower panel: The standard deviation of seasonal temperature. The deviation peaks in the summer season while the fall season shows the smallest standard deviation. The overall standard deviation is 10^oC

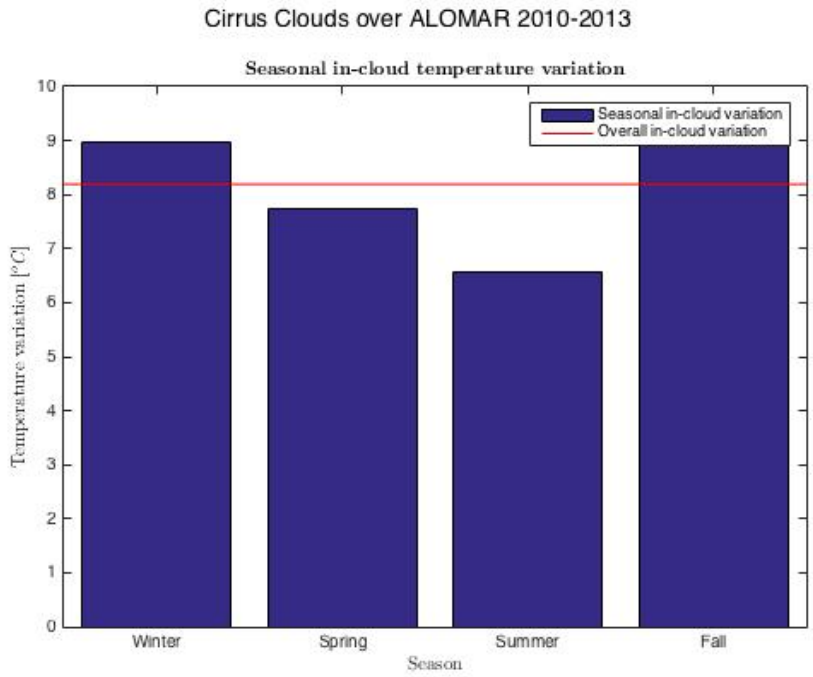

Figure C.6: Seasonal in-cloud temperature variations. The figure shows an overall mean variation of 8^oC. The summer season shows the lowest variations.

/D Distance Measurement

Temperature data for this thesis is obtained from radiosondes released from Bodø at 00:00 and 12:00 UTC every day. The data is entered into the Integrated Global Radiosonde Archive (IGRA) administrated by the National Oceanic and Atmospheric Administration (NOAA) [1].

The distance from Bodø to Andenes is measured using Google Maps. Print screen of the map with distance measured in overhead line is shown in figure C.1. The same figure was presented in the preliminary project paper dated June 2015 (Hanssen, 2015).

1. Details regarding the archive can be found on NOAAs webpage: `http://www.ncdc.noaa.gov/data-access/weather-balloon/integrated-global-radiosonde-archive`. Last checked: Nov. 13th 2015 07:48 UTC

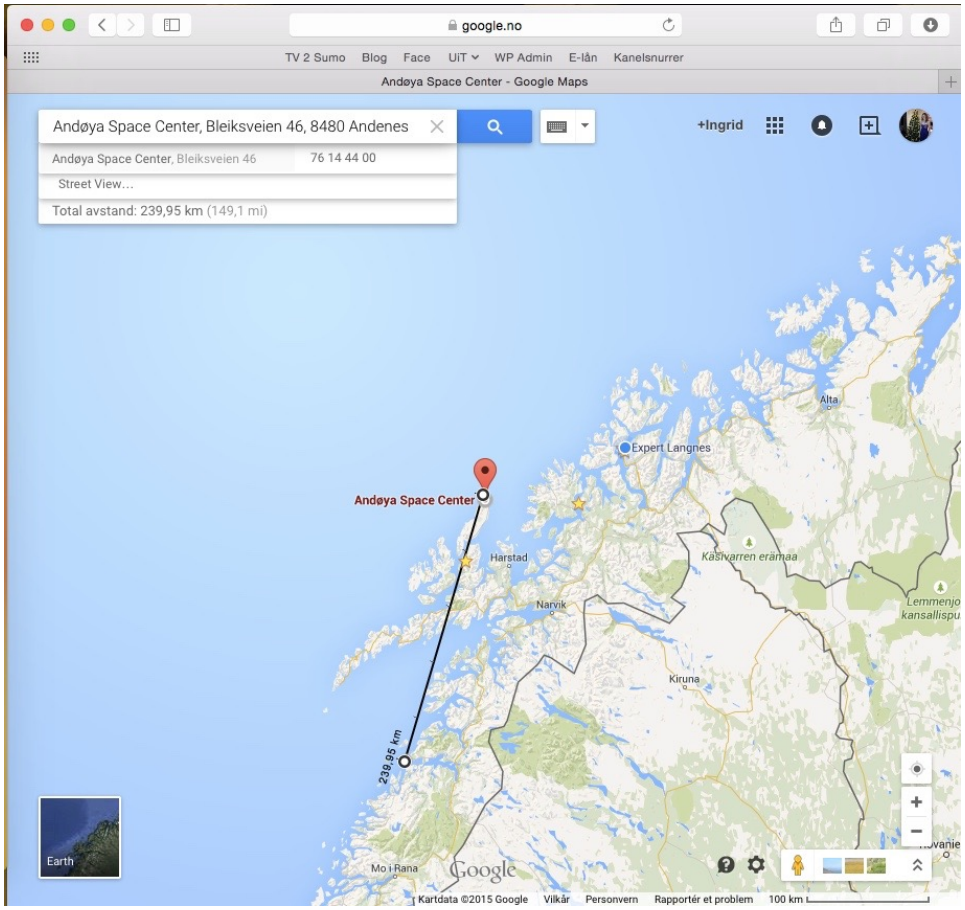

Figure D.1: Distance measurement from Bodø Airport to Andøya Space Center by Google Maps. Temperature data from the Meteorological institute used in this paper stems from the radiosonde station there.